AN ABSTRACT OF THE THESIS OF

Peter Hayden Sprunger for the degree of Doctor of Philosophy in Physics presented on May 18, 2010.

Title: A Study of Actinide De-excitation Through Neutron Emission from the Deuteron Induced Fission of ^{238}U

Abstract approved: _____

Albert Stetz

The process of de-excitation of the actinides is a very important question in both pure and applied science. In this dissertation the process was studied using the neutrons emitted in coincidence with fission induced by the bombardment of ^{238}U with 14.85 MeV deuterons. Neutrons can be emitted at multiple stages during the de-excitation process, with each stage producing its own unique neutron spectrum. The neutron spectrum in the lab frame is broken down into its constituent components using kinematic corrections to place them in their own reference frame.

It was found that 5.270 ± 0.067 prompt neutrons are emitted per fission with an average source temperature of 1.094 ± 0.011. In addition to the prompt neutrons spectrum, a pre$-$equilibrium component of 0.458 ± 0.023 neutrons per fission was observed coming from a source with a temperature of 3.15 ± 0.25 MeV. Unfortunately, the desired compound nucleus components were not resolveable because the magnitudes of the components were smaller than the magnitudes of the errors on the data.

A Study of Actinide De-excitation Through Neutron Emission from the Deuteron Induced Fission of ^{238}U

by

Peter Hayden Sprunger

A THESIS

submitted to

Oregon State University

in partial fulfillment of
the requirements for the
degree of

Doctor of Philosophy

Presented May 18, 2010
Commencement June 2011

Doctor of Philosophy thesis of Peter Hayden Sprunger presented on May 18, 2010

APPROVED:

Major Professor, representing Physics

Chair of the Department of Physics

Dean of the Graduate School

I understand that my thesis will become part of the permanent collection of Oregon State University libraries. My signature below authorizes release of my thesis to any reader upon request.

Peter Hayden Sprunger, Author

ACKNOWLEDGEMENTS

First and foremost I would like to thank my family and friends for their endless support. Most of all I must thank my wife Andrea. Her continuous and persuasive support was my ballast.

I want to thank the current members of my graduate committee for both the education they provided throughout my tenure and their support with matters outside the realm of physics. This group includes Albert Stetz, Ken Krane, Henri Jansen, Todd Palmer, and Douglas Warrick.

I would also like to thank the past and present members of the Oregon State University Nuclear Chemistry Group that aided in setting up the experiment as well as participating in fruitful discusions that provided new insight. These include Walter Loveland, Attukalathil Vinodkumar, Ricardo Yanez, Don Peterson, Radhika Naik, James Neeway, Brent Matteson, and Gustav Peterson. I must also mention the Nuclear Chemistry Group at Indiana University led by Romualdo deSouza where I spent one year before beginning at Oregon State.

Scientists cannot perform their duty alone. Ted Hinke, the machinist in the Chemistry Department, built and aided in the design of many of the detector holders and other unique pieces that allowed this experiment to happen. I would also like to that the staff and scientists at the Nuclear Physics Laboratory at the University of Washington where this experiment was completed. From the computation side I must thank Michael Conrady of the Radiation Center and the Physics Department technical staff for providing computers and maintenance. This especially includes Justin Elser who maintained the physics department computers for many years as well as always willing to help with personal IT issues. A final thank you to the NNSA who supported this work financially.

TABLE OF CONTENTS

TABLE OF CONTENTS (Continued)

TABLE OF CONTENTS (Continued)

LIST OF FIGURES

LIST OF FIGURES (Continued)

LIST OF FIGURES (Continued)

LIST OF TABLES

LIST OF TABLES (Continued)

A STUDY OF ACTINIDE DE-EXCITATION THROUGH NEUTRON EMISSION FROM THE DEUTERON INDUCED FISSION OF ^{238}U

1. INTRODUCTION

1.1 Motivation

The fission process is one of the most complicated naturally occurring processes. It requires hundreds of nucleons to act together, competing against the emission of single neutrons, charged particles, and photons, as a form of de-excitation. Additionally, the applications of fission in power production and weapons are currently some of the most controversial social issues, as they have been in the past and will be in the future. Even if there was an immediate global stoppage in the use of nuclear weapons and nuclear reactors, there would still be the issue of waste disposal. Besides long term storage, there is the possibility of destroying the material by inducing fission via bombardment with light charged particles, neutrons, or photons. With no immediate end to these controversies in sight the physical fission process will be at the heart of policy issues for many years. It is therefore imperative that the process is understood.

The composition of reactors, weapons, and decaying waste are all modeled in the same fashion. One starts with an initial composition of actinide isotopes. The future composition is governed by rates of particle captures and subsequent decays. Both reactors and weapons rely on chain reactions characterized by neutron captures to induce fission. The fission fragments then release an additional $\sim$ 1-4

neutrons into the system which sustains the chain reaction. In a reactor, the operator moderates the neutron flux in order to maintain a steady rate of fission. There is no moderation in a weapon which allows for an exponentially increasing rate of fission.

The prediction of the time rate of change of the composition of a system of actinides is deceivingly simple at first look. One simply estimates the rate of particle capture and nuclear decays and estimates the composition at a future time. The time step is set by the simulator. Due to compounding errors, the problem is accuracy. A small error in the estimate of the neutron flux at the very beginning could drastically change the result. To make an accurate prediction, one must have accurate neutron capture cross section data for all nuclei of interest, *and* an accurate measurement of the neutron flux. Since the neutron flux is created by the fissioning nuclei in the system, one must have accurate data or predictions of the neutrons produced during fission of all nuclei of interest.

Once one has accurate neutron data or predictions, one must also understand the competition between neutron emission, fission, charged particle, and gamma decay, as a function of excitation energy for all nuclei of interest. The number of neutrons emitted from an excited nucleus sheds light on this issue because neutron emission and fission are the two dominant decay modes.

To help illustrate the complexity this process is shown pictorially in Figure 1.1 for some nuclei of interest. Here, only neutron captures, shown with thick horizontal arrows, are considered. Beta decays are represented with vertical thin arrows and alpha decays are thin diagonal arrows. The figure also shows the main decay mode and corresponding half-life of the ground state for each element. In this case long decays are ones with half lives greater than 6000 years. These decays have an activity that is negligible. It should be noted that while not stated in the figure, all of the elements shown in Figure 1.1 can undergo fission.

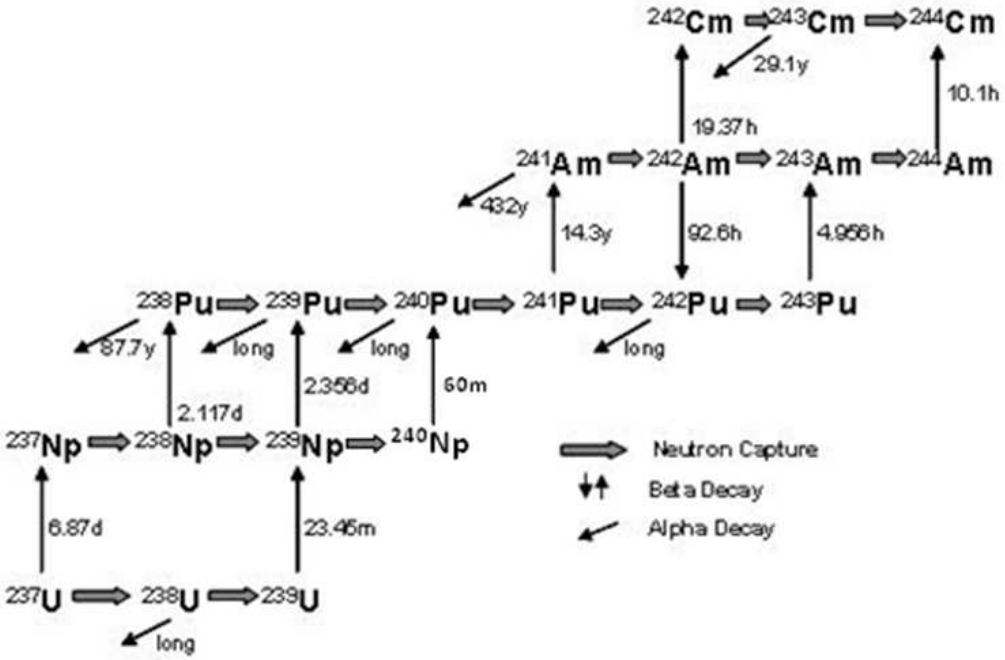

FIGURE 1.1: A network of actinides with Z≥92. This system is fed by neutron capture on lighter uranium isotopes.

Notice the interconnectedness of the system. There are often multiple ways to get from one nucleus to another (but there is often one that is much more likely than all the others). It also must be noted that the decay times are shown only for the ground state. As the excitation energy of a nucleus increases, the decay times drastically reduce. Even this simple case presents a challenging modeling problem. To complete this picture one must add in all other possible captures, decays, and nuclei.

The excitation energies of this experiment are higher than those found in a normal reactor, but are normally found in boosted nuclear weapons. In a boosted weapon a mixture of deuterium and tritium gas is injected into the center of a hollow pit just before the chain reaction occurs. The energy from the surrounding fissions compresses and heats the gas to cause fusion between the deuterium and tritium releasing 14.1 MeV neutrons in the process. If neutrons with this kinetic energy fuse

with ^{238}U, the excitation energy of the ^{239}U is 18.9 MeV, well over the fission barrier of ^{239}U. The excitation energies studied here are between 7 and 23 MeV, similar to the excitation energies obtained in boosted nuclear weapons.

Another practical application of this knowledge is that of transmutation of nuclear waste. The idea is to speed up the decay process of the longer lived actinides by subjecting them to a large energetic particle flux (neutrons, protons, deuterons, etc.) causing them to fission. Optimizing this process to use the least amount of energy to decrease the amount of waste by a desired amount requires detailed knowledge of the decay process for a wide range of excitation energies [1].

In this research, we use a deuteron projectile because it is easy to produce in an accelerator and allows for the exploration of a wider range of nuclei than high energy neutrons. For instance, to study the ^{240}Np nucleus directly one must use a target of ^{239}Np and bombard it with neutrons, or use a target of ^{239}U and bombard it with protons. It is very difficult to use these materials as targets due to their short half lives.

The question then arises as to whether the nucleus created in a deuteron capture is equivalent to the creation of the same nucleus using neutron capture. The key physical difference between the two is the $1/2\ \hbar$ spin difference between the deuteron and neutron. There are three results that suggest that this difference in spin is negligible.

First, Rubchenya *et al.* showed that the mass distributions of fission fragments created in the ^{238}U(d,f) and ^{238}U(d,pf) are nearly identical up to an excitation energy of approximately 50 MeV [2, 3]. This demonstrates that the post-scission fission properties are satisfactorily equivalent. Second, H.C. Britt and J.D. Cramer showed that the fission cross sections as a function of energy are nearly identical for the isotopes ^{235}U, ^{237}U, ^{239}U, ^{241}Pu, and ^{243}Pu created from the (n,f), (t,pf), and (d,pf)

reactions [4]. This suggests that the pre-scission properties are satisfactorily equivalent. Finally, Min and Martinot calculated the average neutron multiplicity emitted from the fission fragments ^{108}Mo and ^{144}Ce and they found that a small change in angular momentum does not significanly change the average neutron multiplicity [5]. Therefore the neutron spectrum between two reactions with a 1/2 $\hbar$ spin difference is satisfactorily equivalent.

An excited nucleus has many different channels open to decay, all of which compete against each other. Each decay modes has its own unique decay rate which is a function of excitation energy. This can be expressed in terms of Fermi's Golden Rule

$$\lambda_{if} = \frac{2\pi}{\hbar}|\langle f|V|i\rangle|^2\rho(E_f^\star) \tag{1.1}$$

where i and f refer to the initial and final states of the system, V is the operator that causes the change in states, and $\rho(E_f^\star)$ is the density of final states at excitation energy $E^\star$. Attempting to predict the decay rate requires detailed knowledge involving fundamental physics of the level structure of the nucleus and information about the interaction that causes the decay. While reliable systematics have been worked out regarding the decay of excited nuclei, the uncertainties are very large. More accurate data are needed to decrease the uncertainties.

This experiment sheds light on this process by studying the neutrons emitted in coincidence with fission from the bombardment of ^{238}U with 14.85 MeV deuterons (^{2}H). This reaction was performed at an excitation energy large enough to allow for multiple neutrons to be emitted before fission. The neutron spectra are decomposed into pre-equlibrium, equilibrium, and post-fission neutrons which will provide insight into the fundamental physics of the competition between neutron emission and fission. This will improve knowledge about what neutrons are present in a system of fission actinides.

1.2 Notation

A large number of symbols will be used in this document. Unless otherwise noted:

- A represents the mass of the nucleus in units of atomic mass units. The conversion to mass in units of MeV/c^2 is given by 1 amu = 931.5 Mev/c^2.
- B represents a barrier energy. The two most common cases in this work are the fission barrier, B_f, and the neutron binding energy, B_n.
- E will represent the kinetic energy of a particle. Unless otherwise noted the particle will be a neutron. Where appropriate, subscripts will be used to not whether the neutron is in the reference frame of the laboratory (lab) or the center of mass reference frame (cm). In some cases the reference frame will be irrelevant but the source will be important. In this case a mass number is used to differentiate between different sources.
- $E^\star$ represents the excitation energy of a nucleus. Also where appropriate, subscripts will be used for differentiation.
- M represents one of two things: the neutron multiplicity of a source, or the total mass of a nucleus. In the context is should be apparent which is meant.
- p represents the momentum of a particle. The same notation rules that applied for the kinetic energy of a particle, apply here.
- T represents the nuclear temperature.
- Z represents the charge, or proton number of a nucleus.
- ϵ represents the kinetic energy per nucleon of a nucleus.

- ε represents the efficiency of the neutron detectors.

1.3 Energetics

The maximum energy of the deuterons available of (14.85 MeV) was used in order to obtain the highest excitation energy possible in the compound nucleus. See Section 2.1 for more details on the beam characteristics.

Assuming a complete fusion of the deuteron and the target, the energy and momentum conservation equations are

$$M(^{2}\mathrm{H}) + M(^{238}\mathrm{U}) + E_{^{2}\mathrm{H}} = M(^{240}\mathrm{Np}) + E_{^{240}\mathrm{Np}} + E^{\star} \tag{1.2}$$

$$p_{^{2}\mathrm{H}} = p_{^{240}\mathrm{Np}} \tag{1.3}$$

Here, $M(x)$ represents the mass energy of the nucleus x. The incoming deuteron has a momentum of 236.05 MeV/c which is completely transfered to the ^{240}Np compound nucleus. This leads to a recoil energy and velocity of 0.125 MeV and 0.0317 cm/ns. Using the masses from [6] the energy conservation equation can be solved yielding an excitation energy of 22.845 MeV.

Complete fusion is only one possibility. Due to the requirement of a fission in the hard trigger, this experiment observes only reactions that end in fission. It is possible that nothing is emitted and the ^{240}Np nucleus immediately fissions. The cross section of the ^{238}U(d,f) reaction is approximately 700 mb [7].

Let us now explore the possibilities of the different decay chains. Once (If) the compound nucleus is formed, it will then begin to de-excite. In this mass and excitation energy range the primary modes of decay of the compound nucleus are neutron emission or fission. While it is possible for the nucleus to decay via γ, β, or charged particle emission, these modes contribute a negligible amount. The

assumption that decay modes besides neutron emission and fission are negligible is very common [8, 9, 10].

At each step in the chain the de-excitation process nucleus will de-excite by either emitting a neutron or by fissioning. The probability of decay via mode i is denoted Γ_i/Γ_τ. Here Γ_i represents the decay width of mode i and Γ_τ represents the sum of all the partial widths or the sum over all i modes.

The probability of choosing neutron emission over fission is modeled by the function

$$\left(\frac{\Gamma_n}{\Gamma_f}\right)_{A,E^\star} \tag{1.4}$$

This is a function of the mass of the nucleus and the excitation energy (as well as a few other things of lesser relevance to this work). This function is discussed more in Section 1.4.4. The probability of the compound nucleus emitting one neutron and then fissioning is written as

$$\sigma_{d,n_{cn}f} = \sigma_{d,capture}\left(\frac{\Gamma_n}{\Gamma_T}\right)_{A=240,E^\star_{240}}\left(\frac{\Gamma_f}{\Gamma_T}\right)_{A=239,E^\star_{239}} \tag{1.5}$$

where $\sigma_{d,capture}$ is the probability of forming a compound nucleus. If a fusion reaction occurs, then then there is just enough excitation energy available for 3 neutrons to be emitted. However, the total kinetic energy of all three neutrons would need to be nearly zero in order for the system to still have enough excitation energy to overcome the fission barrier. This is extremely unlikely. Therefore, pracitcally speakeing, this experiment can observe a maximum of two neutrons per event.

There is also the possibility of a direct reaction occurring where a neutron or proton is emitted before the system is in equilibrium. The most common of these are the (d,p$_{pre}$f), (d,n$_{pre}$f), and (d,n$_{pre}$n'$_{pre}$f). The subscript *pre* has been added for clarity. The excitation energy for the (d,n$_{pre}$) reaction can be calculated from

$$\mathrm{M}(^2\mathrm{H}) + \mathrm{M}(^{238}\mathrm{U}) + E_{^2\mathrm{H}} = \mathrm{M}(^{239}\mathrm{Np}) + \mathrm{M}(\mathrm{n}) + E_{^{239}\mathrm{Np}} + E_{\mathrm{n}} + E^\star \tag{1.6}$$

Assuming the daughter products have zero kinetic energy the resulting excitation energy of the ^{239}Np nucleus is 17.914.

The (d,pf) reaction (of which (d,p$_{pre}$f is a subset) is slightly problematic because the proton will not be observed while the fission will be observed. This will make the (d,pf) reaction indistinguishable from the (d,f) reaction. Luckily, the cross section of the ^{238}U(d,pf) reaction is approximately 1/30 of the ^{238}U(d,f) reaction [11]. In the end these events can be ignored.

Once a compound nucleus is formed the excitation energies of the chain can be calculated. Consider the case of complete fusion again. If a complete fusion occurs, the resulting ^{240}Np nucleus will have an excitation energy of 22.845 MeV. If this nucleus undergoes neutron decay the resulting ^{239}Np nucleus will have an excitation energy of $E^{\star}_{239} = E^{\star}_{240} - B_n - E_n$. Since the neutrons are emitted in a Maxwellian distribution (which will be discussed later in this chapter) the average kinetic energy of the neutron is twice the nuclear temperature (when measured in units of MeV) of the emitting source. The ^{239}Np nucleus can then undergo neutron emission and the excitation energy of the daughter ^{238}Np nucleus can be calculated in the same way. One of the difficulties in modeling the decay is due to the distribution of excitation energies stemming from the distribution of the kinetic energy of the neutrons. This must be taken into account due to the exponential increase in decay rate as a function of excitation energy.

1.4 Previous Work

1.4.1 Experimental

There is a large amount of data describing the prompt neutrons emitted from the fission of nuclei with the mass $A = 239$ and 240. A plethora of data can be found

using the Evaluated Nuclear Data File (ENDF), available on the National Nuclear Data Center (NNDC) website [12, 13]. There are also a number of experiments that have used protons to induce fission [8, 14, 15, 16, 17]. The data from these experiments in the excitation energy range of this experiment are shown in Figure 1.2.

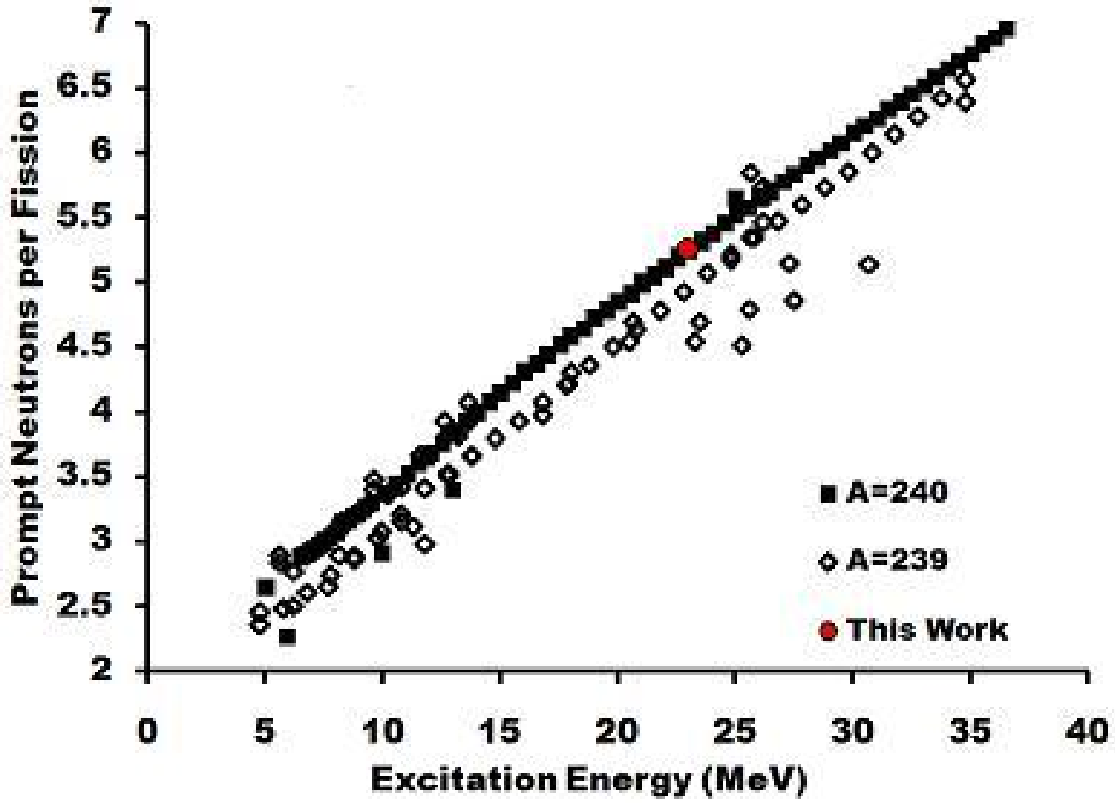

FIGURE 1.2: Total prompt neutrons emitted per fission from systems with $A = 239$ and 240 as a function of the energy of the fully fused system. Data are from [8, 12, 13, 14, 15, 16, 17]

As one can see there is a slight decrease in the total multiplicity with decreasing mass in this region. Also, the relation between total multiplicity and excitation energy is approximately linear. If one goes to higher excitation energies the relation follows [18, 19]

$$\nu = a + b(1 - e^{-cE}) \tag{1.7}$$

where ν is the total number of neutrons emitted, E is the excitation energy of the system, and a, b, and c are fitted constants. It is unclear how this parameterization was derived and since no rigorous derivation is described it appears to be an empirical fit [19][1].

In this experiment we are interested not only in the total number of neutrons emitted, but the source of these neutrons. In this experiment neutrons can be emitted from any of the following

1. The excited but not yet equilibriated compound nucleus
2. The equilibrated compound nucleus
3. During the fission process
4. Prompt neutrons emitted from the excited fission fragments.
5. Delayed neutrons emitted from the excited fission fragment.

These sources and their application to this experiment will be discussed in greater detail in Section 4.2

While there have been many measurements of the prompt neutron multiplicity, there have been only a few experiments performed where the components were separated, and even fewer in the energy range of this experiment. In Figure 1.3 the multiplicity of neutrons emitted from the equilibrated compound nucleus is shown as a function of excitation energy [8, 14, 15, 16, 17]. As one can see there is a large deviation in the compound nucleus neutron multiplicity. If one draws a best fit line

[1]This is not to say that Equation 1.7 is completely without merit. A hand waving argument for the form of Equation 1.7 goes something like this: This total excitation energy is mostly in the form of neutron binding energy. Using the semi-empirical mass formula, a semi-empirical neutron binding energy can be derived. Integrate the semi-empirical neutron binding energy over the number of neutrons emitted to find the total excition energy as a function of neutrons emitted. One of the dominant terms is a logaritic term. And, rearranging Equation 1.7, the total excitation energy is proportional to the logarithm of the number of neutrons emitted.

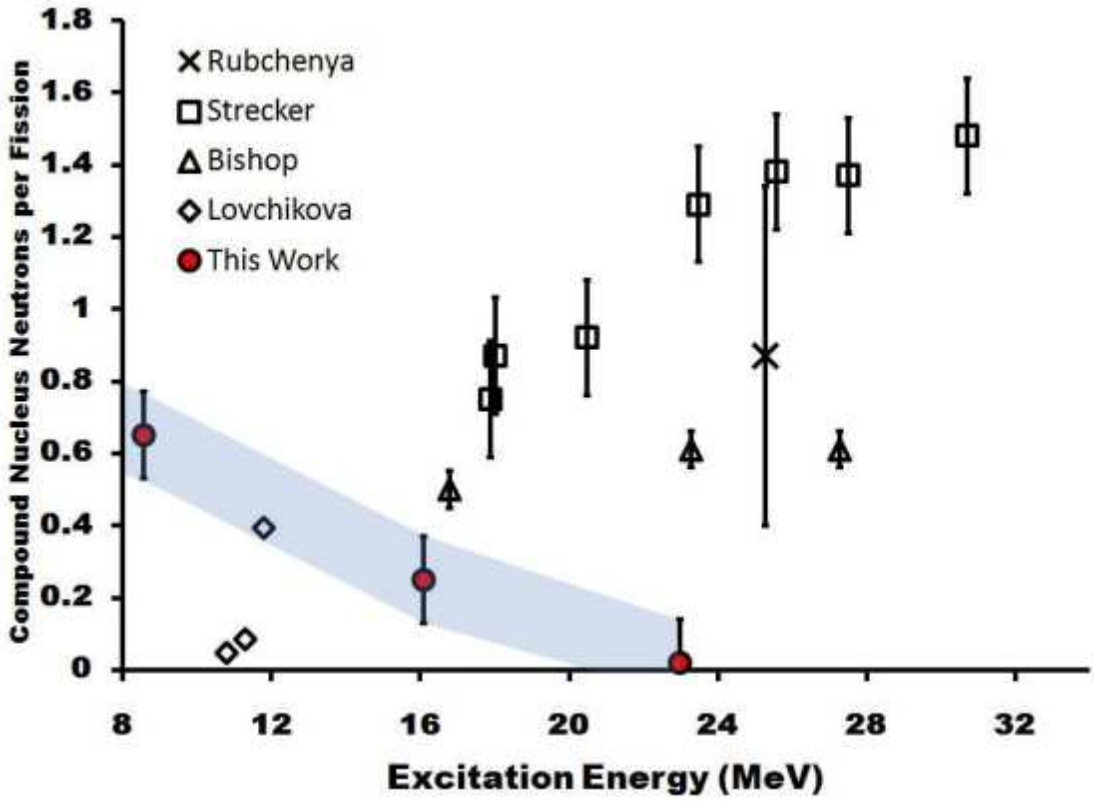

FIGURE 1.3: Data of the multiplicity of the compound nucleus component. Only data from systems with A=239 are available [8, 14, 15, 16, 17]. The result from this experiment is shown in red.

through each of the data sets of Bishop *et al.*, Strecker *et al.*, and Lovchikova *et al.*, separately, it is easy to see that the trends are not in agreement with each other. It is important to note that these data are from nuclei with A =239, not A=240. This experiment is the first of its type to attempt to measure the compound nucleus neutrons at this excitation energy from an A=240 source.

It is commonly stated that the pre-equilibrium process is the least understood neutron component. The data from the experiments most similar to this one adhere to this rule. Strecker *et al.* [15] place their detectors perpendicular to the direction of the beam and assume the pre-equilibrium component is negligible. Lovchikova *et al.* [17] calculated the pre-equilibrium component using the methods of Kalbach and Mann [20]. The calculated temperature is not stated but appears to be very large judging from their plots. Rubchenya *et al.* [16] calculate a pre-equilibrium component *and* then exclude the calculated pre-equilibrium component during the fitting procedure and assume it is absorbed by the prompt neutron component.

Other experiments at significantly different excitation energies from this experiment but using similar methods also have a wide distribution of tactics for dealing with the pre-equilibrium component. Hinde *et al.* [21] assume a Maxwellian distriubtion with a source velocity 1/2 of the beam velocity, calculate the temperature using the BME code and fit the multiplicity to the data. Isaev *et al.* [22] fit both the multiplicity and temperature but claim that the temperature parameter is unphysical and do not give the fitted values. Cabrera *et al.* [23] use a Watt spectrum to model their pre-equilibrium spectrum and fit both multiplicity and temperature *and* report both values. Keutgen *et al.* [24] also use a Watt spectrum to describe the pre-equilibrium neutrons but do not state the temperatures. The model used in this experiment assumes a Maxwellian energy distribution and an angular distribution based on the systematics of Kalbach [21, 25]. The model is discussed in Section 4.3.

1.4.2 Methods

One of the original experiments to separate the neutron spectrum into various components was performed by Harding and Farley using 147 MeV protons on natural uranium [26]. Then, using the kinematics of Fraser [27] and DeBenedetti *et al.* [28], they found that out of 13.1 neutrons emitted per event, 2.5 were emitted after fission with the rest before. The key to this work is that the that neutrons are emitted isotropically in the rest frame of the emitting fragment. This means that neutrons emitted from the moving fragments will be kinematically focused in the fragment direction.

In an experiment of this type, the measured result is a spectrum of neutrons in the lab frame. One must then make assumptions to separate this single spectrum into the prompt, equilibrium, and pre-equilibrium, components. There are two techniques to separate the spectrum: an iterative approach, and a multiple source chi-squared minimization approach [29].

The iterative approach is optimized when the neutron detectors are placed at 0° and 90° with respect to the path of the fission fragment. It has the advantage that no functional form of the neutron distribution needs to be assumed. The only assumption is that the neutrons are emitted isotropically in the respective frame of reference of the emitting source.

The iterative approach proceeds in one of two ways. The first is to assume that all the neutrons in the forward detector (at 0° with respect to the fission fragments) are prompt neutrons. From this assumption it is determined how many prompt neutrons are present in the detector perpendicular to the direction of fission. This is done by transforming the forward component from the lab frame into the rest frame of the fission fragment. The contribution from the fission fragment in the perpendicular detector is then dervived. This derived component is then subtracted

from the perpendicular experimental spectrum, and the remainder is assumed to be neutrons from the compound nucleus. The compound nucleus spectrum is then subtracted from the experimental spectrum in the forward detector and the remainder is the prompt neutron spectrum. No kinematic transformation is needed in this step because the compound nucleus component is emitted isotropically in the lab frame. The process is then repeated to the desired precision.

The second way the iterative approach is done is to first assume that all the neutrons in the perpendicular detector are equilibrium neutrons and subtract this component from the forward detector.

Relevant to this experiment is the work of Bishop *et al.* [8, 14]. They investigated the ^{238}U + p reaction at an energy similar to this experiment and used an iterative approach to separate the compound nucleus component from the prompt neutron component. A pre-equilibrium component was assumed to be negligible because all neutron detectors were perpendicular to the direction of the beam.

One drawback of the iterative method is that only two sources can be used, one that is stationary in the lab frame and one that is in motion. The two sources are taken to be the stationary compound nucleus and the fully accelerated fission fragments. The neutrons from direct reactions, pre-equilibrium processes, and scission neutrons are assumed to be negligible perturbations or are grouped in with the isotropic or kinematically focused component. Furthermore, the method is clearest when only neutrons at 0° and 90° with respect to the beam are used. It is possible to use detectors at other angles but the separation is not as easy and the kinematic equations are more difficult.

The χ^2 minimization methods solves all of these problems. The idea is simple, one first assumes a functional form for each source one would like to isolate. Sum these together to obtain a single equation that governs all the data. Then fit the

equation to the data by minimizing the χ^2 value. The set of parameter values that yields the minimum χ^2 value is taken to be the best reflection of reality [29].

Each neutron source (such as a compound nucleus or a fission fragment) is a hot body. Therefore the neutrons are emitted isotropically in their own reference frame and form a Maxwellian distribution. This idea dates back to Weisskopf′s work in 1937 [30] where he showed that the kinetic energy of neutrons evaporated from an excited compound nucleus follows a Maxwellian distribution

$$N(E_{cm}, T)dE_{cm} = \frac{1}{4\pi T^2} E_{cm} e^{-E_{cm}/T} dE_{cm} \tag{1.8}$$

Translating Equation 1.8 to the lab frame yields [22]

$$\frac{d^2M}{dEd\Omega} = \frac{1}{4\pi T^2} \sqrt{E_{lab}E_{cm}} \exp\left(\frac{-E_{cm}}{T}\right) \tag{1.9}$$

An aside needs to be made about the slope parameter, T, in the preceeding equations. In the case of a nuclear reaction it is uncertain whether the system is in thermodynamic equilibrium. The slope parameter, T, in the preceeding equations is often referred to as the "nuclear temperature". It actually corresponds to the kinetic temperature which can be used whether the system is in thermodynamic equilibrium or not [31]. Since the only way to measure the temperature of a nucleus is to observe the spectrum of particles emitted which is always modeled by a Maxwellian, the T in the equation above is the only measure of the temperature of the nucleus. The T in the equation is in units of energy for convenience and actually represents kT.

The Maxwellian form can be used to describe the compound nucleus emission if one neutron is emitted. It is also used to describe the pre-equilibrium component. While the pre-equilibrium component, by definition, is not in thermal equilibrium, it is nevertheless treated assuming a Maxwellian distribution. This can be done because the temperature parameter is an accurate measurement of the kinetic temperature regardless of whether the system is in thermodynamic equilibrium or not.

In the case of the fission fragment, multiple neutrons are emitted in a cascade. If one assumes that the fission fragments have a constant kinetic energy then the neutron spectrum from the fission fragments was shown experimentally to follow a Watt distribution [32]

$$\frac{dM}{dE} = \frac{M}{2\sqrt{\pi\epsilon T}} \exp\left(\frac{-(E+\epsilon)}{T}\right) \sinh\frac{2\sqrt{E\epsilon}}{T} \tag{1.10}$$

Hilscher *et al.* [33] introduced the form

$$\frac{d^2M}{dE_{lab}d\Omega} = \frac{M}{2(\pi T)^{3/2}} \sqrt{E_{lab}} \exp\left(\frac{-(E_{lab} - 2\sqrt{E_{lab}\epsilon}\cos\theta + \epsilon)}{T}\right) \tag{1.11}$$

where E_{lab} is the lab energy of the neutron, θ is the angle between the fragment direction and the neutron direction in the laboratory reference frame, and ϵ is the energy per nucleon of the fragment. Note that by using the law of cosines the lab energy and center of mass energy of the neutrons are related by

$$E_{cm} = E_{lab} + \epsilon - 2\sqrt{E_{lab}\epsilon}\cos\theta \tag{1.12}$$

Furthermore, integration of Equation 1.11 over all angles results in (the experimentally proven) Equation 1.10 [33].

Equations 1.8 and 1.11 are the functional forms that are normally used in the χ^2 minimization method. When only one neutron is expected from a source Equation 1.8 is used while if multiple neutrons are emitted the cascade approximation (Equation 1.11) is used. In theory all of the parameters in Equation 1.11 can be fit but usually a value (or values if the fission fragments are assumed to be asymmetric) for ϵ is assumed and θ is set by the placement of the detectors. This leaves the multiplicity and temperature as the fitted parameters. Furthermore, a good portion of the time the temperatures are calculated and held constant; this decreases the number of free parameters. This method has been used multiple times [21, 22, 23, 33, 34, 35, 36].

1.4.3 Disclaimers on previous experimental work.

Now that the body of experimental work has been explained it is time to go back and take a second look at the data shown in Figure 1.3

The experiment by Rubchenya *et al.* [16] uses the χ^2 minimization method as decribed above but does not discuss the temperatures or the χ^2 value of the resulting fits. It can therefore not be said that the fits are statistically relevant or to what extent the data actually agree with any other data because only 1/2 of the parameters (the multiplicities) are given. Furthermore, only neutrons of energy greater than 2 MeV are considered which means that only the small tail of the compound nucleus component is observed. The pre-equilibrium component is not included in the fitting procedure and is assumed to be part of the prompt fission component.

Strecker *et al.* used a hybrid approach by first separating the components using an iterative method and then determining the multiplicities and temperatures of each component by fitting them separately using the χ^2 minimization method. The measured fission fragment temperatures range from 0.93 MeV to 1.02 MeV for excitation energies from 17.9 to 30.7 MeV. The pre-equilibrium component is not included because all neutron detectors are perpendicular to the beam direction. The resulting χ^2 values are not given either, therefore one cannot make the conclusion that they are statistically significant.

Lovchikova *et al.* provide the most detailed experiment which includes reduced χ^2 values of 1.42, 0.5, and 1.16 for bombarding neutron energies of 6.0, 6.5, and 7 MeV repectively. However, the data are measured relative to the neutron spectrum from the spontaneous fission of ^{252}Cf and it is assumed that the temperatures are equivalent. The temperature of the ^{252}Cf prompt fission neutron spectrum is approximately 1.4 MeV which does not match the results of Strecker *et al.*

Each one of these experiments make some questionable assumptions or do not disclose relevant findings that could possibly cast a shadow on the quality of the results. The fact that each of these experiments was not conducted in the same fashion and that some aspects are in contradiction with other experiments explains the lack of consistency amongst the data shown in Figure 1.3.

1.4.4 Theory Behind Γ_n/Γ_f

One last topic that needs to be introduced is the classic theory for the level width for a neutron decay. The decay width can be expressed as

$$\Gamma_n = \frac{D}{2\pi}\sum T \tag{1.13}$$

where D is the level density of the compound nucleus and in this section T is the transmission coefficient, not the temperature. A similar relation can be drawn for the fission width.

At excitation energies well over the barrier, the transmission coefficients approach unity. The competition between neutron decay and fission decay then becomes a statistical question based on the number of daughter states available. For neutron decay the number of states is calculated for the daughter nucleus, and for fission it is calculated at the saddle point.

Also, at high excitation energies there are many possible angular momentum states available. These new angular momentum states must be considered in the sum over the transmission coefficient in Equation 1.13. The range on the sum spans from $l = 0$ to the maximum spin allowable, l_m. In the excitation energy regime of this experiment there are many states available and the sum can be replaced with an integral. Integrating over these possible angular momentum states yields

$$\int_0^{l_m} (2l+1)T_l dl = l_m^2 \tag{1.14}$$

Here T_l is assumed to be 1. l_m can be estimated by $Rp/\hbar$ where R is the radius of the nucleus and p is the linear momentum of the neutron at the edge of the nucleus. Since $E = p^2/2m$, where E is the kinetic energy of the neutron and m is the mass,

$$l_m^2 = 2mER^2/\hbar^2 \tag{1.15}$$

Plugging this result into Equation 1.13 and integrating over energy one obtains

$$\Gamma_n = \left(\frac{D}{2\pi}\right)\left(\frac{2mR^2g}{\hbar^2}\right)\int_0^{E^\star - B_n} E\rho(E^\star - B_n - E)dE \tag{1.16}$$

where $\rho(E)$ is the level density of the daughter nucleus. The factor g is due to the two neutron spin states (up and down) and has a value of 2 in this case. See Chapter 7 of [37] for a more thorough discussion.

One can do a similar calculation for the fission width. Dividing the neutron width by the fission width results in the classic theory of the competition between neutron emission and fission:

$$\frac{\Gamma_n}{\Gamma_f} = \frac{gA^{2/3}}{K_0}\frac{\int_0^{E^\star - B_n} E\rho(E^\star - B_n - E)dE}{\int_0^{E^\star - E_f}\rho(E^\star - B_f - K)dK} \tag{1.17}$$

where K is the kinetic energy of the fission fragments along the axis of fission. K_0 is the angular momentum of the nucleus. Assuming a Fermi Gas level density this expression becomes

$$\frac{\Gamma_n}{\Gamma_f} = \frac{4A^{2/3}a_f(E^\star - B_n)}{K_0 a_n[2a_f^{1/2}(E^\star - B_f)^{1/2} - 1]}\exp[2a_n^{1/2}(E^\star - B_n)^{1/2} - 2a_f^{1/2}(E^\star - B_f)^{1/2}] \tag{1.18}$$

where a_f and a_n are the level density parameters for neutron emission and fission respectively.

2. EXPERIMENTAL SETUP

2.1 Beam Characteristics

The deuteron beam for this experiment was provided by the Tandem Van de Graaff accelerator at the Center for Experimal Nuclear Physics and Astrophysics (CENPA) of the University of Washington. The booster was not available during the experiment therefore instead of using an 18 MeV deuteron beam a 14.85 MeV beam was used. Since measuring the cross section of the reaction was not a goal of this experiment a rigorous measurement of the beam intensity was not performed. The current was allowed to vary between roughly 25-75 electrical nanoamperes and was adjusted when the data collection rate was deemed either too high or too low. More can be found on the accelerator at the CENPA website [38].

2.2 Target

The target used during the experiment was made by Dr. Walter Loveland of the nuclear chemistry group at Oregon State University [39]. Made by evaporation of UF_4, it consisted of 1.1 mg/cm^2 U on a backing of 0.15 mg/cm^2 natural Ag. Depleted uranium was used ensuring that over 99% of the uranium is ^{238}U. No correction was made for other isotopes in this experiment.

2.3 Chamber and Detectors

A thin walled vacuum chamber was built for this experiment. It consists of a 1/16 inch (1.59 mm) thick stainless steel central cylinder with a radius of 9 inches

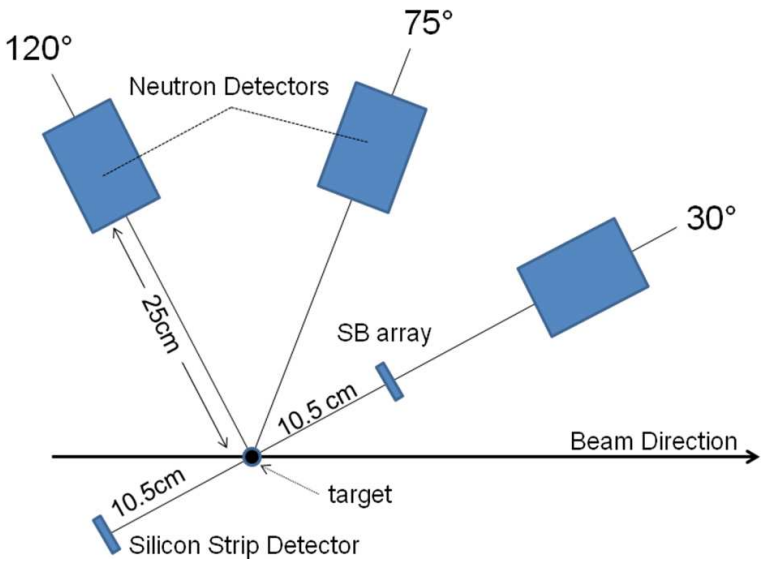

FIGURE 2.1: Schematic of the detector setup.

(22.86 cm) and a width of 5.25 inches (13.34 cm). The cylinder was placed such that its radial axis was parallel to the ground and was capped with two 1/8 inch (3.18 mm) thick aluminum domes. The domes have 1 inch (2.54 cm) wide lips that sit in flanges fixed to the cylinder. A rubber gasket is placed between the dome and flange to make a seal. Each in-plane neutron detector then viewed only 1/8 (3.18 mm) of aluminum. All feedthrough ports were located on the cylinder.

A schematic of the setup is shown in figure 2.1. Four Saint Gobain BC-501a liquid scintillator detectors were used to detect the neutrons in this experiment. They consist of an aluminum cylinder 8 cm long and 8.9 cm in diameter leading to an active cylindrical volume 7.8 cm long with a 3.75 cm radius. Henceforth they will be referred to as N0, N1, N2, and N3. N1, N2, and N3 were placed in-plane with the charged particle detectors with their front face 25 cm from the target at 30°, 75°, and 120°, respectively, with respect to the direction of the beam. N0 was placed directly above the target with the front face at 45 cm. The mean interaction depth is 3.3 cm [40] meaning the three in plane detectors covered 15.1° across the diameter

(0.054 steradians) and N0 covered 8.9° across the diameter (0.019 steradians).

The uncertainty in the placement of the neutron detectors is approximately 1 cm. When the detectors were set in place the measuring implement's finest scale was in millimeters. Care was taken to set the detectors at exactly 25.0 cm from the source. The original uncertainty was on the order of a couple of millimeters. However it was discovered later in the experiment that the detectors had shifted for two reasons. The first comes from stresses applied by the power and signal cables. The second was that the table on which the detectors were setting was not fixed to the floor and it was found to have moved a few millimeters during the experiment. While the shifts due to the cables and the table were both on the order of millimeters, the location at the time of data collection is unknown. Furthermore, there is an uncertainty of a few millimeters in the mean interaction depth simulated by Pozzi *et al.* [40]. For all these reasons, an uncertainty of 1 cm is assumed.

An array of four 300 mm^2 surface barrier detectors (SBD or SBDs) was housed in a 1/2 inch thick aluminum block with its center located 30° from the beam at a distance of 10.5 cm. Henceforth they will be referred to as S0, S1, S2, and S3, and as a group will be referred to as "the array". A schmatic of the array is shown in Figure 2.2. The centers of the detectors were 1.4 cm above and below the plane of the neutron detectors and 1.7 cm to the left and right of the center of the block. They are at a distance of 10.72 cm from the target. Each detector covered 10.6° across the diameter (0.206% of 4π). S0 and S1 are above the plane, while S2 and S3 were below. S0 and S2 are further from the beam at 40° than S1 and S3 at 22°.

Sitting directly opposite the array is a double-sided silicon strip detector (DSSD). The detector was 5 cm x 5 cm square and was divided into 16 separate strips aligned vertically in this experiment. The signals from the 16 vertical strips were added together in groups of four adjoining strips bringing the total number of

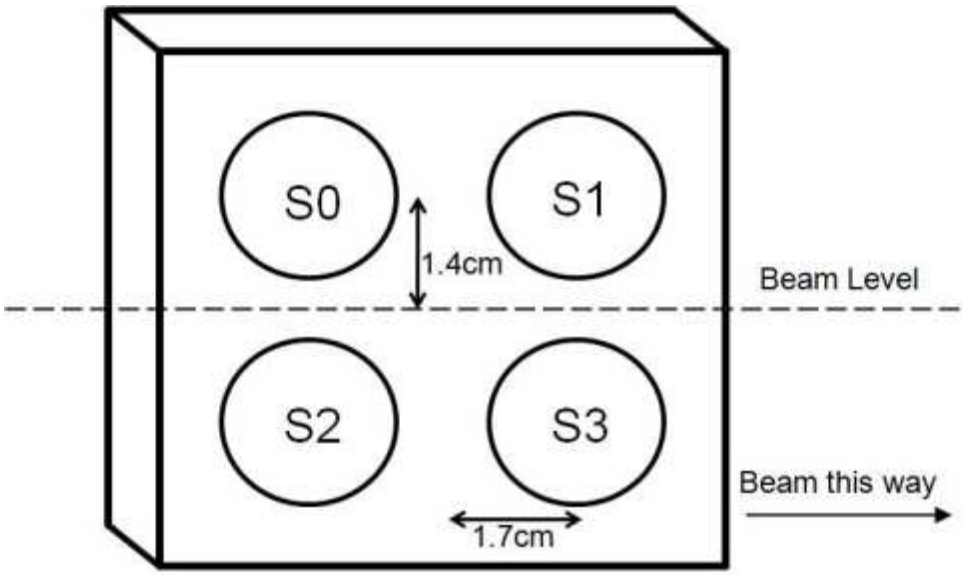

FIGURE 2.2: Schematic of the surface barrier detector array. The perspective is that of looking through the array towards the target.

unique output signals from 16 down to four. These four "strips"will henceforth be referred to as S4, S5, S6, and S7. S4 is centered at 140° with respect to the beam, S5 147°, S6 153°, and S7 160°.

The angles in degrees between the good (see section 3.5) charged particle and neutron detectors are listed in the Table 2.1. Only S0, S1, S3, and S7 are listed due to issues with the other silicon detectors. The uncertainties were determined by simulation with a Monte Carlo method. The code (similar to the one shown in Appendix C.1) randomly generates two points on a sphere. These two points were taken to be the direction of the "fission"and the "neutron". If the fission intersected the location of a fission detector and the neutron intersected the location of a neutron detector the angle between the two vectors was recorded. A minimum of 100,000 events was required to assure a smooth distribution. The distributions were then fit with a Gaussian function. The validity of the use of a Gaussian to describe the

	N0	N1	N2	N3
S0	82 ± 4	12 ± 5	37 ± 5	81 ± 5
S1	82 ± 4	12 ± 5	54 ± 5	99 ± 5
S2	98 ± 4	12 ± 5	37 ± 5	81 ± 5
S7	90 ± 4	166 ± 5	144 ± 5	99 ± 5

TABLE 2.1: Coincident angles between the silicon detectors and neutron detectors. Uncertainties were determined by fitting a Gaussian to a spectrum generated by a Monte Carlo method.

angular distributions of both the SBD's and the strips is evident in Figure 2.3 which shows the spectra for an S1-N3 coincidence and an S7-N3 coincidence.

2.4 Electronics

A diagram of all the electronics is shown in Figure 2.4. Each signal from the fission detectors was taken out of the chamber and fed directly into one of two 8 channel Mesytec MSI-8 modules. These MSI-8 modules contain both a preamplifier and an amplifier/shaper. The slow signal from the MSI-8 was sent to a Philips 7164 ADC (analog to digital converter) whose output was read by the computer. The fast signal was fed into a constant fraction discriminator (CFD) which was used to eliminate the low energy signals (the noise). The CFD logic pulses were then fed into fan-in/fan-out (FIFO) modules that served to "OR" the fission signals together. The signal from the individual neutron detectors was first input into a pre-amplifier and the output fast signal was sent into a Caen 808 CFD. No FIFO's were needed to create a neutron OR because the Caen 808 CFD created its own OR output.

The OR signals from the fission detectors provided the input into the gate

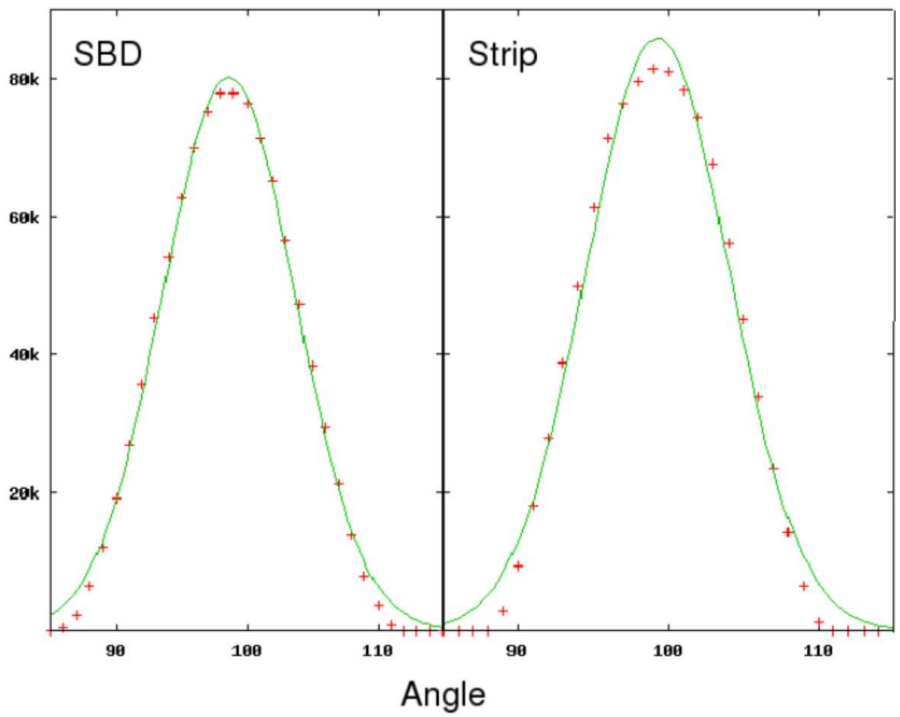

FIGURE 2.3: Simulated spectrum and resulting gaussian fits to a surface barrier detector - neutron detector combination (right) and a strip detector - neutron detector combination (left).

generator which created our master gate signal. The master gate generator is a CO-4010 module and has the dual function of also being a logic module. The OR signal from the neutron detectors (via the Caen 808) was also input into this module. If desired one can then use the logic capabilities to produce a master gate on only a fission signal, only a neutron signal, the AND of the two signals, or the OR of the two signals. The master gate signal width was set at 4μs to ensure it encompassed the entire signal sent from the MSI-8 module. The master gate was fed into the master gate input of the CAMAC modules.

The timing was done using a Philips 7087 time to digital converter (TDC). A second fission OR signal from the FIFO was sent to the universal "start"while the CFD outputs of the neutron signals were sent to the individual "stops". Not

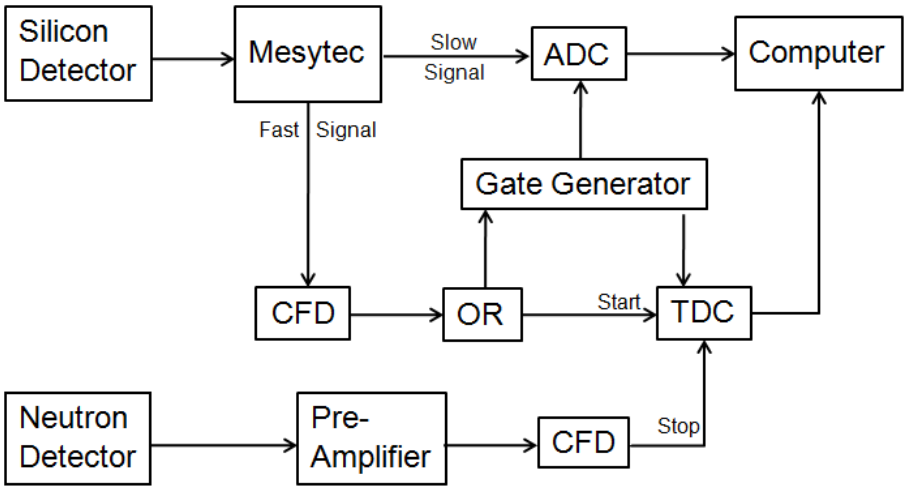

FIGURE 2.4: Schematic of the electronic setup in this experiment.

discussed in the preceeding paragraphs was the various cables added as necessary that acted as passive delays. These cables assured that all signals reached the ADC and TDC within the window of the mastergate.

The data from the ADC and TDC was recorded using a SpecTcl system custom built by Ron Fox of Michigan State University. This system also allowed us to control the CAMAC crate and all modules within that crate. More can be found at the SpecTcl site on the MSU website [41].

3. CALIBRATION AND EVENT REJECTION

3.1 Fission Detectors and Fission Event Rejection

As mentioned before there were eight silicon detectors used in the experiment. Four were 300 mm^2 surface barrier detectors arranged in an array situated in-plane nominally 30° from the beam. The other four were part of a double-sided silicon strip detector situated in-plane centered at 210° with respect to the beam (180° from the array).

The raw calibration ADC spectrum from each fission detector is shown in Figures 3.1 and 3.2. The spectrum is that of a ^{252}Cf source which was shown on the array and DSSD just prior to data collection. Schmitt and Pleasonton [42] claim that a fission detector with good resolution should have a light peak to valley ratio of at least 2.85 and a light peak to heavy peak ratio of 1.3 (for a ^{252}Cf spectrum). These numbers were determined in an experiment that was set up to measure the performance of detectors. To isolate the detector behavior new detectors were used and the source was very thin.

In this experiment the detectors have been used before and energy dissipation in the source was significant. The array detectors have light peak to valley ratios of approximately 1.2 to 1.3 and light to heavy ratios of approximately 1.0 to 1.2. The DSSD performed a little better with light peak to valley ratios of 1.3 to 1.5 and light to heavy peaks ratios of 1.2 to 1.4. These numbers are based on double peaked gaussian fits to the data and rounded to the nearest 0.1. The fact that these ratios do not match with those of Schmitt and Pleasonton does not mean that they are bad. Instead, it means that the fission fragment spectrum was distorted by their passage through the source material. The data is still usable because the fission

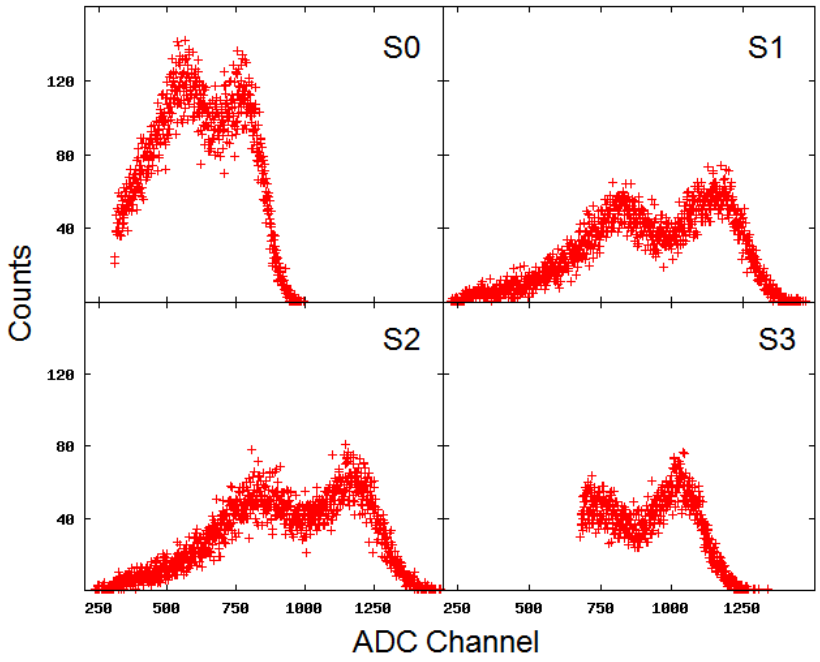

FIGURE 3.1: The calibration spectrum from each of the four surface barrier detectors in the array. The spectra are fission fragment spectra from a ^{252}Cf source.

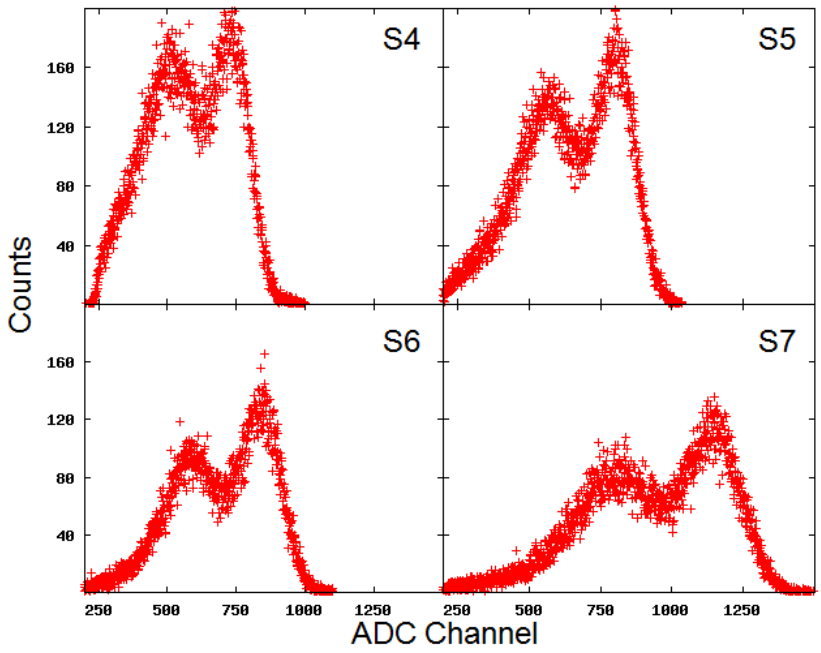

FIGURE 3.2: The calibration spectrum from each of the four backward strip detectors. The spectra are fission fragment spectra from a ^{252}Cf source.

fragment peaks are distinct. With the exception of the region near the edges (which is discussed later) it is clear that an event in this region is a fission fragment rather than some random event.

It appears that the threshold on S3 was set too high, cutting out a good portion of the lower energy fission fragments, therefore it is used only as a veto for a double array event or to identify bad coincident events.

While it is possible to calibrate the fission detectors in order to determine the energy and mass of the fission fragment on an event by event basis, [43] it is not necessary. In the analysis of the neutrons, the only place where knowledge of the fission fragment energy (or velocity) is useful is in the transformation from the lab frame to the center of mass reference frame. Since the source of the neutron is an unknown in this experiment then the velocity of the source is unknown. Therefore a thorough calibration of the fission detectors is not necessary (i.e. one where the energy as a function of ADC channel is determined). An average velocity is assumed for each desired source. See Section 4.2 for more details.

The raw experimental ADC spectra are shown in Figures 3.3 and 3.4. The resolution is satisfactory enough to easily separate a fission fragment signal from a lower energy signal produced by spallation or other random noise. The low end cut-off was set at the the approximate location of the valley between the spallation products and the heavy peak. The high end cut-off was determined by examination of the data with the value of the vertical axis on a log scale. The Gaussian peaks appear as inverted parabolas in this view. The point where the behavior of the data deviated from the parabola was set as the cut-off. These values are listed in Table 3.1. The low and high cut-offs are greater than three standard deviations away from the centroids. Therefore the amount of real data above and below the cut-offs that is ignored is on the order of 0.1%.

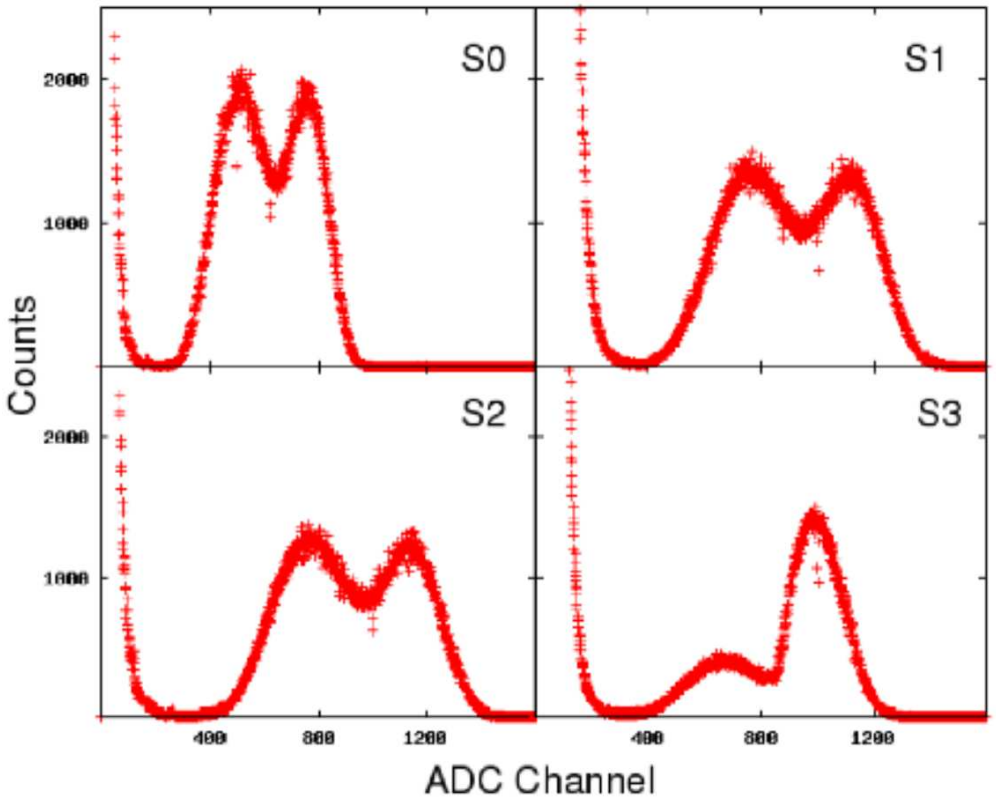

FIGURE 3.3: The raw experimental ^{238}U(d,f) fission fragment spectrum from each of the four surface barrier detectors in the array.

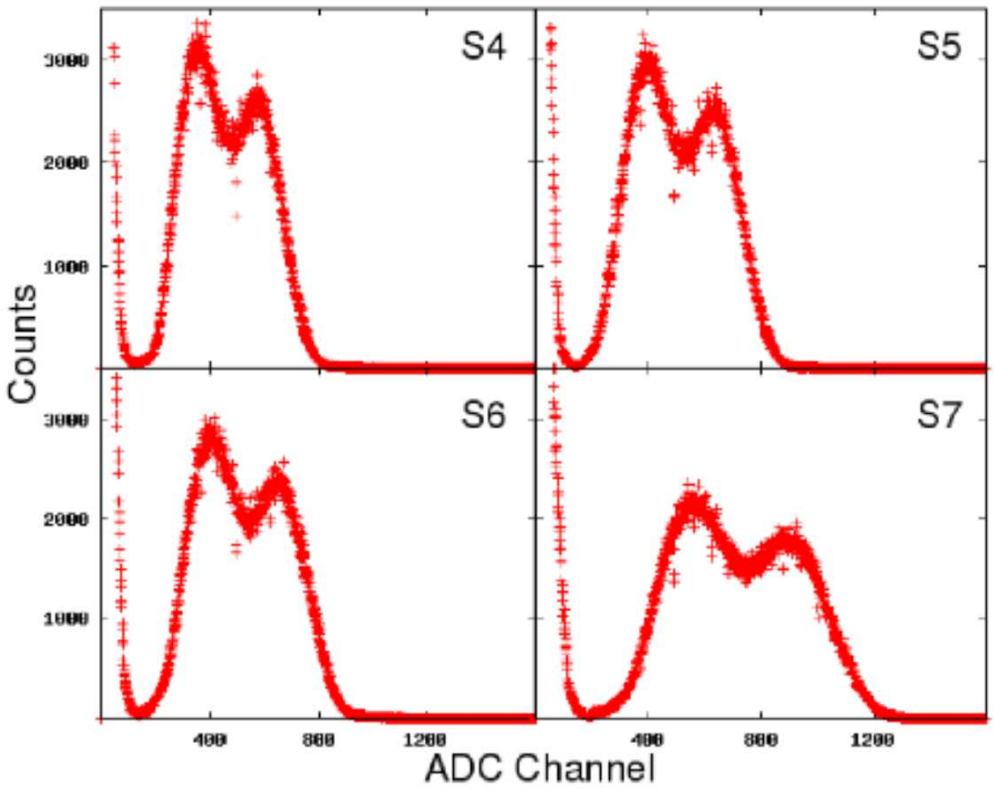

FIGURE 3.4: The raw experimental ^{238}U(d,f) fission fragment spectrum from each of the four backward strip detectors.

Detector	Low Channel Cut−off	High Channel Cut−off
S0	225	1025
S1	375	1525
S2	325	1500
S3	325	1325
S4	125	850
S5	150	925
S6	150	950
S7	200	1375

TABLE 3.1: Cut−off channels chosen for each of the fission detectors. The raw experimental data was used.

All fission detectors were treated as single detectors without considering the effects of good coincident events between the array and the strip detector. This was done for the following reasons.

First, the singles spectra and the coincident spectra have the same shape which demonstrates that there is no bias introduced by ignoring the coincidences. These spectra are shown in Appendix B.1.

Second, this experiment could be conducted with only *one* fission detector at an arbitrary location. All of the data analysis with only one detector would be carried out in the same manner and the addition of detectors only strengthens the experiment. Third, the knowledge that a particular fission fragment is in coincidence with another fission fragment adds no additional information as to which fragment emitted the neutron.

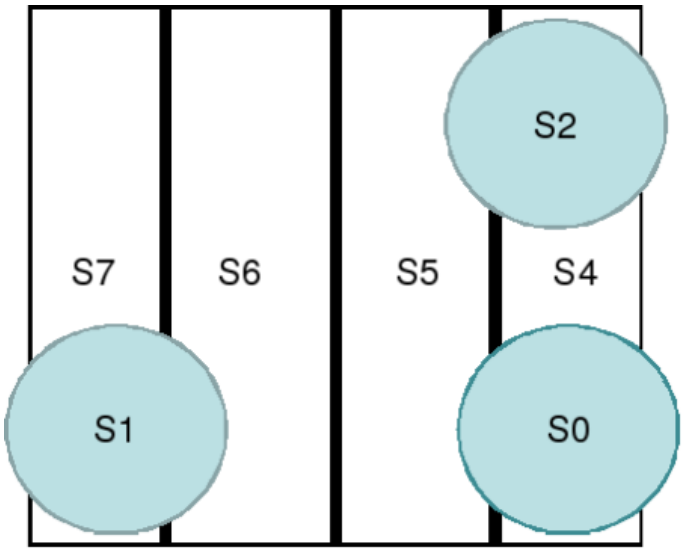

FIGURE 3.5: The area of the strip detector (white, in background) that is 180 degrees across (relative to the target) from a detector in the array (blue, foreground).

Lastly, there is the fact that the detectors to not cover the entire coincident area. In otherwords, if a fission fragment is observed in the strip detector is not certain that the other fragment will appear in one of the array detectors. Figure

3.5 shows the regions of the strip detector that lie 180° from a detector in the array. As one can see there are events that might register in the array but miss the strip detector and vice versa. If one takes the dispersion due to the fragments traveling through the target and the emission of neutrons the borders of the area of coincidence smears out. Therefore, by requiring a coincident between an array detector and its corresponding strip detector, a large portion of good singles data would be eliminated.

One last set of events that was removed from the data were those that were random coincidences. While it is never certain that two events are or are not in coincidence, there are certain types where it is extremely unlikely that the two fission fragments are in coincidence. Such events are those where there are two or more fission fragments in the array or in the DSSD. The smaller the angle of coincidence is between two fission fragments, the more likely that they are a random coincidence rather that a real fission fragment pair.

The number of coincident events observed (i.e. a good fission fragment in both detectors) between S0 and S1 is 11,830, S0 and S2 is 10,523, and S1 and S2 is 11,241. Since these detectors are all forward these are all assumed to be random coincidences. The number of coincidences between the array detectors and the strip detectors is shown in Table 3.2. Notice that the coincidence rates of S1-S4, S1-S5, S0-S6, S2-S6, S0-S7, and S2-S7 are about 11,000 or less. This suggests that they are random coincidences and that when those detector pairs both observed a good fission fragment that they come from separate events rather than the same event.

Furthermore, the asymmetries in the rates all point to a small rotation of one of the detectors. Relative to Figure 3.5 this rotation would be the equivalent of rotating the strip detector clockwise, which would be a counterclockwise direction in the lab frame. This is based on the asymmetry of the data in Table 3.2 and is

	S0	S1	S2
S4	396136, 170°	2999, 159°	124086, 170°
S5	85411, 166°	7109, 162°	363365, 166°
S6	3011, 162°	416604, 166°	6077, 162°
S7	6697, 159°	111346, 170°	11652, 159°

TABLE 3.2: Number of coincident events between fission fragment detector pairs and angle in degrees between the center of each detector.

not recorded in any of the lab books.

The code found in Appendix C.2 was used to separate the events with a good fission from the raw event file. To summarize, events that had any of the following characteristics were eliminated:

- A coincidence between two or more detectors in the array or two or more detectors in the strip.
- Any fission fragment with an energy either too low or too high as defined in Table 3.1.
- All events in S3 due to the cutting of some of the low energy fissions.
- A coincidence between an array detector and a strip detector that do not overlap in Figure 3.5. These pairs are S0-S6, S0-S7, S1-S4, S1-S5, S2-S6, S2-S7.

3.2 Calculation of the Neutron Detector Efficiency

The detector calibrations were made by comparing a measured ^{252}Cf neutron spectra with the data of Bowman *et al.* [44]. The source was a ^{252}Cf single−sided source with an activity of 15μCi. The 15μCi was calculated using the activity of the source at a given data by the manufacturer. This was validated by measurement of the alpha spectrum just after the experiment.

The neutron energy was determined by time-of-flight (TOF) measurements. The fast signal from a fission detector served as a start signal while a fast signal from a neutron detector served as a stop. The γ-peak was used to obtain an absolute TOF. Pulse shape discrimination is also used quite often to distinguish between the neutron and γ-peaks. In this experiment the two peaks were separated enough that this was not needed. Determining the efficiency of the neutron detectors consists of two parts. The first is the calibration of the TDC, and the second is the comparison of the measured data to a known standard.

3.2.1 TDC Calibration

The TDC was calibrated during the experiment by comparing two consecutive data collection runs, one of which had an 80 nanosecond cable added to the fast signal from each of the neutron detectors. All other variables were kept the same. By comparing the location of the centroids of the $\gamma-$peaks the number of nanoseconds per TDC channel was obtained by

$$\frac{\Delta t}{\Delta \text{Channel}} = \frac{80(\text{ns})}{(\gamma_1 - \gamma_2)(\text{channels})} \tag{3.1}$$

where γ_1 and γ_2 are the centroids of the two γ-peaks.

The raw TDC spectrum and corresponding fit is shown in Figures 3.6 and 3.7 for one of the neutron detectors. The background, shown in red in Figure 3.6, was

determined by summing over a region that was clearly outside of the real data peaks and dividing by the total number of channels in the region. The background is 0.36 counts per channel for N0, 0.35 for N1, 0.27 for N2, and 0.33 for N3. This number was subtracted from each channel in the raw TDC spectrum and the remaining spectrum was fit with a double Gaussian function using Gnuplot 4.2 [45]. The quality of fit is evident in Figure 3.7.

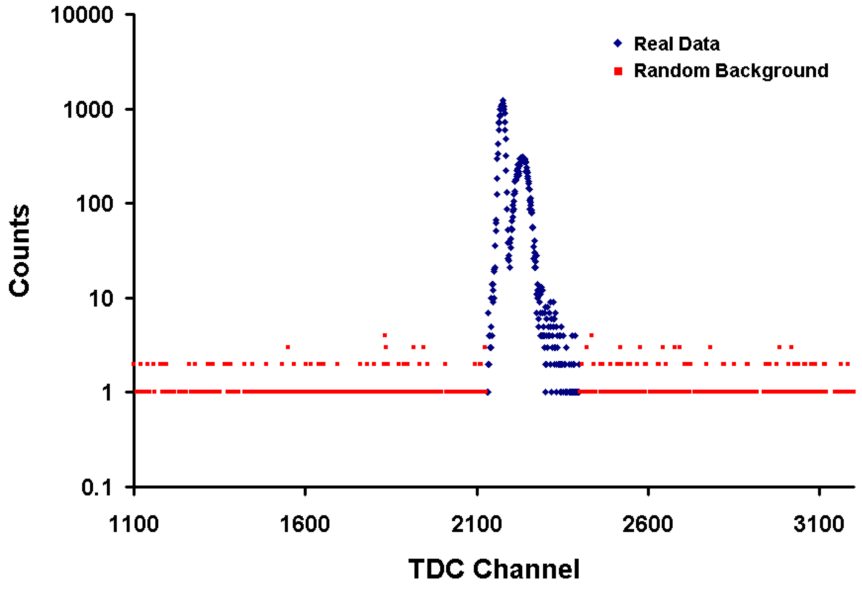

FIGURE 3.6: The raw TDC data for N0. The events considered as random background are shown in red while the gamma and neutron events are shown in blue.

In theory, the Gaussian is not the proper function to describe the shape of the neutron peak. The energy of the neutrons as a function of the time of flight is

$$E = \frac{1}{2}mv^2 = \frac{1}{2}m\left(\frac{d}{t}\right)^2 \tag{3.2}$$

where m is the mass of a neutron, d is the distance from target to detector, and t is the time of flight of the neutrons. If one assumes the energy distribution of neutrons is Maxwellian then the substituting the energy in Equation 1.8 with Equation 3.2,

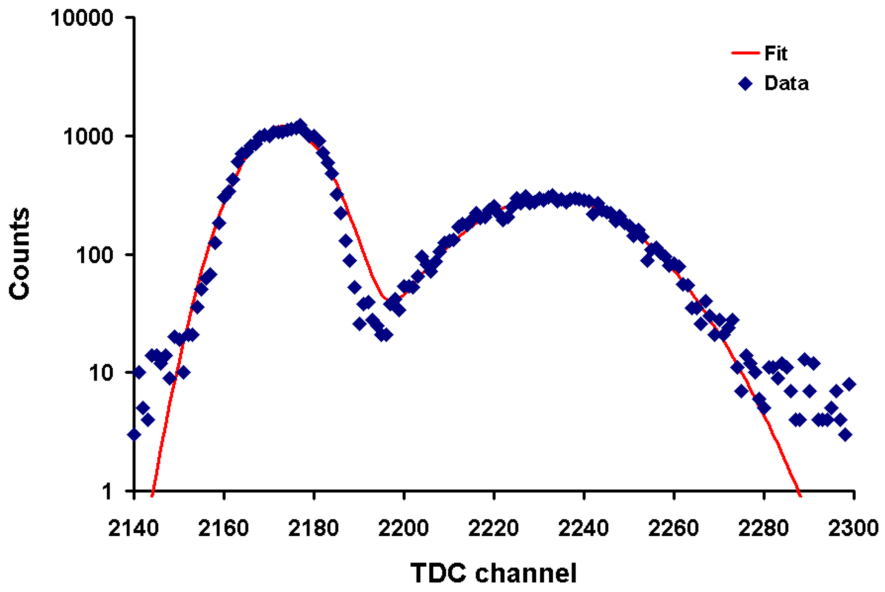

FIGURE 3.7: A close-up of Figure 3.6 including the double Gaussian fit. The Gaussian fit is applicable to the data.

the TDC spectrum would look like

$$P(t) \propto \frac{1}{t^2} \exp[-t^{-2}] \tag{3.3}$$

If the neutron energy distribution follows Equation 1.11 then the TDC spectrum would fall off with 1/t instead. These functions are very similar in shape to a Maxwellian distribution. See Section 3.4 for more on the abnormal shape of the data.

Each fission-neutron detector pair has a slightly different TDC calibration. Since fission detectors were swapped during the experiment between the data collection run and neutron detector calibration run the average over all fission detectors used during the TDC calibration was used in the analysis of the data. The data from the neutron detector calibration run are shown below in Table 3.3. The data from S3, S4, S5, and S6 are not included because they are flawed (see Sections 3.1 and 3.5). The uncertainties of these numbers are negligible due to the large number

of counts in the γ-peaks.

	N0	N1	N2	N3
S0	0.1912	0.1959	0.1955	0.1954
S1	0.1917	0.1959	0.1979	0.1951
S2	0.1915	0.1970	0.1956	0.1961
S7	0.1892	0.1957	0.1946	0.1890
average	0.1909	0.1962	0.1959	0.1932

TABLE 3.3: ns/TDC Channel for each neutron detector and fission fragment detector combination. The average over fission detectors was used in the analysis.

3.2.2 Comparison with ^{252}Cf

The efficiency of the neutron detectors was done by a comparison of the data to that of the neutron spectra measured by Bowman *et al.* [44] which has been used in previous experiments to calibrate neutron detectors [8, 46, 47]. The method of comparing a measured spectrum to some standard has the advantage that it takes all aspects of the measurement (geometrical efficiency, detector size, signal processing electronics, etc.) into account simultaneously. No simulation is needed.

Bowman *et al.* reported their data as a neutron density, $\rho(V,\theta)$, determined by the function

$$N(V,\theta) = R\omega\varepsilon\rho(V,\theta)V^2\Delta V \tag{3.4}$$

where $N(V,\theta)$ is the number of counts observed for in given velocity and angular bin, R is the number of fissions observed, ε is the efficiency, ω is the solid angle coverage in steradians, V is the velocity, and ΔV is the velocity width of the bin.

The Bowman data have the advantage that they are reported in the lab frame. This eliminates the need for a fission detector that covers a 2π solid angle. All four

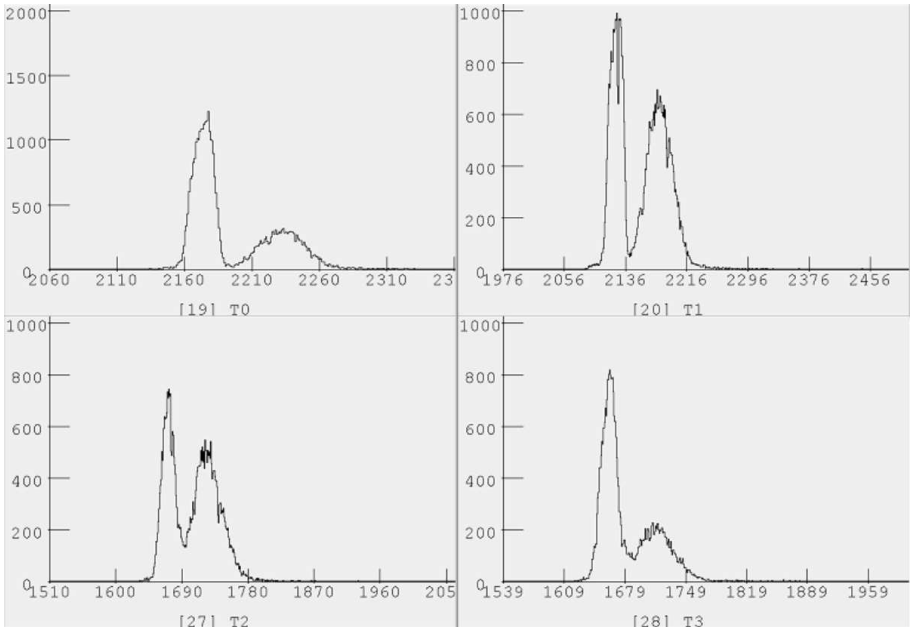

FIGURE 3.8: The raw calibration spectra for each neutron detector. The valley between the gamma peak (left) and the neutron peak (right) correspond to neutron energies between 18 and 20 MeV. Thus the separation between the neutron and gamma peaks is sufficient.

neutron detectors were calibrated simultaneously using one fission fragment detector (S0) and a 15μCi ^{252}Cf source. The fission fragment detector was placed in plane at 90° to the beamline at a distance of 5.5 cm. The neutron detectors were set up at angles of 11° and 45° to the fission fragment detector to match angles the angles of Bowman *et al.* This setup ensured that the aluminum dome was perpendicular to all four neutron detectors and simplified the analysis by reducing the number of unique angles to two. The raw calibration spectra are shown in Figure 3.8.

3.2.2.1 Geometrical Correction

A geometrical correction was applied to the Bowman data to remove the effect of differences in detector size. During the calibration, the radius of fission fragment detector spanned 10° and the radius at the location of the mean interaction depth the neutron detectors spanned 15.1°. In the experiment performed by Bowman *et al.*

the radius of the fission fragment detectors spanned 2.9° and the neutron detector radius spanned 3.2°. Since the angular acceptance of our detectors was much larger than that of Bowman *et al.* it was assumed that their detectors were point detectors.

In order to account for the finite width of our detectors an angular distribution of Bowman's neutron density for each energy was determined by fitting the data to the function

$$F(\theta) = A\cos(B\theta) + C \tag{3.5}$$

It represents the density that Bowman *et al.* would have measured at the angle θ. This function was chosen solely because it matched the data.

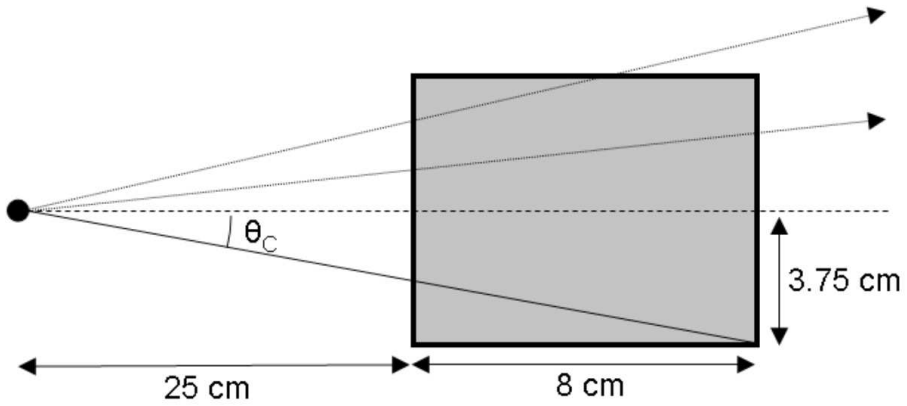

FIGURE 3.9: The geometry of a neutron detector. The active area is shown in grey and the source is represented by the dot.

The other component needed to compare our data to the data of Bowman *et al.* is the correction to the angular distribution due to the finite depth of our detectors. A neutron that impinges on the detector slightly off the detector axis will have a greater chance of detection because it passes through more scintillator material. This is shown in Figure 3.9. A probability of interaction due to the detector depth at a given angle was determined using a Monte Carlo method. The code and a description is found in Appendix C.4. The output of this code is the function $W(\theta)$ which represents the probability for a neutron to interact at an angle

θ. The function is normalized such the sum over all angles of $W(\theta)$ is 1.

The neutron density Bowman would have obtained if using detectors in our placement and dimensions is then

$$\rho = \sum_{i=1}^{180} F(\theta_i) W(\theta_i) \tag{3.6}$$

It was summed in one−degree increments. This new neutron density was used in comparison with our data.

The uncertainties from the Bowman data were used in the fitting of $F(\theta)$ and the uncertainties in the fitted parameters including their correlations were used in determining the uncertainty in $F(\theta)$. The uncertainty of $W(\theta)$ was negligible compared to that of $F(\theta)$ and was therefore not included. The uncertainty in ρ was then determined by

$$\sigma_\rho = \sum_{i=1}^{180} \sigma_{F(\theta_i)} W(\theta_i) \tag{3.7}$$

where $\sigma_{F(\theta)}$ is the uncertainty in $F(\theta)$ at a given angle.

3.2.2.2 Comparison with the Standard

The front faces of the neutron detectors were 25 cm from the target during the calibration run with an estimated uncertainty of 1 cm. This is not optimal for T0 which was placed at 45 cm during the experiment; a correction was made for this difference and is discussed later. The average γ interaction is then 29 cm from the target [40]. The centroid of the gamma peak therefore corresponds to a real time of

$$t = \frac{d}{c} = \frac{29 \text{ cm}}{30 \text{ cm/ns}} = 0.967 \text{ ns} \tag{3.8}$$

Using this and the TDC calibration the time of flight of the neutron in nanoseconds is

$$TOF = m(b - c) + 0.967 \tag{3.9}$$

where TOF is the time of flight, m is the TDC calibration in ns/channel, b is the TDC bin in which the event was observed, and c is the γ-peak centroid for the unique fission detector-neutron detector combination.

Once the time of flight has been found, the velocity and energy can easily be derived from non-relativistic mechanics (see Equation 3.2). It follows that the uncertainty in the energy is due to the uncertainties in the distance traveled and the time of flight, both of which manifest themselves in the width of the γ-peak. Table 3.4 lists the standard deviations in the γ-peaks. In order to account for the uncertainty in the energy the uncertainty of the distance was set to 0 and the width of the γ-peak was used as the uncertainty in the time of flight.

	N0	N1	N2	N3
S0	1.83	1.91	1.96	2.13
S1	1.53	1.59	1.85	1.69
S2	1.87	1.78	1.81	1.94
S7	2.12	2.04	2.33	1.92

TABLE 3.4: The widths (one standard deviation) of the γ-peaks in nanoseconds for each neutron detector - fragment detector combination.

As mentioned before, Bowman *et al.* calculate the number of neutrons per fission per steradian per $(\mathrm{cm/ns})^3$ using

$$\rho(V,\theta) = \frac{N(V,\theta)}{R\omega\varepsilon V^2 \Delta V} \tag{3.10}$$

The number of fissions observed during the calibration run (R) determined by the area of the fission spectra was 8,458,120. (The low and high cut$-$offs were determined in the same manner as in Chapter 3.1.) The uncertainty in the number of fissions was negligible.

With the area of the detector set at $\pi 3.75^2$, and the distance from target to detector set at 28.3 cm, the solid angle in steradians is 0.0552. The uncertainty in the solid angle was set at 0.0037. This was done by assuming an uncertainty in the detector distance of 1 cm and then calculating the solid angle at ± 1 cm from the average of 28.3 cm.

The number of events per bin was determined by first converting the raw TDC channel into a velocity and then summing the number of counts in each TDC bin to match the Bowman bins. In the case where a TDC bin spanned two different velocity bins, the fraction of the neutrons placed into the first velocity bin is equal to the fraction of the TDC bin that overlaps with the first velocity bin. The rest were placed into the second velocity bin. The uncertainty in the number of counts in the bin is the square root of the number of counts measured.

The efficiency of our detectors is then

$$\varepsilon(V) = \frac{\rho_E(V,\theta)}{\rho_B(V,\theta)} \tag{3.11}$$

where ρ_B is the density measured by Bowman *et al.* and ρ_E is our experimental density (excluding the efficiency term). The resulting efficiency data is shown in Figure 3.10.

The fit (red line in Figure 3.10) is of the form

$$\varepsilon(E) = \frac{c + dE + eE^2 + fE^3}{1 + \exp[(a - E)/b]} \tag{3.12}$$

where a, b, c, d, e, and f are fitted parameters. The numerator governs the behavior of the function at energies larger than ~ 2 MeV. The denominator, modeled after the Woods-Saxon potential in nuclear physics, governs the low energy drop-off in the efficiency. The values of the fitted parameters for each detector are listed in Table 3.5. More will be said on this choice of function to model the data in Section 3.4.

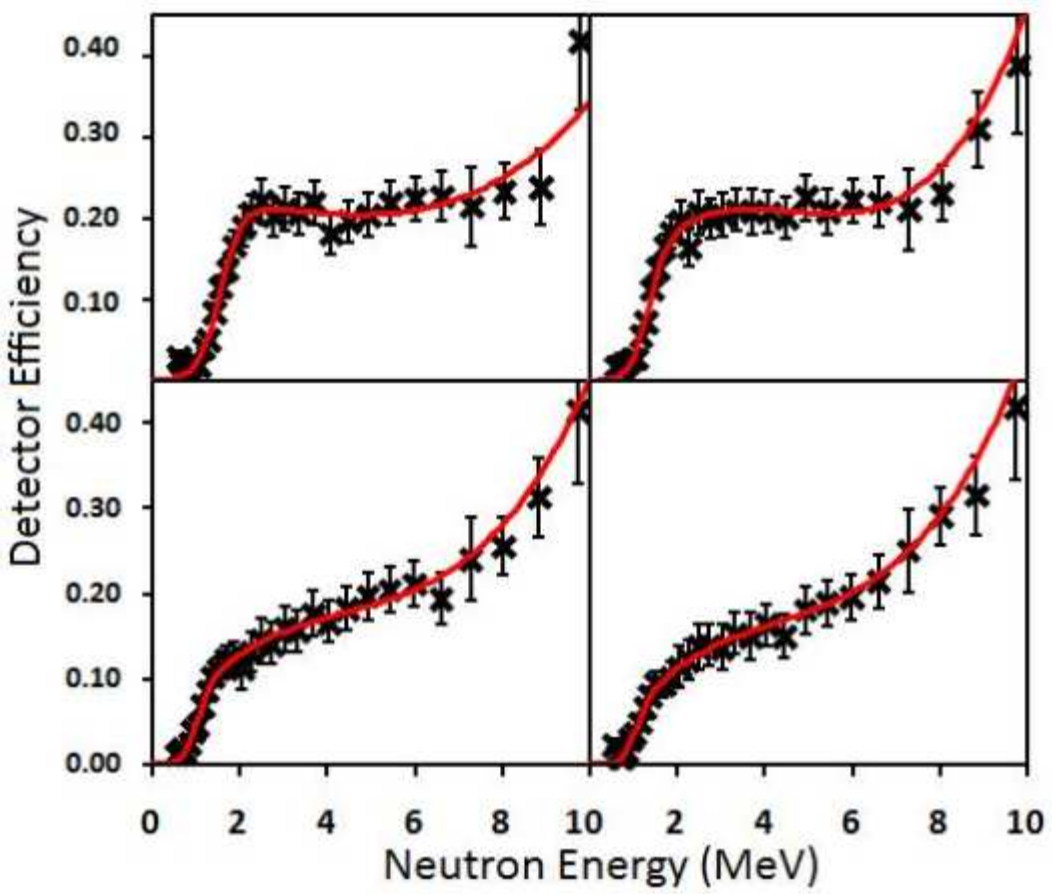

FIGURE 3.10: Detector efficiencies for the four neutron detectors. Raw data are shown in black and the fit (Equation refeq:efficiency) is shown in red.

	a	b	c	d	e	f
N0	1.5496	0.2567	0.2356	-0.0052	-0.0020	0.00036
N1	1.2750	0.2154	0.0650	0.1024	-0.0233	0.0017
N2	0.9814	0.1624	0.0223	0.0778	-0.0145	0.0011
N3	1.0073	0.1632	-0.0030	0.0839	-0.0155	0.0012

TABLE 3.5: The fitted parameters from Equation 3.12 for the four neutron detectors.

Not all of the efficiency data were used in determining the fit. Going to lower energies (<1 MeV), the efficiency levels off and in some cases begins to increase again. In the TDC spectrum this is in the region far away from the gamma peak where the number of real counts is roughly the same as the number of background counts. The four lowest energy points ($E = 0.576$, 0.635, 0.7, and 0.771 MeV) were excluded.

3.3 Corrections due to the support structure

The corrections for the neutron energy lost in the support structure in the chamber are negligible. This was demonstrated with MCNP simulations [48]. The geometry of the simulations consisted of a 1/2 inch thick sphere of aluminum at a distance of 10.5 cm from the target to represent the block holding the four forward silicons and a sphere of 1/8 inch thick aluminum at a distance of 20.3 cm to represent the domes. The input file is shown in Appendix C.5. Using the average energy loss in each element and then calculating the resulting change in the time-of-flight it was found that a 1 MeV neutron loses 0.0039 MeV and a 5 MeV neutron loses 0.0028 MeV.

Another possible correction is that of the more energetic neutrons interact at a larger depth on average in the detector than lower energy neutrons. This results in a different distance of flight. The uncertainty in the velocity of the neutron can be found by the equation

$$\left(\frac{\Delta V}{V}\right)^2 = \left(\frac{\Delta d}{d}\right)^2 + \left(\frac{\Delta t}{t}\right)^2 \tag{3.13}$$

Making reasonable estimates of Δd and Δt shows that the time term is over an order of magnitude larger than the distance term. Therefore no corrections were made for the uncertainty in the distance.

3.4 Neutron Detector Efficiency Curve Discussion

The measured efficiency curves increase at higher energies in this experiment. This behavior does not match previous measurements for a BC-501 scintillator (which is identical to NE-213), see [39, 40, 49, 50, 51, 52, 53] and Figure 3.11. Shown in Figure 3.11 is the efficiency data from detector N1 (red line and red crosses) along with other previous experimental and simulated data. The differences at lower energy can be explained by the different thresholds used.

From a physical standpoint the idea that the neutron efficiency increases with energy is not correct. First, an efficiency over 1, which occurs if one extends Equation 3.12 out to higher energies, is simply not possible because it implies particle creation in the detector. The efficiency should decrease with increasing energy. The probability for a neutron to interact with the detector is

$$\varepsilon = 1 - \exp^{-nd\sigma(E)} \tag{3.14}$$

where ε is the efficiency, n is the number density of atoms in the detector, d is the length of the detector, and $\sigma(E)$ is the energy dependent cross section. Since

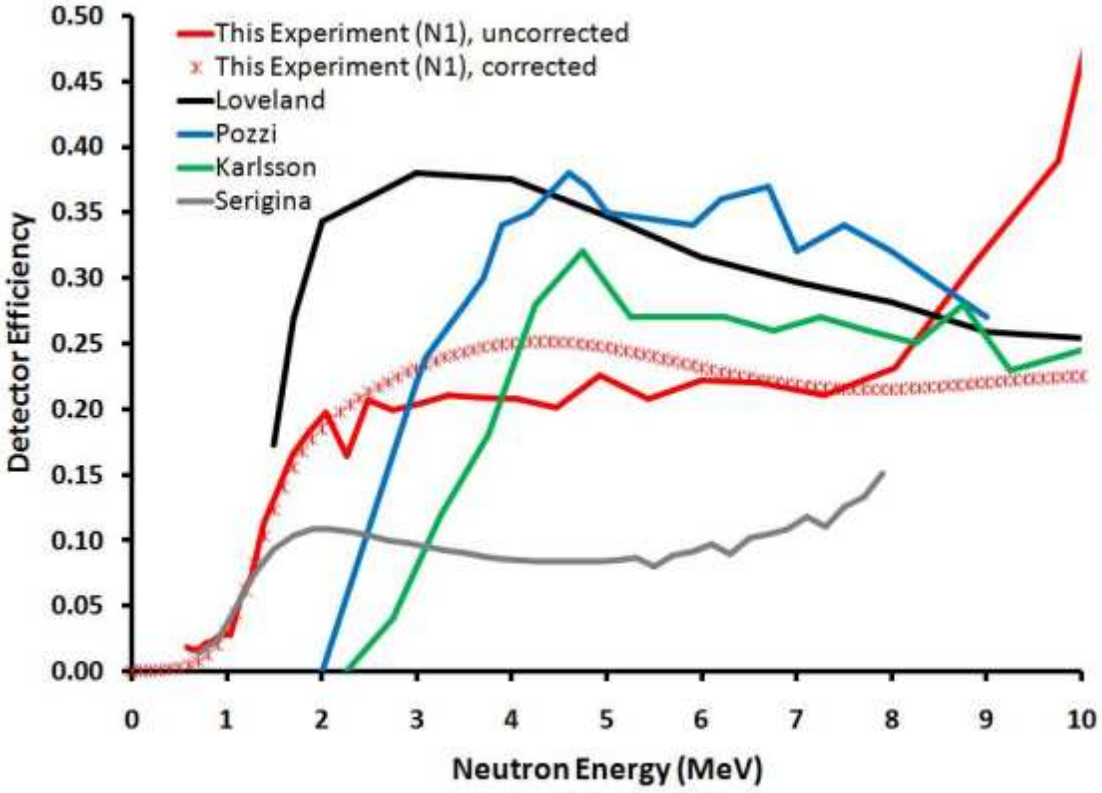

FIGURE 3.11: Comparison of the neutron detector efficiencies from this experiment and previous experiments. Data is from Loveland [39], Pozzi *et al.* [40], Karlsson [53], and Serigina [52].

the neutron cross section decreases with increasing energy, as the neutron energy increases the efficiency decreases.

Before diving into the details specific to this experiment let us investigate the implications of comparing the measured data to a known standard. The functional form of the Bowman data follows a Watt distribution with an exponential decay. At high energies the term $exp(-E/T_B)$, where T_B is the slope parameter of the Bowman data, governs the decay. Similarly the experimental data also follow a distribution with an exponential decay which can be represented as $exp(-E/T_{exp})$. Therefore according to Equation 3.11 at higher energies the efficiency curve will

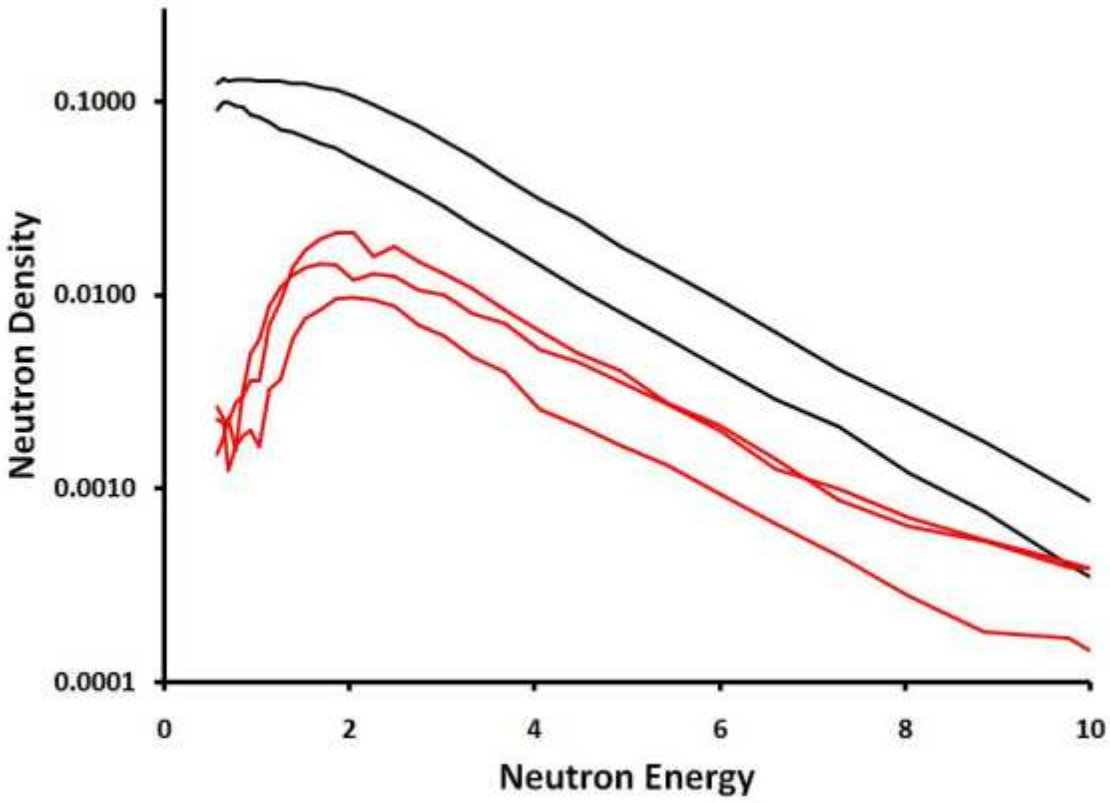

FIGURE 3.12: Neutron densities of the Bowman data (black) and this experiment (red).

have the form

$$exp\left(-E\left(\frac{1}{T_{exp}}-\frac{1}{T_B}\right)\right) \tag{3.15}$$

Normally, T_{exp} is smaller than T_B resulting in an exponentially *decreasing* function. In this experiment however, T_{exp}, is greater than T_B, so the efficiency function increases exponentially. As seen in Figure 3.12 our experimental data falls off exponentially as expected, just not as rapidly as the Bowman data.

An exponential function was initially used in an attempt to model the neutron detector efficiencies. It was found that a function that fit all four detectors required at least 4 parameters. A polynomial was used for its simplicity. The connection between the two functions is that the exponential function can be expanded into

a polynomial. The use of a polynomial also alleviates any confusion of the physics behind the equation. Since the desire was to simply find a function that extrapolates between the data points, no physics was sought. Therefore a physically relevant equation is not needed.

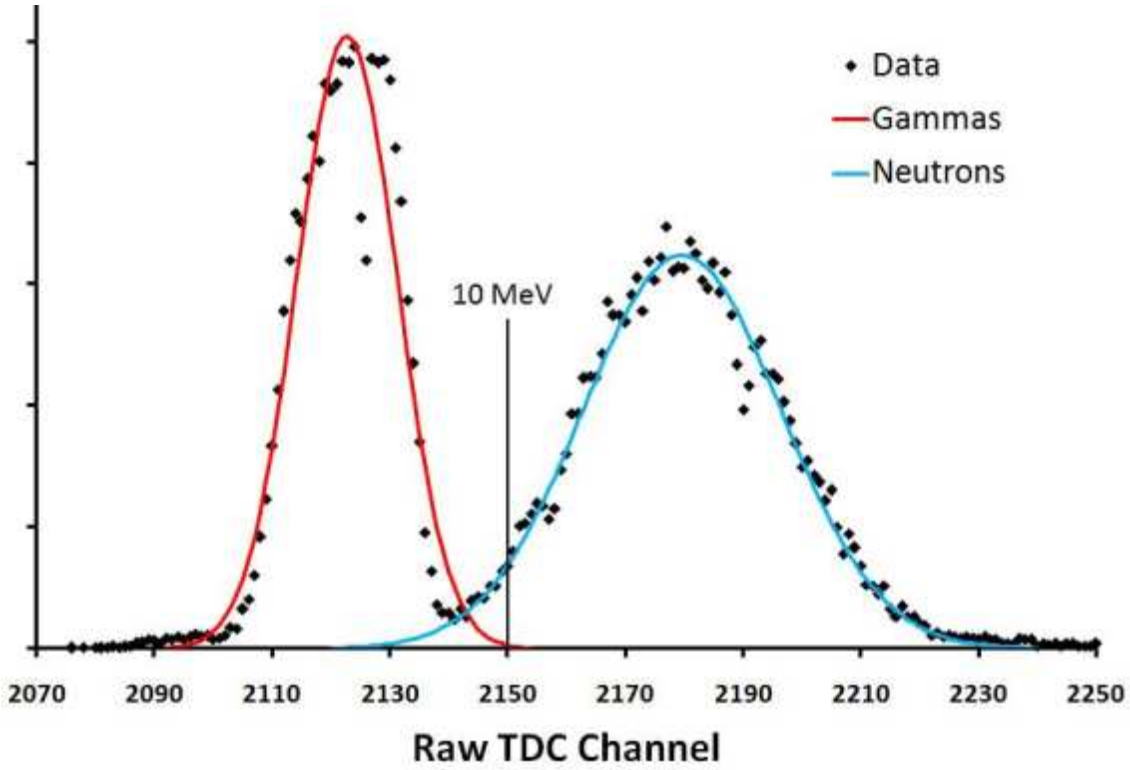

FIGURE 3.13: Raw TDC spectrum from N1 highlighting the ratio of the neutron peak to the $\gamma-$peak at 10 MeV.

The increase at higher efficiencies is not due to γ's that are counted as neutrons. Figure 3.13 shows the same data as Figures 3.6 and 3.7. Also shown is a vertical line corresponding to the location of a 10 MeV neutron. For this particular data set, the N1 data, the ratio of the neutron peak to $\gamma-$peak at this location is 37.9. The ratio at 10 MeV for N0 is 41.6 and for N2 is 63.6. (N3 is not included because the data were not satisfactory. See Section 5.1.1 for more details.) To the right of the 10 MeV line the neutron peak rapidly increases while the $\gamma-$peak rapidly

decreases. Therefore the contamination from γ's is less than 3%. A correction was made for this small amount by multiplying the total number of counts in each TDC bin by the factor $N_n/(N_n + N_\gamma)$ where N_n is the fitted height of the neutron peak for the given bin and N_γ is the fitted height of the $\gamma-$peak.

The increase in efficiency at higher energies is due to large relative error in the time of flight due to the proximity of our detectors to the source and the electronics. Since the energy is inversely proportional to the square of the time of flight (Equation 3.2), as the time-of-flight decreases the error in the measurement time-of-flight causes incorrect energy binning with a bias towards higher energy neutrons.

For example, consider a beam of 4 MeV neutrons impinging on a detector 100 cm from the source. The flight time is 36.1 ns. If one assumes what is generally considered to be a "good" uncertainty in the time of flight of 1.27 ns (one standard deviation is 1.27 ns, FWHM = 3 ns) then the distribution of these 4 MeV neutrons would range from 3.7 to 4.3 MeV. If the detector is 28 cm from the source, the flight time would be only 10.1 ns and the energy distribution would be 3.1 to 5.7 MeV. Note the asymmetry of the energy distribution skews the data to higher energies. This is what occurred in our measurements and the reason behind the lack of decrease in efficiency at higher energy.

Shown in Figures 3.14 and 3.15 are the results of simulations done to model the convolution. A Maxwellian curve of magnitude 1,000,000 and T=1.4 was divided into 0.1 MeV bins. The TOF was calculated for each energy, and then each count in the bin was convoluted and rebinned. The convolution was done assuming a 1.7 ns uncertainty (σ=1.7, FWHM = 4 ns) in the TOF. To ensure a Gaussian distribution a possible change in the TOF was generated using

$$\Delta t = 8\sigma(R - 0.5) \tag{3.16}$$

where R is a random number between 0.0 and 1.0. This generated a uniform distri-

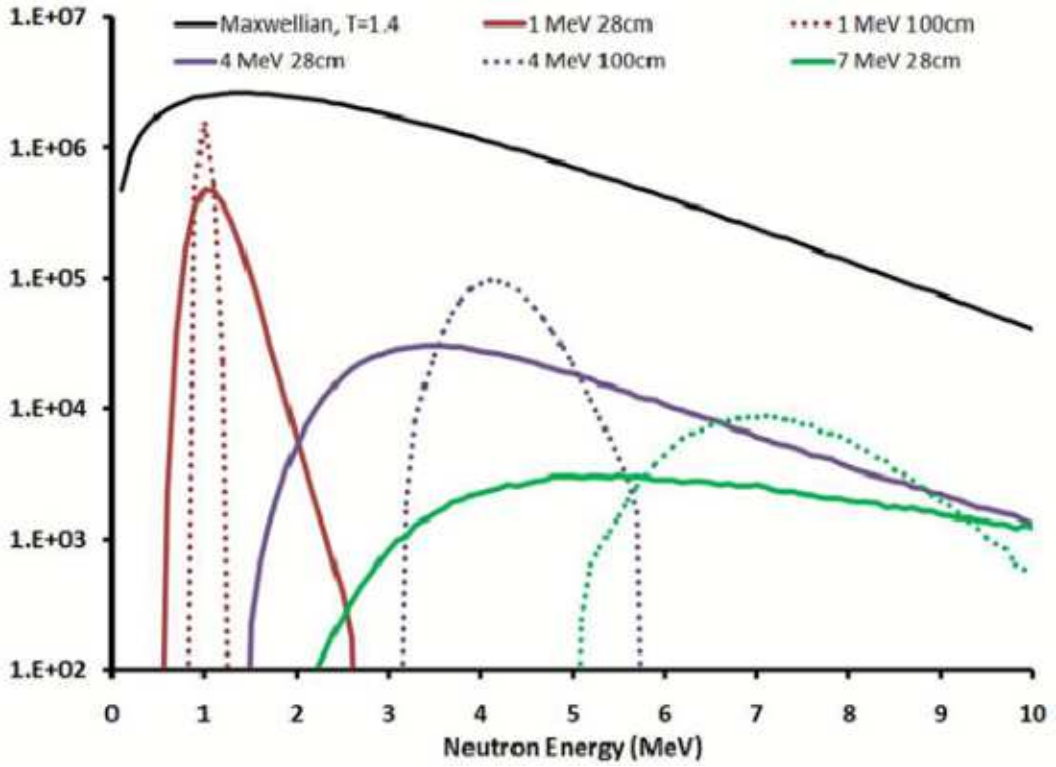

FIGURE 3.14: Specific cases of the effective spreading of the neutron energy spectrum due to TOF uncertainty. The red curves are generated using 1.1 MeV neutrons, the purple curves using 4.2 MeV neutrons, and the green curves used 7.0 MeV neutrons. A detector distance of 28 cm is shown using solid lines and a distance of 100 cm is shown using dotted lines.

bution within 4 standard deviations from the norm. If the Δt passed the criteria

$$R < \exp\left(\frac{\Delta t^2}{2\sigma^2}\right) \tag{3.17}$$

(where R is a different random number than in the previous equation) then Δt was added to the TOF, a new energy was calculated and the event was rebinned. If 3.17 did not hold true a new Δt was generated and the process was repeated until it passed.

Figure 3.14 shows the spreading of the data. Shown are three cases of the spread of 1.1, 4.2, and 7.0 MeV neutrons at detector distances of 28 cm and 100 cm as well as the generating Maxwellian spectrum of T=1.4. Notice that at 10 MeV

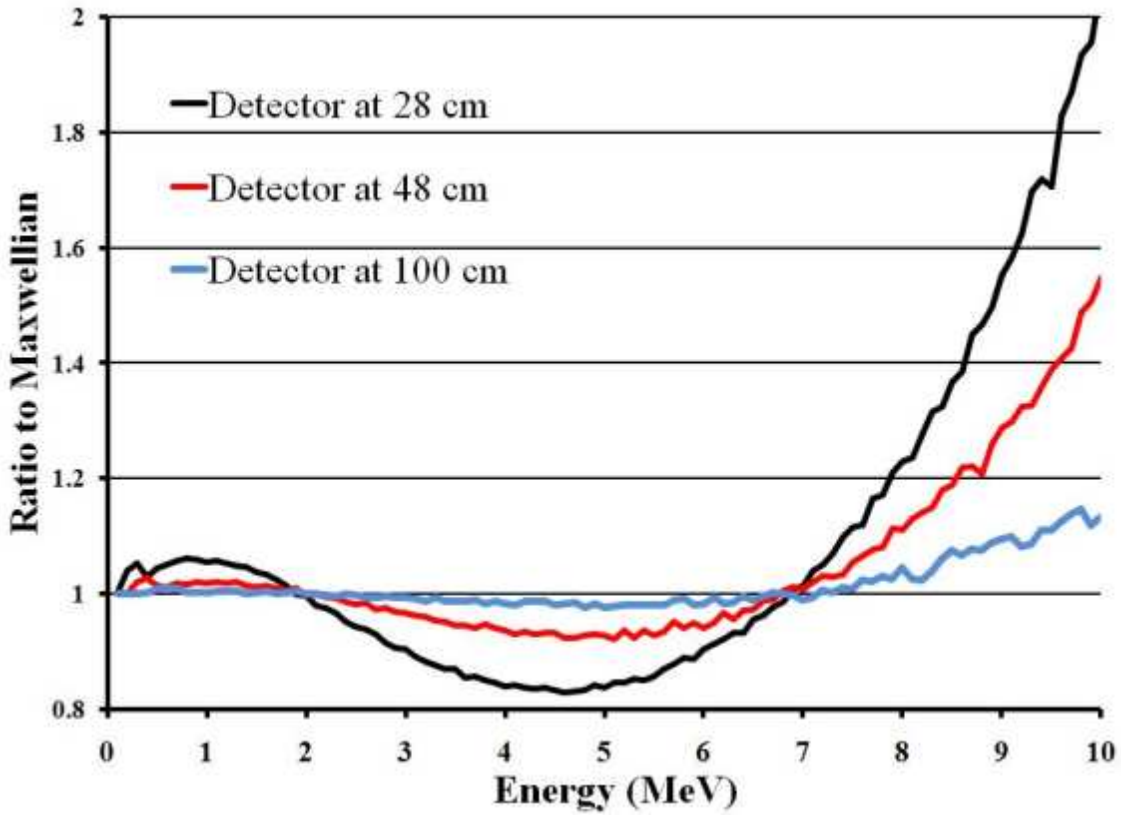

FIGURE 3.15: Ratio of the convoluted energy spectrum to the original spectrum. The black curve is the ratio for a detector distance of 28 cm, the red curve is for a detector at 48 cm, and the blue line is for a detector at 100 cm.

the contribution to the spectrum is equal parts 4.2 and 7.0 MeV neutrons. Figure 3.15 shows the total convoluted spectra if all energies are included. The change is very small for detectors placed 100 cm from the source. As the detector is moved closer to the source, the efficiency becomes more distorted with a bias towards higher energies.

The equation for the efficiency, Equation 3.12,

$$\varepsilon(E) = \frac{c + dE + eE^2 + fE^3}{1 + \exp[(a - E)/b]} \tag{3.18}$$

should not be taken to be a physically meaningful equation. This equation simply provides a smooth curve that matches the data. Since there was never any intent

to derive any physics from the efficiency curve, nothing is lost.

This discussion revolved around the distance of detector to source as the cause of the poor time of flight resolution. It should be noted that an improvement in the electronics could also improve the resolution.

This shift towards higher energies does not make our efficiency at higher energies useless, or "wrong", since the detectors were at the same distance for the calibration and for the experiment. The exception is N0 which was placed at 48 cm from the target during the experiment and 28 cm from the source during the calibration. For this reason a correction was made to the data from the N0 detectors. The N0 data was divided by the 28 cm : 48 cm ratio before the weighted−efficiency correction. (The weighted−efficiency is discussed in Section 4.1.)

Returning to Figure 3.11 there are two different curves showing our data. The solid red curve is the measured efficiency that was used to create the fit that was used in the experiment. The uncertainty in the time of flight was corrected for by dividing the measured efficiency by the "28 cm"curve shown in Figure 3.15. This corrected data is shown with the red x's. The corrected data matches rather well with the previous measurements, so it appears that the increase at higher energies is due to a poor time-of-flight resolution. It is possible that the Serigina data suffer from the same ailment.

Every efficiency curve depicts a low energy cut−off. The energy at which this cut−off occurs is set by the experimenter operator through a combination of photomultiplier voltage and CFD threshold. As seen in [40, 50], by increasing the threshold the cut−off energy increases. In this experiment the threshold was set during the experiment at a level just above the noise. If the thresholds were decreased our data acquisition system could not handle the data flux. Also, the higher energy bias as described above pushes our low energy cut−off to a higher

energies.

Compared with previous neutron efficiency data, the measured cut-off is not unreasonable. The neutrons that have an energy near or on the steep slope can still be used if the flux at that energy times the efficiency at that energy is significantly greater than the background rate. The point corresponding to 1.0 MeV in the raw TDC plots was always outside of the background while the point 0.75 MeV was not. Therefore, only data over 1.0 MeV was used in this experiment.

In conclusion, while the efficiency curves look odd they are still correct. The low energy cut−off of 1 MeV is comparable to other experiments, and the high energy increase is due to the large uncertainty in the time-of-flight. The efficiencies, while unconventional in appearance, are still 100% usable for N1, N2, and N3 because the detectors are the same distance from the source in the calibration as in the experiment. Any biasing of the data during the experiment is also present in the efficiency calibration. Since correcting the data for this biasing effect brings the efficiency curves in line with previous measurements it appears that this is the only significant problem. Therefore the N0 data is satisfactory once the efficiency curve is corrected for the differences between a distance of 48 cm and 28 cm.

3.5 Neutron Event Rejection

After the bad fission events were eliminated, the events containing a bad neutron event were eliminated. The raw TDC spectra for each fission−neutron detector pair are shown in Appendix B.2 while the data from N1 is shown below in Figures 3.16 and 3.17. The neutron spectra show similar behavior for the same fission detector while showing different behavior for different neutron detectors.

The data from the array and S7 is satisfactory because the γ-peak is clearly

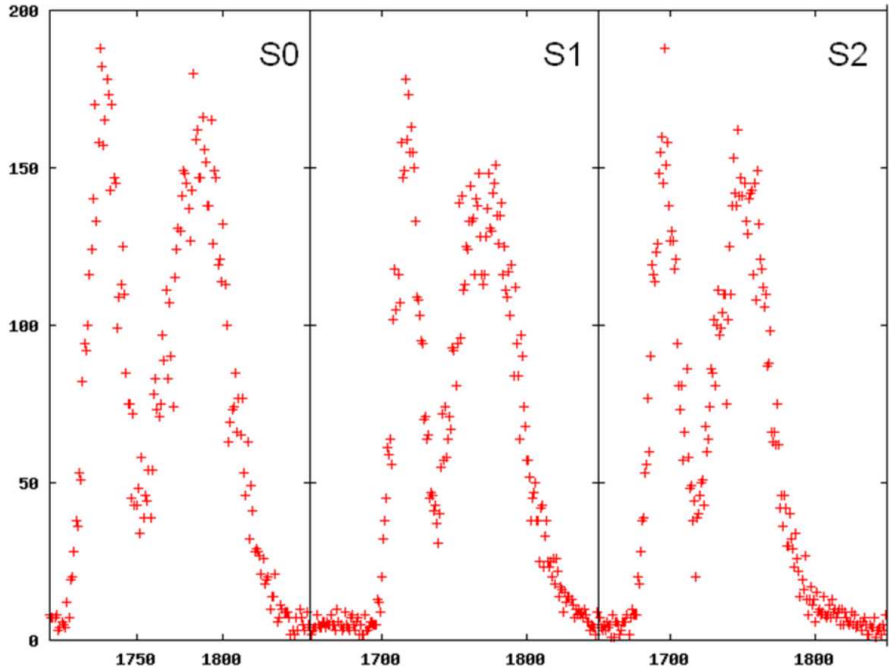

FIGURE 3.16: Neutrons from N1 detected in coincidence with the array detectors.

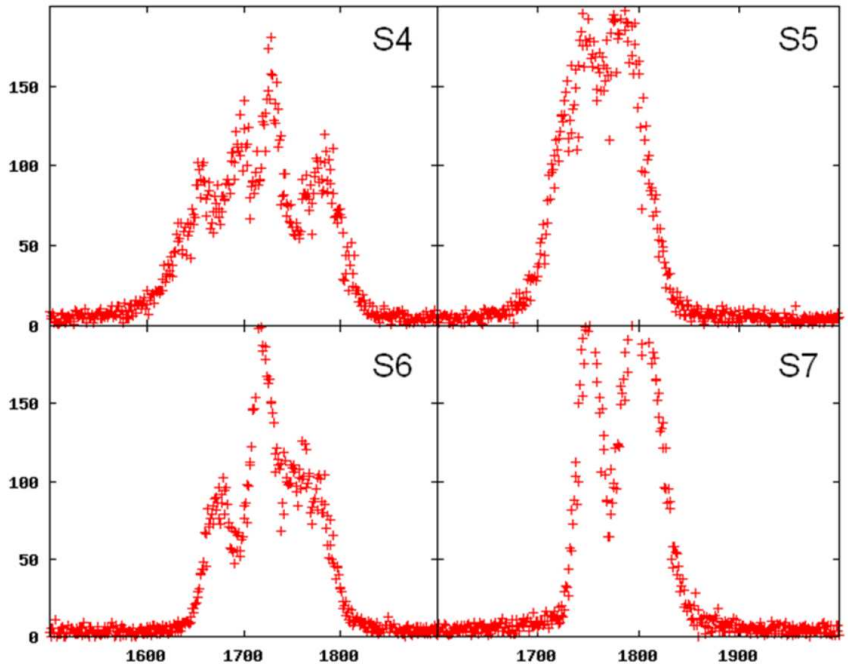

FIGURE 3.17: Neutrons from N1 detected in coincidence with the strip detectors.

defined. The data from S4, S5, and S6 is not as clear however. S4 and S6 display multiple peaks which could be due to a discrete gain shift (or shifts) or at a specific time(s) during data collection. This can be solved by dividing the data collection into multiple temporal parts each with their own γ-peak location. The γ-peak is not as clearly defined in S5 which suggests that if a gain shift occurred it is continuous rather than discrete. A continuous shift cannot be remedied.

However, a gain shift is not the cause of the multiple peaks in this experiment. Figure 3.18 is identical to Figure 3.17 except that it shows roughly the first temporal half of the data collected. One can see that the shape of the spectra are the same as in Figure 3.17 but with only 1/2 the number of counts. Therefore the multiple peaks are not caused by discrete shifts that can be separated. Only data from S7 can be used.

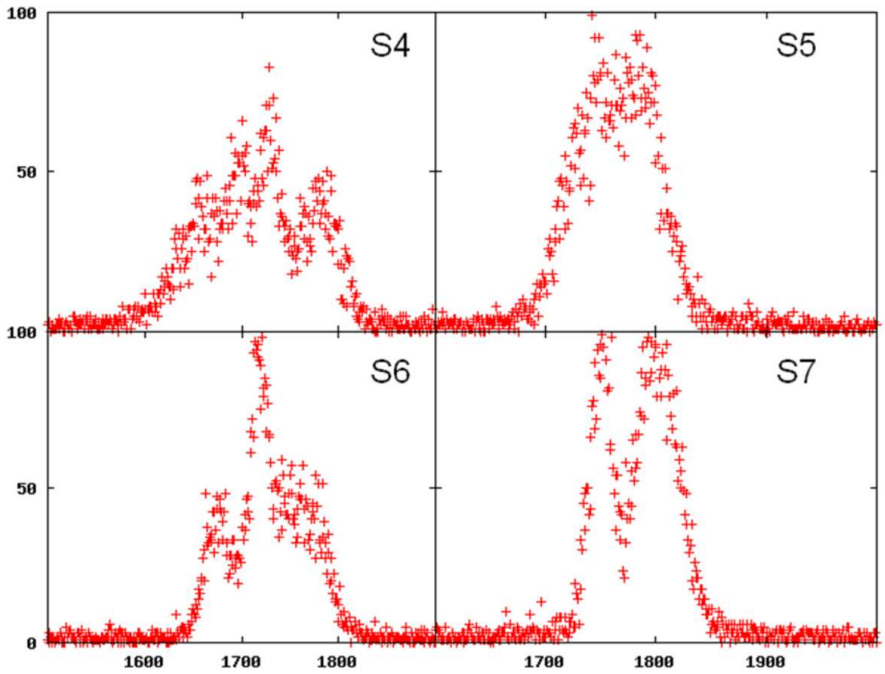

FIGURE 3.18: Identical to Figure 3.17 except that only about half of the data is used.

The neutron energy was then determined for each event using the method

outlined in Section 4.1. The code used for processing the events with a satisfactory neutron can be found in Appendix C.3. This code calculates the time-of-flight and from that, the energy. If the energy is between 1.0 and 10.0 MeV the event is output into a separate file.

4. DATA REDUCTION AND ANALYSIS

4.1 Data Reduction

Once all the the unsatisfactory events are eliminated, the neutron spectra are formed. In review, the lab energy of the neutrons is calculated from the time-of-flight (TOF). The velocity of a γ is a constant which allows for the use of the γ-peak as a measure of the absolute time of the reaction. During the experiment the front faces of N1, N2, and N3 were all placed at 25 cm from the target while N0 was 45 cm away. Assuming the an average γ interaction depth of 4 cm [40], the γ-peaks are at

$$t = \frac{d}{c} = \frac{29\text{cm}}{30\text{cm/ns}} = 0.967\text{ns} \tag{4.1}$$

for N1, N2, and N3, and

$$t = \frac{d}{c} = \frac{49\text{cm}}{30\text{cm/ns}} = 1.633\text{ns} \tag{4.2}$$

for N0. Using this and the TDC calibration (Table 3.3) the time of flight of the neutron in nanoseconds is

$$TOF = n(B - C) + t_\gamma \tag{4.3}$$

where n is the TDC calibration in ns/channel, B is the TDC bin in which the event was observed, C is the γ-peak centroid for the unique fission detector - neutron detector combination, and t_γ is the flight time of the γ. The lab energy of the neutron can then be calculated using non-relativistic mechanics,

$$E = \frac{1}{2}mv^2 = \frac{1}{2}m\left(\frac{d}{TOF}\right)^2 \tag{4.4}$$

The neutrons from each fission-neutron detector pair were then binned into 1/2 MeV wide bins. It was necessary to keep each detector pair separate because

each has a unique angle relative to the beam and to the fission fragments. This results in 16 different neutron spectra.

The goal is to obtain a spectrum that can be described using Equations 1.8 and 1.11

$$\frac{d^2M}{dE_{cm}d\Omega} = \frac{M}{4\pi T^2} E_{cm} e^{-E_{cm}/T} \tag{4.5}$$

$$\frac{d^2M}{dE_{lab}d\Omega} = \frac{M}{2(\pi T)^{3/2}} \sqrt{E_{lab}} \exp\left(\frac{-(E_{lab} - 2\sqrt{E_{lab}\epsilon}\cos\theta + \epsilon)}{T}\right) \tag{4.6}$$

Both of these equations have units of neutrons per MeV per steradian. Assuming a full momentum transfer the maximum velocity of the compound nucleus recoil is 0.0317 cm/ns in the direction of the beam. Since this is much less than the velocity of a fission fragment, the compound nucleus is therefore assumed to be at rest in the lab frame.

At this point the spectra are in units of total counts per energy bin. This must be transformed into a spectrum with units of real counts per MeV per steradian. First the background was subtracted from the raw number of counts per bin. The units at this point are neutrons per 1/2 MeV per detector area. Therefore this quantity is multiplied by 2 and is divided by the solid angle in steradians to obtain units of neutrons per MeV per steradian. The number of counts per bin is also divided by the efficiency. Mathematically this is written as

$$\frac{d^2M}{dEd\Omega} = \frac{2}{\Omega\varepsilon}(R - b) \tag{4.7}$$

where the left hand side is the multiplicity per MeV per steradian, Ω is the solid angle of the detector, ε is the efficiency, R is the raw number of counts in the given energy bin, and b is the number of background counts in the given energy bin.

The background was measured by taking the average number of counts per TDC bin far away from the γ and neutron peaks. (See Section 3.2.1 and Figure 3.6 for more details.) The total number of background counts per 1/2 MeV bin is the

number of TDC bins within the given energy bin, times the average background per TDC bin.

The efficiency is calculated at the midpoint of the energy bin using the fitted efficiency equation, see Equation 3.12 and Table 3.5. This application of the efficiency is correct only if there is a linear dependence of multiplicity versus neutron energy across the bin. This is obviously not correct. To correct for this non-linearity, each spectrum was fit with a Maxwellian distribution in which the magnitude and temperature were allowed to vary. This intermediate Maxwellian represents the neutron spectra with the correct units, but a slightly incorrect efficiency. A new weighted–efficiency was then found for each bin using the equation

$$\varepsilon_{new} = \frac{\sum_{i=E_{low}}^{E_{high}} P(E_i)\varepsilon(E_i)}{\sum_{i=E_{low}}^{E_{high}} P(E_i)} \tag{4.8}$$

where ε is the efficiency, E_{low}, E_{high} are the energy limits on the bin, and *P(E)* is the value of the intermediate Maxwellian at energy E. The sum was carried out in increments of 0.01 MeV. This new efficiency was then used to calculate a new number of counts for the bin and the process was repeated until the change in the efficiency in all bins was less than 0.0001. This occured in 2-3 iterations. The correction was most effective for lower energies where the curvature of the distribution was greatest. The correction was virtually zero at higher energies where a linear approximation was appropriate.

In a χ^2 minimization fit, the magnitude of the error in data is just as important as the magnitude of the value of the data. The uncertainty for each data point is found by doing propagation of errors on Equation 4.7.

- σ_R **and** σ_b are taken to be the square root of the number of raw counts and

the number of background counts in each bin since both processes follow a Poisson distribution. These two uncertainties dominate at higher energies due to a small number of counts per bin.

- σ_ϵ is calculated from the uncertainties in the individual efficiency data points (see Section 3.2.2). The uncertanties from the efficiencies dominate the lower energies.

- σ_Ω is estimated assuming a 1 cm uncertainty in the distance traveled. This 1 cm is rather arbitrary and comes from a guess of the uncertainty of placement of the detectors as well as an uncertainty of the interaction depth. Solid angles were calculated at $\pm$ 1 cm from the average interaction depth and found to be 0.0037 steradians different than the solid angle calculated at the average interaction depth, 0.0552 steradians.

The final results including the fits to the data are shown in Figures 5.1, 5.2, 5.3.

4.2 Analysis

Attempts were made to decompose the spectra shown in Figures 5.1, 5.2, and 5.3, using both an iteration method and a χ^2 minimization method. The following sections will describe these methods as they pertain to this experiment. A discussion of the results of the analysis is presented in Chapter 5.

The source velocity of the compound nucleus is 0.0317 cm/ns in the direction of the beam. A neutron emitted with no kinetic energy would have a lab energy of 0.0005 MeV. Since this is much less than both the neutron detector threshold and much less than the uncertainty in the energy of a neutron (see Section 3.4) the

compound nucleus is assumed to be at rest in the lab frame.

An average kinetic energy of 1.01 MeV/nucleon was assumed for the light fragment and 0.52 MeV/nucleon was assumed for the heavy fragment. From Figures 3.3 and 3.4, it is clear that that the assumption of asymmetric fission must be used. But to what degree is the system asymmetric? Since the kinetic energy release is only weakly dependent on excitation energy (see Section 8.2.C.4 of [54]), it is assumed that the experimental spectra are very similar to the spectra from a nucleus in its ground state. The total kinetic energy released in fission is calculated using the Viola Systematics [55].

$$TKE = 0.1189\frac{Z^2}{A^{1/3}} + 7.3 \text{ MeV} \tag{4.9}$$

where TKE is the total kinetic energy release in MeV, Z is the proton number and A is the mass in amu. Assuming Z=93 and A=240 the average total kinetic energy release in fission is 172.8 MeV. It is then assumed that 1 neutron is emitted prior to fission and the heavy fragment has a mass of 139 amu and the light fragment has a mass of 100 amu (see Figure 13.15 of [56]). Using momentum conservation one then arrives at the result that the heavy fragment has a kinetic energy of 0.52 MeV/nucleon and the light fragment has a kinetic energy of 1.01 MeV/nucleon.

4.2.1 χ^2 Minimization

The definition of χ^2 is

$$\chi^2 = \sum_i \left(\frac{y_i - f(x_i, a_j)}{\sigma_i} \right)^2 \tag{4.10}$$

where y_i and σ_i represent the experimental value and uncertainty of data point i. $f(x_i, a_j)$ is the function in question evaluated at x_i with parameters a_j. Here, $f(x_i, a_j)$ is a combination of Equations 4.5 and 4.6.

The minimization fits were performed either with a brute force method code written by the author (found in Appendix C.6) or Gnuplot 4.2 [45]. Gnuplot was

used for single spectra but proved inadequate when attempting a fit that included detectors at different angles. The brute force code works by looping through different parameter values set by the user, calculating the χ^2 value for each set, and outputting the set of parameters that yielding the lowest χ^2. While this method is computationally inefficient, the simplicity and intuitiveness of the program made it a viable solution. The code was tested by analyzing the data of Bowman *et al.* [44]; the code repeated their fits perfectly. When comparing the results of Gnuplot to that of the brute force it was found that the deviations of the parameter values were less than 1% and always well within the uncertainties.

A simple first assumption is to use the cascade approximation for the pre-fission de-excitation. The general form of $f(x_i, a_j)$ is then

$$\frac{d^2M}{dE_{lab}d\Omega} = \sum_{i=1}^{n} \frac{M_i}{2g_i(\pi T_i)^{3/2}} \sqrt{E_{lab}} \exp\left(\frac{-(E_{lab} - 2\sqrt{E_{lab}\epsilon_i}\cos\theta_i + \epsilon_i)}{T_i}\right) \qquad (4.11)$$

Each term in the sum represents one of the n sources. Each source can have its own unique multiplicity M, temperature T, relative angle with respect to fission θ, and lab energy ϵ. Also included is a configurational degeneracy term g_i. This is 1 in the case of pre-fission neutrons and 2 in the case of fission fragments.

For example, if one compound nucleus source and fission fragments are considered then there are 5 sources:

1. A compound nucleus source with a lab energy of 0
2. A light fission fragment moving in the forward direction
3. A heavy fission fragment moving in the backward direction
4. A light fission fragment moving in the backward direction
5. A heavy fission fragment moving in the forward direction.

The degeneracy g_i is needed because either sources 2 and 3 are present or sources 4 and 5 are present. In other words, in half of the fission events the light fragment is moving forward and the heavy fragment is moving backwards, and in the other half of the fission events the heavy fragment is moving forwards and the light fragment is moving backwards. The factor of 1/2 is needed to prevent double counting.

If a Maxwellian is used to model the compound nucleus de-excitation, Equation 4.5 is used for the pre-fission term. If this model is used it must be remembered that the Maxwellian model describes only single neutron emission. Therefore to describe a decay chain multiple terms must be used. As each neutron is emitted the excitation energy, and therefore the temperature, decreases.

Assuming the compound nucleus behaves like a Fermi gas then the temperature can be calculated from the excitation energy using the equation $E^\star = aT^2$ where $E^\star$ is the excitation energy of the nucleus, a is the level density parameter and T is the nuclear temperature. The level density parameter is linearly related to the mass of the nucleus A, $a = kA$ where k is taken to be 1/9.5 in this case. This particular value is discussed in Section 5.1.2. The compound nucleus component can then modeled as [21]

$$\frac{d^2M_{cn}}{dEd\Omega} = \sum_{i=0}^{n} \frac{M_i}{4\pi T_i^2} E e^{-E/T_i} \tag{4.12}$$

No mention of the refernce frame is given because the lab and cm frames are identical. Each term in the sum represents a different nucleus in the neutron decay chain. There are up to n neutrons emitted before fission. Each time a neutron is emitted the excitation energy, and therefore the temperature in the excited compound nucleus decreases. Assuming an initial excitation energy of the nucleus, the average excitation energy of the daughter nucleus can be calculated using $E_2^\star = E_1^\star - B_n - 2T$. Here B_n is the binding energy of the nucleus, $2T$ is the average kinetic energy of the neutron, and $E_1^\star$ and $E_2^\star$ are the excitation of the

parent and daughter nuclei.

The neutron separation energies for ^{240}Np, ^{239}Np, and ^{238}Np are 5.056 MeV, 6.217 MeV, and 5.488 MeV respectively. If the level density parameter is $a = A/9.5$, and the initial excitation energy ($E_1^\star$) of the ^{240}Np nucleus is 22.85 MeV, then the initial temperature (T_1) of the compound nucleus is 0.95 MeV. The average kinetic energy of an emitted neutron is then 1.9 MeV. The average excitation energy of the daughter nucleus ($E_2^\star$) will be 15.9 MeV, and the temperature will be 0.79 MeV. Continuing in this fashion we find that $E_3^\star = 8.1$ MeV, $T_3 = 0.57$ MeV, and $E_4^\star = 1.47$ MeV. While it is energetically possible for the compound nucleus in our system to emit three neutrons, the remaining excitation energy is below the fission barrier. Therefore it is not possible for us to observe this decay due to our fission−only trigger.

It is technically incorrect to use only the averages to determine the temperatures due to the distribution of kinetic energy distributions, which results in a range of excitation energies. Since the the probability to emit a neutron is dependent on excitation energy, there is a bias on the average excitation energy due to the fission−only trigger used in this experiment.

The standard deviations in the parameter values are determined by holding all other parameters constant and increasing the given parameter until the χ^2 value increases by 1 [57, 58]. The derivation of this is as follows for a single parameter system. For notational clarity let $\chi^2(x) = S(x)$. Expanding $S(x)$ around the minimum a (in this case a is a dummy parameter and should not be confused with the level density parameter) yields

$$S(x) = S(a) + \frac{\partial S}{\partial x}(x-a) + \frac{1}{2}\frac{\partial^2 S}{\partial x^2}(x-a)^2 \tag{4.13}$$

Since this function is evaluated at the minimum

$$\partial S/\partial x = 0 \tag{4.14}$$

and

$$\frac{1}{2}\frac{\partial^2 S}{\partial x^2} = \frac{1}{\sigma^2} \tag{4.15}$$

Evaluating this function at the point $x = a + \sigma$ yields the result of

$$S(x + a) = S(a) + 1 \tag{4.16}$$

Similarly, evaluating the function at $x = a + 2\sigma$ yields an increase in the minimum χ^2 value of 4.

This can be extended to multiparameter systems. Excluding the first order terms, Equation 4.13 in two dimensions, x and y, expanded around $x = a$ and $y = b$ is

$$S(x, y) = S(a, b) + \frac{1}{2}\frac{\partial^2 S}{\partial x^2}(x - a)^2 + \frac{1}{2}\frac{\partial^2 S}{\partial y^2}(y - b)^2 + 2\frac{\partial^2 S}{\partial x \partial y}(x - a)(y - b) \tag{4.17}$$

The partial derivatives are evaluated at $x = a + \sigma_a$ and $y = b + \sigma_b$. If the parameters are independent of each other then

$$\frac{\partial^2 S}{\partial x \partial y} = 0 \tag{4.18}$$

Using Equations 4.14 and 4.15 then evaluation at $x = a + \sigma_a$ and $y = b + \sigma_b$ yields Equation 4.16. A similar result will be found evnaluating $S(x, y)$ at $x = a$ and $y = b + \sigma_y$.

4.3 Shape of the Pre-Equilibrium Component

There are two mechanisms that create pre-equilibrium neutrons, the break up of the deuteron before it interacts strongly with the nucleus, and nucleon-nucleon interactions once the projectile enters the nucleus. The neutrons from deuteron breakup are not observable in this experiment. If a deuteron with a kinetic energy of 14.85 MeV breaks up into a proton and neutron then there will be 12.6 MeV left

over which will be shared by the daughter nucleons. Assuming a symetric energy split, this will amount to 6.3 MeV per nucleon. According to the Bass model [59], the Coulomb potential energy that a proton must overcome to interact with ^{238}U is 12.8 MeV. Therefore the protons from a deuteron breakup will interact elastically with the nucleus and the nucleus will not have enough energy to fission. Since there is no fission, the event will not be observed in this experiment.

The model used to describe the pre-equilibrium component is based on the exciton model originally devised by Marshall Blann and then extended in multiple articles [25, 60, 61, 62, 63, 64]. The angular and energy-dependent cross section for pre-equilibrium neutrons has been parameterized by Kalbach [25] as

$$\frac{d^2\sigma}{d\Omega dE} = \frac{1}{4\pi}\frac{d\sigma}{dE}\frac{a}{\sinh a}\left[\cosh(a\cos\theta) + f_{MSD}\sinh(a\cos\theta)\right] \tag{4.19}$$

Here $d\sigma/dE$ is modeled using Equation 1.9 [21]. As mentioned in the introduction, the most commonly used form to model the pre-equilibrium component is a Maxwellian spectrum with a source velocity 1/2 that of the beam velocity [21, 22, 23, 24][2].

f_{MSD} is the fraction of neutrons emitted from a direct equilibrium process (i.e. those that are emitted before multiple nucleon collisions occur during the reaction), θ is the angle of emission, and a is an energy-dependent parameter. For the excitation energy ranges in this experiment, a is small (<0.5) [25], and the angular distribution portion of the cross section is close to 1.

The model of the source velocity is rather simple: The initial interaction between two nuclei is between one nucleon of the projectile and one nucleon of the target. The momentum of the projectile nucleon will be shared equally between

[2]There is an interesting sequence of referencing here. Hinde *et al.* [21] specifies the use of a Maxwellian form to model the pre-equilibrium component. Isaev *et al.* [22], Cabrera *et al.* [23], and Keutegen *et al.* [24] all reference [21] when discussing the origin of their pre-equilibrium models but [23] and [24] choose to use a Watt spectrum to model their pre-equilibrium components.

the two nucleons. After the initial interaction a number of further interactions may (or may not) take place, smearing out the distribution of emitted nucleon(s) [61].

5. RESULTS AND DISCUSSION

5.1 Data Discussion

Non-linear multi-variable fits are difficult. Mathematically obtaining a solution is easy, obtaining a physically reasonable one is more tricky. Due to the number of free parameters considered in this experiment, the possibility of over-fitting must be considered. This occurs when too many parameters are used to describe a set of data. Some parameters are then superfluous. If over-fitting occurs the best case scenario is that the fit will make sense but the reduced χ^2 value will be small. Over fitting can also occur when trying to distinguish between two very similar components. If the error bars are too large the two components may be statistically indistinguishable.

Over fitting becomes a real problem when the statistically excess parameters allow the outlier data points to dominate the fit. If this occurs, the fit may converge to parameter values that are far from being physically reasonable. One must also be aware of the possibility of convergence on a local, rather than global minima. For these reasons many different fits were performed to make sure the fit only contained statistically reasonable parameters and was in a global minimum. For the sake of brevity, only a cross section of the fits to the data performed during the analysis will be shown and discussed here.

5.1.1 Fits to Individual Detector Pairs

The program Gnuplot 4.2 was used to fit each individual fission−neutron detector pair neutron spectrum. The results using only a fission component are listed in Table 5.1. The initial guess for the multiplicity and temperature of the fission fragment component is M_f=5.0 and T_f=1.4. The key feature to note is the rela-

tively high temperature values for N3. Examining the raw TDC spectra, shown in Appendix B.2, the centroid of the neutron peaks corresponds to a neutron energy of $\sim$ 4 MeV for detectors N0, N1, and N2, but corresponds to an energy of $\sim$ 6 MeV for N3. It is unclear what caused this shift. This will be examined more in later fits.

Detector Pair	M_f	T_f	Reduced χ^2
S0N0	4.79±0.45	1.25±0.07	0.53
S1N0	8.87±0.97	0.93±0.05	0.78
S2N0	7.71±1.02	1.06±0.07	0.52
S7N0	6.57±1.06	1.14±0.09	1.52
S0N1	5.37±0.19	1.140±0.044	1.07
S1N1	5.12±0.26	1.260±0.082	2.22
S2N1	5.10±0.24	1.142±0.062	1.83
S7N1	5.77±0.17	1.343±0.048	0.76
S0N2	5.50±0.28	1.260±0.062	1.52
S1N2	4.69±0.32	1.570±0.098	1.6
S2N2	5.34±0.26	1.190±0.051	1.22
S7N2	5.98±0.28	1.506±0.055	0.83
S0N3	5.77±0.39	1.636±0.058	0.68
S1N3	4.94±0.63	1.88±0.15	2.46
S2N3	5.97±0.46	1.682±0.069	0.99
S7N3	5.05±0.46	1.654±0.081	1.31

TABLE 5.1: Fit results for the individual detector pairs. This set excludes a compound nucleus component.

More components, such as a compound nucleus with a lower temperature than

the prompt component and a pre-equilibrium component with a temperature larger than that of the prompt component were then explored. These results are not shown here because they did not yield any new information. Each detector pair showed evidence for two components, but adding a third component only produced over fitting. The over fitting was evident from two physically reasonable components and the third was governed by a stray data point or two and yielded an unphysical result.

5.1.2 Analyzing all Detector Pairs Simultaneously

Since the neutrons are emitted at multiple stages during de-excitation from a source at rest in the lab frame,

$$\frac{d^2M_{cn}}{dEd\Omega} = \sum_{i=0}^{n} \frac{M_i}{4\pi T_i^2} E e^{-E/T_i} \tag{5.1}$$

was used to describe the compound nucleus component where each term represents one stage of de-excitation. A similar term was used to describe the pre-equilibrium component [22, 23, 24].

$$\frac{d^2M_{cn}}{dE_{lab}d\Omega} = \sum_{i=0}^{n} \frac{M_i}{4\pi T_i^2} \sqrt{E_{lab}E_{cm}} e^{-E_{cm}/T_i} \tag{5.2}$$

Notice that if $E_{lab} = E_{cm}$ then Equation 5.2 reduces to Equation 5.1. The results of these fits are shown in Table 5.2. The prompt component was modeled using a Watt distribution, Equation 4.11 [33, 34].

$$\frac{d^2M}{dEd\Omega} = \frac{M}{2(\pi T)^{3/2}} \sqrt{E_{lab}} \exp\left(\frac{-E_{cm}}{T}\right) \tag{5.3}$$

The fitting was performed using the brute force code discussed in Section 4.2 and shown in Appendix C.6. The procedure started with the fission fragment component and then added in additional terms one at a time. The fission fragment component was done first because it is the largest producer of neutrons in this experiment and thus the dominant term. This is fit 1 in Table 5.2. This fit does not include the data from N3.

It was assumed that the excitation energy per nucleon remained constant during fission. Using the Fermi gas model the temperature of the two fragments is then identical. This assumption has been used quite often [22, 23, 24, 34]. Since it is assumed that the mass of the heavy fragment is 1.4 times that of the light then the heavy fragment will have 1.4 times the total excitation energy as the light fragment.

Therefore, on average, 1.4 times as many neutrons will be emitted from the heavy fragment as the light fragment. This ratiowas held constant during the fit.

Next a pre-equilibrium component was then added to the fit. The result of this fit is number 2 in Table 5.2. The pre-equilibrium magnitude and temperature stated in the table is that of the fit itself. In the case of the pre-equilibrium component the best fit values are not assumed to be the physical values that represent reality because of a biasing as a result of the requirement of a fission. The physical magnitude and temperature is 0.458±0.023 and 3.15±0.25 MeV. This is discussed in Appendix A.

After the pre-equilibrium component was found, the compound nucleus components were included. Fit 3 in Table 5.2 shows the most simple case with only one compound nucleus component. This result is not physically realistic for two reasons.

First, the temperature 0.39 is too low. The excitation energy and the temperature of the nucleus can be related using the equation $E = aT^2$ where a is the level density parameter. The level density parameter is somewhere between $A/12$ and $A/8$. For the nuclei of interest in this experiment the value is approximately $A/(9.5 \pm 1)$ [65, 66, 67]. The excitation energy of the emitting source of compound nucleus neutrons is then approximately 3.8 MeV. This value is below both the fission barrier and the neutron separation energy. Therefore, no events can be observed in this experiment from a source with an excitation energy this low.

The second reason that this source cannot be correct is that the multiplicity is larger than 1.0. Assuming a Maxwellian distribution for the equilibrium neutrons implies that only one neutron is emitted from a given source (as opposed to a Watt distribution which assumes multiple neutrons and an average temperature over the cascade). Therefore, for each fission a maximum of 1 neutron can be observed per source. One cannot conclude that the multiplicity larger than 1.0 is due to

there being multiple sources of compound neutrons that are modeled with only one component. If this were true, one source would have a temperature larger than 0.39 and one would have a temperature smaller than 0.39. Since 0.39 is already too low, it is not possible that this component is a combination of two or more sources.

Since letting the temperature of the equilibriated nucleus vary did not yield physically realistic results, the next attempt at determining the compound nucleus neutrons was done by holding the temperatures of the different sources constant [21, 22, 23, 33, 34, 35, 36]. It was decided to look for three different sources: a ^{240}Np created in a complete fusion reaction, a ^{239}Np created after the emission of a neutron from a ^{240}Np created in a complete fusion reaction, and a ^{239}Np created after the ^{240}Np emits a pre-equilibrium neutron. The details of this decision are discussed in Appendix A.

For a complete fusion of the deuteron, this results in a compound nucleus temperature of 0.97. This is fit 4 in Table 5.2. Notice that the reduced χ^2 value increases by adding in this component and that the uncertainty in the magnitude is about 380%. The next source that was searched for was that of a ^{239}Np nucleus created from the emission of a pre-equilibrium neutron. The temperature was assumed to be 0.58 MeV. The results of this fit are shown as Fit 5. One last source was searched for; this was that of a ^{239}Np nucleus created from the decay of an equilibriated ^{240}Np. The temperature for this source is 0.78. The results of this fit is number 6 in Table 5.2.

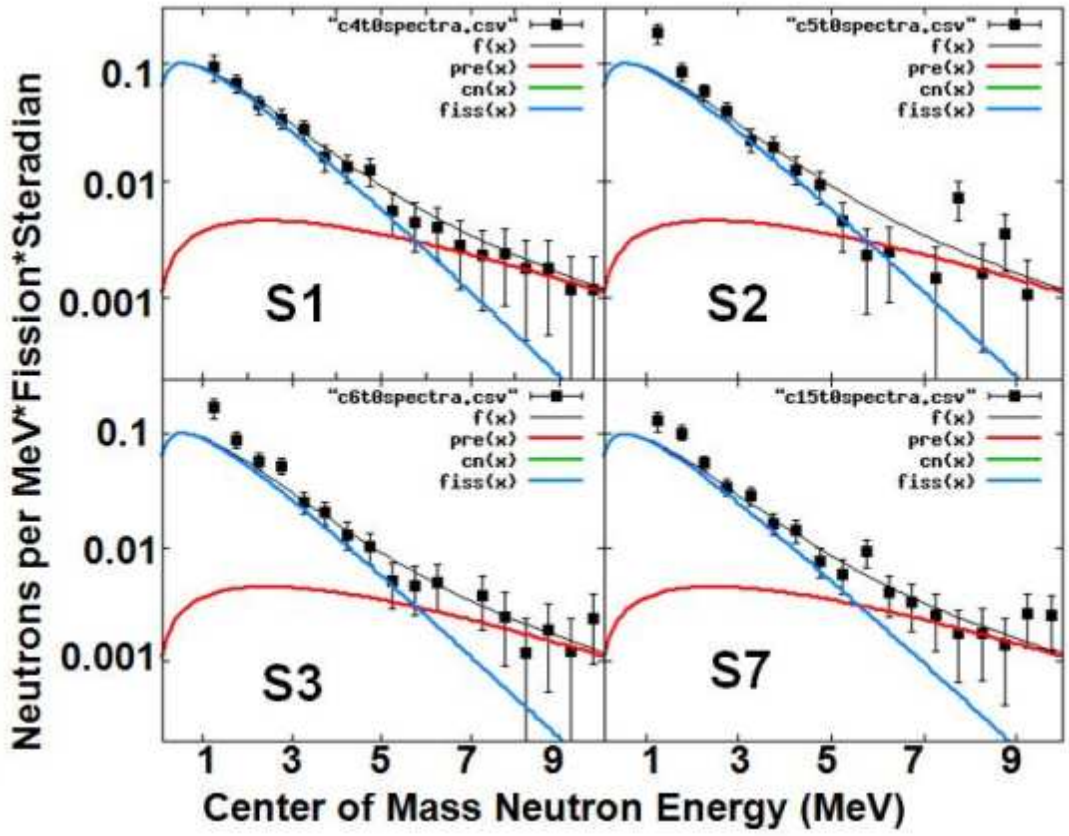

FIGURE 5.1: Neutron spectra from N0 and the results of Fit 2. The black line is the sum of the fission fragment component (blue) and pre-equilibrium component (red).

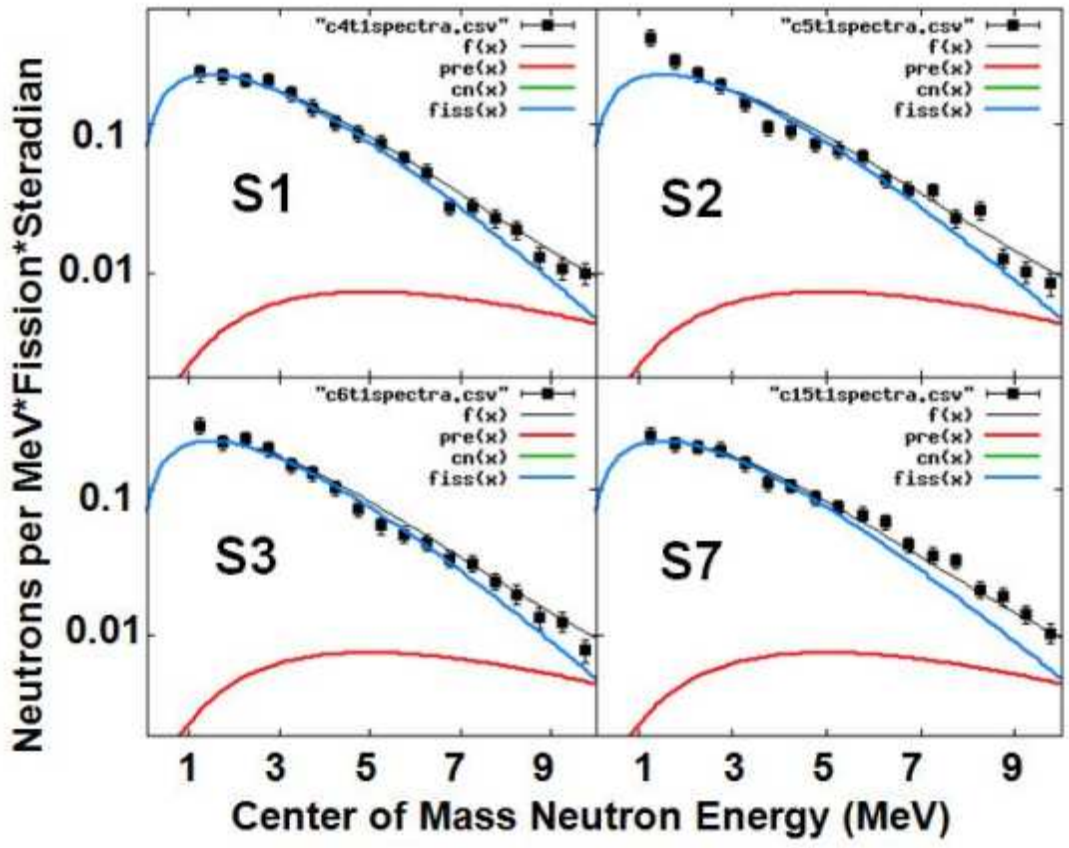

FIGURE 5.2: Neutron spectra from N1 and the results of Fit 2. The black line is the sum of the fission fragment component (blue) and pre-equilibrium component (red).

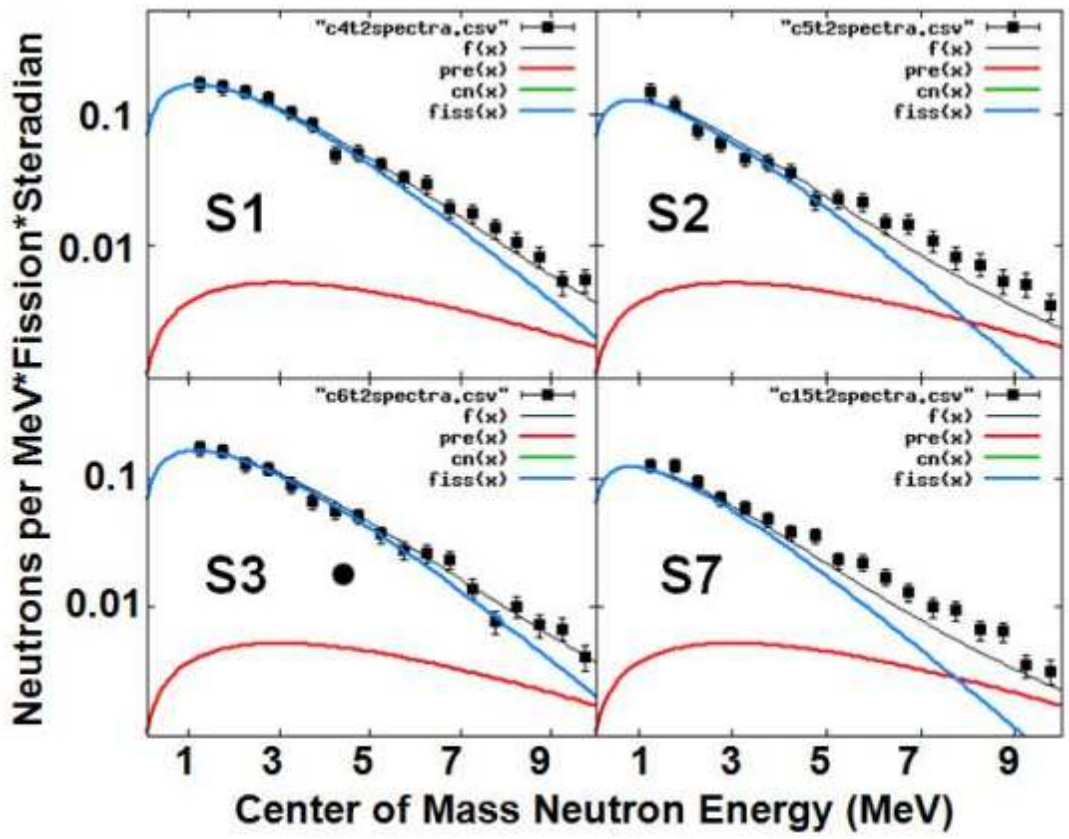

FIGURE 5.3: Neutron spectra from N2 and the results of Fit 2. The black line is the sum of the fission fragment component (blue) and pre-equilibrium component (red).

index	M_{cn}	T_{cn}	M_{pre}	T_{pre}	M_f	T_f	χ^2	Reduced χ^2
1	***0***	**-**	***0***	NA	5.66	1.25	541.94	2.53
2	***0***	**-**	0.492 ± 0.025	2.77 ± 0.22	5.270 ± 0.067	1.094 ± 0.011	466.57	2.201
3	1.24	0.39	0.52	2.58	5.0	1.11	444.99	2.12
4	0.019±0.072	***0.97***	0.495	2.77	5.255	1.093	466.54	2.211
5	0.65±0.12	***0.58***	0.565	2.55	4.939	1.089	451.27	2.14
6	0.25±0.09	***0.78***	0.55	2.63	5.07	1.08	462.92	2.194

TABLE 5.2: Fit results looking at multiple detectors simultaneously. Italics and boldface mean the value was held constant. Fit 1) Data used from all S0, S1, S2, and S7, and N0, N1, and N2. Only a prompt neutron component was considered. Fit 2) Same as fit 1 but with the addition of a pre-equilibrium component. Errors represent 1σ. Fit 3) Same as fit 2 but with the addition of a compound nucleus component. Fit 4) Same as fit 3 but with the compound nucleus source representing an equilibriated ^{240}Np. Fit 5) Same as fit 4 but assuming a compound nucleus source of a ^{239}Np created after the emission of a pre-equilibrium neutron. Fit 6) Same as fit 4 but assuming the compound nucleus comes from a ^{239}Np created from the neutron emission of a equilibriated ^{240}Np.

5.2 Discussion

The final result of this experiment is taken to be that of fit 2 from Table 5.2. This decision was reached because fit 2 has a lower reduced χ^2 value than fit 1 indicating the significance of the pre-equilibrium component. The addition of compound nucleus components did add statistically signficant components, but the physical reality of these components is questionable. The details are discussed below.

The multiplcity of the prompt neutrons of 5.270±0.067 per fission is the same as the ENDF data at this excitation energy, as can be seen in Figure 1.2. Compared to experiments that performed a similar data analysis at a similar excitation energy, it is higher than previously measured values of Rubchenya *et al.*, 4.51±0.31 [16], Bishop *et al.* 4.54±0.14 [8], and Strecker *et al.* 4.79±0.10 [15]. Direct comparisson of these experiments is not completely fair because this experiment created a nucleus of mass 240 while the others created a nucleus of mass 239. The higher mass will naturally create more neutrons.

The temperature of the fission fragments match well with that of Bishop *et al.*, 0.99 and 1.09 [14], and Strecker *et al.*, 1.0±0.02 [15]. Rubchenya *et al.* [16] did not report the fitted temperature.

The theory of the pre-equilibrium component in such reactions is the least understood aspect. Some authors have skirted this by not fully detailing the results of their modeling of the pre-equilibrium component, such as not stating the temperature, or by stating their results are unphysical. The problem with this line of reasoning is that they only consider the pre-equilibrium component to be unphysical. This relegates it to some mathematical construct used to fit the data that cannot be explained by the other components.

The observed neutrons in the experiment, in relation to the individual components, can be written mathematically as

$$DATA = Fission + Compound\ Nucleus + Pre\text{–}Equilibrium \tag{5.4}$$

Rearranging this we get

$$Pre\text{–}Equilibrium = DATA - Fission - Compound\ Nucleus \tag{5.5}$$

If the claim is made that the pre-equilibrium is not physical, then the LHS of the above equation is an nonphysical component. Therefore something on the right hand side must also be nonphysical in order to balance this out. If one assumes that part or all of the fission or compound nucleus component is false then the results are irrelevant. This is analogous to working with an equation with both real and imaginary parts. All the imaginary parts of the equation on one side and leave all the real parts on the other. Therefore in this work the pre-equilibrium component will be considered to be a component as real as all other data.

While the temperature of 3.15 MeV of the pre-equilibrium component is not a true thermodynamic temperature, it does represent a kinetic energy distribution of neutrons. To the author's knowledge, this has not been experimentally measured before. Few authors state the pre-equilibrium temperatures, so quantitatively comparing this temperature to others is difficult. Grusha *et al.* simulated the pre-equilibrium component in the ^{238}U + d reaction at E_d = 12 MeV and found a temperature of about 6 MeV.

One possibility of the discrepancy is the model used to transform the fitted 2.77 MeV to 3.15 MeV (see Appendix A). The most simple model possible was used to simulate the decay cascade. Two assumptions in this model are questionable. First, this model does not take into account the double-humped nature of the fission barrier. Second, it assumes a level density parameter of A/9.5 rather than using

more accurate level density parameters such as those found in the RIPL-2 database [68]. An attempt was made to use a more complex model. The endeavour was abandoned because of the difficulty of obtaining a pre-equilibrium neutron shape that matched the experimental data.

The value of 0.02 compound neutrons from the completely fused system does not match any previous model or data. It is true that the number of compound nucleus neutrons emitted from a ^{240}Np nucleus with an excitation energy of 23 MeV has never been measured before, and therefore this is the only experimental value in existence. To claim that there are no compound nucleus neutrons emitted is equivalent to claiming that the nucleus fissions 100% of the time. This does not match any models of Γ_n/Γ_f that have ever been discussed. Using the classic formula for Γ_n/Γ_f, Equation 1.17 yields a value of approximately 23. In other words, the nucleus fissions in just over 4% of the events.

At excitation energies far above both the neutron binding energy and fission barrier the choice of mode of decay becomes a detailed balance problem. Therefore the most valueable parameter is that of the level density parameter. The level density is proportional to

$$exp(E^{\star} - B) \tag{5.6}$$

where $E^{\star}$ is the excitation energy of the nucleus and B is the barrier to overcome for decay. The fission barrier for ^{240}Np is approximately 6.15 MeV and the neutron binding energy is 5.05 MeV, therefore there are many more levels available for neutron decay than for fission.

The reason for the null result appears to be a simple matter of not being able to adequately resolve the compound nucleus components because the magnitude of the components is smaller than the magnitude of the error bars. Figure 5.4 shows the absolute normalized magnitude of our data on the vertical axis verses the neutron

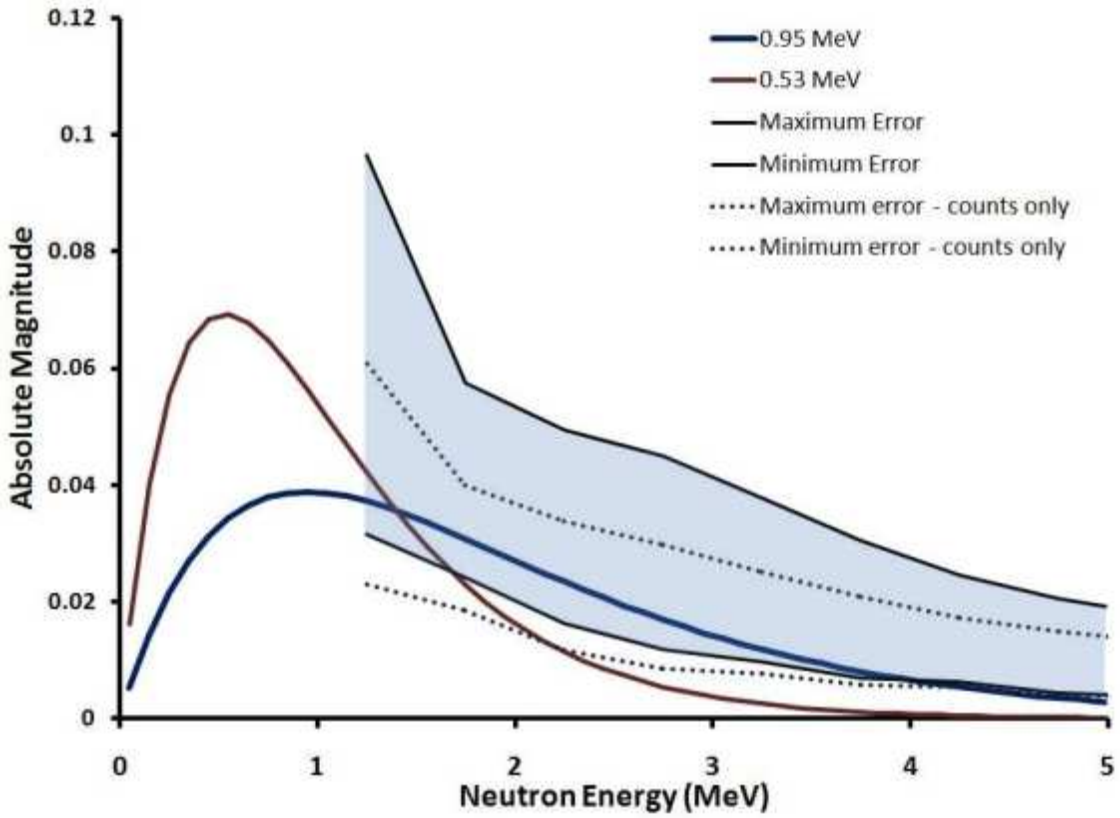

FIGURE 5.4: Absolute magnitude of sought after compound nucleus components and errors up to 5 MeV. A Maxwellian with magnitude 1.0 and T=0.95 (T=0.53) is shown as a solid smooth blue (dark red) line. The solid jagged black lines show the maximum and minimum error of the data for each energy point. The dotted blue lines are the maximum and minimum errors due to only the uncertainty in the number of counts.

energy on the horizontal axis. Two Maxwellian curves of magnitude 1 are shown; the first with T=0.95 and the second with T=0.53. These represent the compound nucleus components. Also shown are the largest and smallest errorbar magnitude of the 12 different detector combinations for each energy point. Notice that the magnitude of the compound nucleus curves are smaller than the size of some of the errorbars. Furthermore, the magnitudes of the Maxwellian curves are set to 1.0 whereas in reality the magnitudes are probably smaller.

On a further note, not shown in Table 5.2 are the 2σ values. As stated before, increasing a parameter by 2σ should increase the χ^2 value by 4. In all of the statistically relevant parameters the measured 2σ value was double that (within 10%) of the 1σ value. While this sounds obvious, if this was not the case it would suggest something could be wrong in the analysis. As it is this stongly suggests that the parameters are acting independently of each other and justifies the use of a χ^2 minimization to model the data.

6. CONCLUSIONS

In conclusion, neutrons from fission induced by the bombardment of ^{238}U by 14.85 MeV deuterons were observed at multiple lab angles. The neutron spectra were broken down into their constituent parts using the χ^2 minimization method.

5.270 ± 0.067 neutrons per fission were measured from fission fragments. The average nuclear temperature of the fragments is 1.094 ± 0.011 MeV. These numbers agree well with previous experiments and demonstrate the the null result of the compound nucleus component is not due to some gross error in the experiment or analysis.

A pre-equilibrium source of 0.458 ± 0.023 neutrons per fission was measured with a temperature of 3.15 ± 0.25 MeV.

Evidence for a compound nucleus component was observed but unresolveable due to the ratio of the magnitude of the errorbars to the magnitude of the relevant components.

No work is ever complete. After doing any experiment there are always things that could have been done differently that would have improved the data in some fashion. Most of the time these short-comings are small and the experiment can still be considered a success. This experiment was not one of the successful experiments. This section discusses improvements and changes that should be made to this experiment to make it successful.

The original goal of this experiment was to measure the charged particles emitted in coincidence with fission fragments and neutrons. By measuring the kinetic energy of an emitted charged particle, the excitation energy of the nucleus can be derived. If a sufficient amount of fission events are collected in coincident with charged particles, the data can be divided up by the excitation energy of the nuclei.

This would allow for a determination of the emitted neutrons at a given excitation energy and a direct measurement of Γ_n/Γ_f.

This aspect of the experiment ultimately failed for two reasons, both of which were discovered after the experiment was completed. First, the random coincident rate between (d,f) and (d,pf) events was too large. This was determined theoretically by using the cross sections to calculate the expected rates of the (d,f) and (d,pf) reactions. While there are a number of different assumptions that can be made that will change the end result, such as an uncertainty in the cross section and angular distribution, the lowest calculated random coincidence rate was 20%. There are two possible solutions to this is problem. The first is to simply decrease the overall reaction rate by decreasing the beam current. The second is to make the solid angle of the detectors smaller. This can be done either with collimation or by moving the detector farther away from the target.

The second reason why this aspect of the experiment failed is because of an incorrect choice of charged particle detectors. The identification of charged particles is done by requiring the particle to travel through one particle detector and implant into a second. Based on the energy deposited in the detectors, the mass and charge of a particle can be determined. In the case of this experiment however, the first detector was too thick. A large amount of energy (about 6 MeV) was required for the particle to punch through the first detector and implant in the second. Therefore, no charged particles with energy less than 6 MeV could be identified. If the charged particle cannot be identified, neither can the excitation energy of the nucleus. Because of the requirement that only charged particles with energy over 6 MeV yield useful data, the energetics were such that a nucleus could not emit both a charged particle, a neutron, and fission in this experiment.

The preceeding discussion of the charged particle measurements has direct

consequences to the material discussed in this work. The magnitude of the error bars of the data are too large to resolve the compound nucleus component. There are a number of things that can be done to decrease their magnitude. The first is what every experimenter wants: to collect more data. In the case of this experiment, this is a very feasible option. Most of the beamtime was spent using a hard trigger that required both a charged particle and a fission. All data collected with this trigger was not useable. This experiment consisted of 21 days of beam totalling 378 hours (18 hours a day) but only 31 minutes of useful data was collected. Roughly half of the magnitude of the errors was due to an uncertainty in the number of counts. This number could easily have been reduced if more time was spent using a fission−only trigger.

The uncertainty in the distance between the target and the neutron detector also contributes to the magnitude of the error bars. The uncertainty in the position of the neutron detectors could be reduced by taking more care in their placement. While the error was on the order of a few millimeters, the solution of anchoring them into a fixed location is rather simple. It is not actually the absolute error that matters, but rather the relative error. If the detectors are moved further away from the source the relative error decreased even if no other improvements are made. Furthermore, moving the detector away from the source will decrease the relative error in the time−of−flight, and the increase in the efficiency at higher energies might be remedied.

Moving the detectors further away from the source comes at the cost of a decreased solid angle and therefore a reduction in the number of counts. Much thought must be put into this interplay. Once the experimenter decides where he/she would like to run the experiment, the experimenter must determine where to place the detectors based on what is known about the detectors that will be used, the expected

beamrate at the accelerator, and the desired beamtime. Once the experimenter is approved for beamtime, the amount of beamtime may be different from what was requested and the setup might need to be modified. If the experimenter is lucky, no changes will be needed during the experiment itself.

In this experiment were repeated with only changes in the beamtime and solid angle, the calculation might go something like this: If four days of beamtime are available, the increase in the amount of data collected would be a factor of 144 (based on 18 hours of beamtime per day and 1/2 hour of data collected in this experiment). If the detectors are moved back to 100 cm away, the amount of data collected would be reduced by a factor of 4. The net result is a 36 fold increase in the amount of data. The error due to the number of counts would then be reduced by roughly a factor of 6.

The errors in the efficiencies are primarily due to the errors in the Bowman data. The errors of the neutron densities of this experiment are between 5 and 10% at the lower energies of this experiment. This uncertainty is due primarily to the uncertainty in the solid angle, about 7%, and not due to the uncertainty in the number of counts, which is less than 1%. These errors cannot be changed. An alternative is to simulate the detector efficiency. Care must be taken to make sure that realistic uncertainties are used that are base on the uncertainties in the underlying physics, and that the error in the efficiencies are not due just to statistical error.

If the experiment were to be repeated, care would be taken to increase the amount of data collected at neutron energies lower than 1.0 MeV. It is unclear how much the cut−off can be lowered. As can be seen in Figure 3.11 a 1 MeV cut−off seems to be the limit with this type of detector. It is hard to do a post-experiment analysis on this because the cut−off is due largely to the setting on the threshold

which is set during the experiment at some point just above the noise.

While not needed, pulse shape discrimination should be considered. This is needed if the experimenter is unsure about the separation between neutrons and γ's. However, since the separation was satisfactory in this experiment, and the detector should not be closer to the source in the repeat experiment, this would be a simple back up.

BIBLIOGRAPHY

1. G. Aliberti, G. Palmiotti, M. Salvatores, and G. C. Stenberg. *Nuclear Science and Engineering*, 146:13, 2004.

2. V.A. Rubchenya, W.H. Trzaska, J. Aysto, A.A. Alexandrov, I.D. Alkhazov, Brinkman K.T., A.V. Evsenin, S.V. Khlebnikov, A.V. Kuznetsov, V.G. Lyapin, M. Mutterer, Yu.E. Penionzhkevich, O.I. Osetrov, Z. Radivojevich, Yu. G. Sobolev, G.P. Tjurin, and D.N. Vakhtin. *Physics of Atomic Nuclei*, 65:697–702, 2002.

3. C.M. Zoeller. PhD thesis, Technischen Hochschule, Darmstadt, 1995.

4. H.C. Britt and J.D. Cramer. *Physical Review C*, 2:1728–1768, 1970.

5. D.P. Min and M. Martinot. *Nuclear Science and Engineering*, 68, 1978.

6. Jagdish K. Tuli, editor. *Nuclear Wallet Cards*. 6 edition, 2000.

7. George L. Bate, R. Chaudhry, and J. R. Huizenga. *Phys. Rev.*, 131(2):722–734, 1963.

8. C.J. Bishop, I. Halpern, R.W. Shaw Jr., and R. Vandenbosch. *Nucl. Phys. A*, 198:161–187, 1972.

9. F. Deak, S. Gueth, J. Inczedy, and A. Kiss. *Acta Physica Academiae Scientia Hungaricae*, 38(3):209–213, 1975.

10. R.M. Lessler, W.M. Gibson, and R.A. Glass. *Nuclear Physics*, 81:401–416, 1966.

11. John A. Northrop, Richard H. Stokes, and Keith Boyer. *Phys. Rev.*, 115, 1959.

12. M.B. Chadwick, P. Obložinský, M. Herman, N.M. Greene, R.D. McKnight, D.L. Smith, P.G. Young, R.E. MacFarlane, G.M. Hale, S.C. Frankle, A.C. Kahler, T. Kawano, R.C. Little, D.G. Madland, P. Moller, R.D. Mosteller, P.R. Page, P. Talou, H. Trellue, M.C. White, W.B. Wilson, R. Arcilla, C.L. Dunford, S.F. Mughabghab, B. Pritychenko, D. Rochman, A.A. Sonzogni, C.R. Lubitz, T.H. Trumbull, J.P. Weinman, D.A. Brown, D.E. Cullen, D.P. Heinrichs, D.P. McNabb, H. Derrien, M.E. Dunn, N.M. Larson, L.C. Leal, A.D. Carlson, R.C. Block, J.B. Briggs, E.T. Cheng, H.C. Huria, M.L. Zerkle, K.S. Kozier, A. Courcelle, V. Pronyaev, and S.C. van der Marck. *Nuclear Data Sheets*, 107(12):2931–3118, 2006.

13. www.nndc.bnl.gov.

14. C.J. Bishop, R. Vandenbosch, R. Aley, R.W. Shaw Jr., and I. Halpern. *Nucl. Phys. A*, 150:129–142, 1970.

15. M. Strecker, R. Wien, P. Plischke, and W. Scobel. *Phys. Rev. C*, 41(5):2172–2187, 1990.

16. V.A. Rubchenya, W.H. Trzaska, D.N. Vakhtin, J. Aysto, P. Dendooven, S. Hankonen, A. Jokinen, Z. Radivojevich, J.C. Wang, I.D. Alkhazov, A.V. Evsenin, S.V. Khlebnikov, A.V. Kuznetsov, V.G. Lyapin, O.I. Osetrov, G.P. Tiourin, A.A. Alesandrov, and Yu.E. Penionzhkevich. *Nucl. Inst. Meth. A*, 463:653–662, 2001.

17. G.N. Lovchikova, A.M. Trufanov, M.I. Svirin, V.A. Vinogradov, and A.V. Polyakov. *Physics of Atomic Nuclei*, 67:1246–1263, 2004.

18. Arthur C. Wahl. *Los Alamos Report*, LA-13928, 2002.

19. T. Ethvignot, M. Devlin, H. Duarte, T. Granier, R.C. Haight, B. Morillon, R.O. Nelson, J.M. O'Donnell, and D. Rochman. *Phys. Rev. Lett.*, 94:052701, 2005.

20. C. Kalbach and F.M. Mann. *Phys. Rev. C*, 23:112 – 123, 1981.

21. D. J. Hinde, D. Hilscher, H. Rossner, B. Gebauer, M. Lehmann, and M. Wilpert. *Phys. Rev. C*, 45(3):1229–1259, 1992.

22. S. Isaev, R. Prieels, Th. Keutgen, J. Van Mol, Y. El Masri, and P. Demetriou. *Nucl. Phys. A*, 809:1–29, 2008.

23. J. Cabrera, Th. Keutgen, Y. El Masri, Ch. Dufauquez, V. Roberfroid, I. Tilquin, J. Van Mol, R. Régimbart, R. J. Charity, J. B. Natowitz, K. Hagel, R. Wada, and D. J. Hinde. *Phys. Rev. C*, 68(3):034613, 2003.

24. Th. Keutgen, J. Cabrera, Y. El Masri, Ch. Dufauquez, V. Roberfroid, I. Tilquin, A. Ninane, J. Van Mol, R. Régimbart, R. J. Charity, J. B. Natowitz, K. Hagel, R. Wada, and D. J. Hinde. *Phys. Rev. C*, 70(1):014611, 2004.

25. C. Kalbach. *Phys. Rev. C*, 36:2350–2370, 1988.

26. G.N. Harding and F.J.M Farley. *Proc. Phys. Soc.*, 69:853–857, 1952.

27. J. S. Fraser. *Phys. Rev.*, 88(3):536–541, 1952.

28. S. Debenedetti, J. E. Francis, W. M. Preston, and T. W. Bonner. *Phys. Rev.*, 74(11):1645–1650, 1948.

29. D. Hilscher and H. Rossner. *Annales de Physique*, 17(6), 1992.

30. V. Weisskopf. *Phys. Rev.*, 52(4):295–303, 1937.

31. Dimitri Mihalas and Barbara Weibel-Mihalas. *Foundations of Radiation Hydrodynamics*. Dover, 1999.

32. B. E. Watt. *Phys. Rev.*, 87(6):1037–1041, 1952.

33. D. Hilscher, J. R. Birkelund, A. D. Hoover, W. U. Schröder, W. W. Wilcke, J. R. Huizenga, A. C. Mignerey, K. L. Wolf, H. F. Breuer, and V. E. Viola. *Phys. Rev. C*, 20(2):576–591, 1979.

34. H. Rossner, D. Hilscher, D. J. Hinde, B. Gebauer, M. Lehmann, M. Wilpert, and E. Mordhorst. *Phys. Rev. C*, 40(6):2629–2640, 1989.

35. E. Holub, D. Hilscher, G. Ingold, U. Jahnke, H. Orf, and H. Rossner. *Phys. Rev. C*, 28(1):252–270, 1983.

36. W. P. Zank, D. Hilscher, G. Ingold, U. Jahnke, M. Lehmann, and H. Rossner. *Phys. Rev. C*, 33(2):519–536, 1986.

37. Robert Vandenbosch and John R. Huizenga. *Nuclear Fission*. Academic Press, 1973.

38. www.npl.washington.edu.

39. Walter Loveland, personal communication.

40. Sara A. Pozzi, James A. Mullens, and John T. Mihalczo. *Nuclear Instruments and Methods A*, 524:92–101, 2004.

41. http://docs.nscl.msu.edu/daq/spectcl.

42. H.W. Schmitt and Frances Pleasonton. *Nuclear Instruments and Methods*, 40:204–208, 1966.

43. H.W. Schmitt, W.E. Kiker, and C.W. Williams. *Phys. Rev.*, 137:B837–B847, 1965.

44. Harry R. Bowman, Stanley G. Thompson, J.C.D. Milton, and Wladyslaw Swiatecki. *Phys. Rev.*, 126:2120–2136, 1962.

45. www.gnuplot.org.

46. E. Cheifetz, Z. Fraenkel, J. Galin, M. Lefort, J. Péter, and X. Tarrago. *Phys. Rev. C*, 2(1):256–288, 1970.

47. Z. Fraenkel, I. Mayk, J. P. Unik, A. J. Gorski, and W. D. Loveland. *Phys. Rev. C*, 12(6):1809–1825, 1975.

48. X-5 Monte Carlo Team. *LA-UR-03-1987*, 2003.

49. I. Tilquin, Y. El Masri, M. Parlog, Ph. Collon, M. Hadri, Th. Keutgen, J. Lehmann, P. Leleux, P. Lipnik, A. Ninane, F. Hanappe, G. Bizard, D. Durand, P. Mosrin, J. Peter, R. Regimbart, and B. Tamain. *Nucl. Inst. Meth. A*, 365:446–461, 1995.

50. R.A. Cecil, B.D. Anderson, and R. Madey. *Nuclear Instruments and Methods*, 161(3):439–447, 1979.

51. M. Drosg. *Nuclear Instruments and Methods*, 105:573–584, 1972.

52. E.A. Serigina. *Measurements and Analysis of Angular-Energy Distribution for Cf-252(sf)*. PhD thesis, Obninsk, 1985.

53. Martin Karlsson. Master's thesis, Lund University, 1997.

54. Cyriel Wagemans, editor. *The Nuclear Fission Process*. CRC Press, 1990.

55. V.E. Viola, K. Kwiatkowski, and M. Walker. *Phys. Rev. C*, 31:1550–1552, 1985.

56. Kenneth S. Krane. *Introductory Nuclear Physics*. John Wiley & Sons, 1988.

57. William R. Leo. *Techniques for Nuclear and Particle Physics Experiments*. Springer-Verlag, 2 edition, 1994.

58. Philip R. Bevington and D. Keith Robinson. *Data Reduction and Error Analysis for the Physical Sciences*. McGraw-Hill, 3 edition, 2002.

59. Walter D. Loveland, David Morrissey, and Glenn T. Seaborg. *Modern Nuclear Chemistry*. Wiley-Interscience, 2001.

60. Jacob Gilat, Alain Fleury, Hughes Delegrange, and John M. Alexander. *Phys. Rev. C*, 16:694–705, 1977.

61. D.J. Hinde. personal communication.

62. P. Demetriou and S. Goriely. *Nuclear Physics A*, 695:95–108, 2001.

63. V.A. Rubchenya. *Physical Review C*, 75:054601, 2007.

64. O.V. et al. Grusha. *Izvestia Academii Nauk SSSR, Seriia Fizicheskiya*, 52:932–935, 1988.

65. Till von Egidy and Dorel Burcurescu. *Phys. Rev. C*, 72, 2005.

66. E. Erba, U. Facchini, and Saetta-Menichella E. *Nuovo Cimentio*, 22, 1961.

67. A.N. Behkami. *Phys. Rev. C*, 66, 2001.

68. http://www-nds.iaea.com/RIPL-2.

69. B. B. Back, H. C. Britt, Ole Hansen, B. Leroux, and J. D. Garrett. *Phys. Rev. C*, 10(5):1948–1965, 1974.

70. P. Moller, Arnold J. Sierk, Takatoshi Ichikawa, Akira Iwamoto, Ragnar Bengtsson, Henrik Uhrenholt, and Sven Aberg. *Phys. Rev. C*, 79, 2009.

APPENDICES

A Modelling

As stated in Section 1.4.4 the classical model of the competition between neutron emission and fission is

$$\frac{\Gamma_n}{\Gamma_f} = \frac{4A^{2/3}a_f(E^\star - B_n)}{K_0 a_n[2a_f^{1/2}(E^\star - B_f)^{1/2} - 1]} \exp[2a_n^{1/2}(E^\star - B_n)^{1/2} - 2a_f^{1/2}(E^\star - B_f)^{1/2}] \quad \text{(A.1)}$$

where

- a_f and a_n are the level density parameters for neutron emission and fission respectively. They were set equal to each other at the value $a = A/9.5$.
- B_n is the neutron binding energy calculated from [6].
- B_f is the fission barrier. The fission barriers for the nuclei in question in this work have been studied various times. A sample of the results are listed in Table 0.1. The average value was used in the modelling.
- A and E are the mass in amu and excitation energy of the nucleus.
- $K_0 = 12$ MeV [37]

Author	^{240}Np	^{239}Np	^{238}Np
Back *et al.*	-	5.85	6.0
RIPL-2	6.3	5.9	6.0
Moller *et al.*	6.01	5.57	5.36
average	6.15	5.77	5.79

TABLE 0.1: Fission barriers for nuclei relevant to this experiment. The barrier for the first saddle is listed first, the second saddle potential is second. The data are from [68, 69, 70]. Uncertainties for the data by Back *et al.* is given as ± 0.30 while the uncertainties for the other two data sets are not obvious.

A Monte Carlo approach was used due to the distribution of excitation energies present during the decay. The code can be found in Appendix C.7. The model was fairly straight forward and proceded by the following steps:

1. Generate an initial compound nucleus excitation energy. This was done by using Equation 1.2 for the fusion reaction. For the case where a pre-equilibrium neutron is emitted, the excitation energy can be calculated from Equation 1.6 using the fitted temperature. A kinetic energy for the neutron was created by first using a random number generator to create an energy between 0 and 10 MeV. The kinetic energy was kept if the next random number was less than the value of a Maxwellian at that energy. The kinetic energy of the recoil was much less than the distribution of neutron kinetic energies so it was assumed to be zero.

2. Determine Γ_n/Γ_f for calculated excitation energy and from that calculate the probability of fission. If a random number (between 0 and 1) is less than the probability for fission then the event fissions. Else it undergoes neutron decay.

3. If the nucleus undergoes neutron decay, calculate the temperature using $E^\star = (A/9.5)T^2$. Randomly choose a kinetic energy for the neutron using the calculated temperature as the slope parameter in a Maxwellian. Calculate the resulting excitation energy of the daughter nucleus using $E^\star_{A-1} = E^\star_A - B_{n,A} - 2T_n$.

4. Repeat until the nucleus is below both the neutron binding energy and the fission barrier.

One million events were used to ensure that the uncertainties due to the Monte Carlo process were minimal. The events that ended in fission (approximately 1/2) were sorted based on the particular path of the decay. For each path the temperature

of the neutron sources were determined by histogramming the events into 0.1 MeV wide bins and then fitting the histogram to a Maxwellian.

It was found that when the reaction would form a fully equilibriated ^{240}Np, the ^{240}Np would have a temperature of 0.97 MeV and the ^{239}Np would have a temperature of 0.78 MeV. A negligible amount of events emitted a third neutron and then fissioned.

The pre-equilibrium component was more difficult because of the requirement that the event underwent fission. Because of this the final excitation energy must be greater than 6 MeV or so. After the emission of the pre-equilibrium neutron, the maximum excitation energy of the nucleus is 17.9 MeV. Therefore, there is only 11.9 MeV available for the combination of kinetic energy for the pre-equilibrium neutron and the total (kinetic plus binding) energy of any equilibrium neutrons emitted. The binding energy of a neutron in a ^{239}Np nucleus is 6.2 MeV. *If* the ^{239}Np nucleus is to emit a neutron before fission, then the total kinetic energy available for the pre-equilibrium neutron and the equilibrium neutron is $11.9 - 6.2 = 5.7$ MeV. If the pre-equilibrium neutron has more kinetic energy then this, second chance fission *is not* possible. If the pre-equilibrium neutron has a kinetic energy less than this, second chance fission *is* possible.

There are therefore two components to the pre-equilibrium neutron spectrum: the component that results in first chance fission and the component that results in second chance fission. The component that results in 2nd chance fission is a select subset of the total pre-equilibrium events that have a small enough kinetic energy to allow for second chance fission. Therefore the measured temperature of the total pre-equilibrium spectrum is smaller than the real system because of this extra low temperature component. Using the simulation it was found that setting the pre-equilibrium neutron temperature at 3.15 MeV yielded a total temperature of 2.77 MeV.

Furthermore, as has already been stated the maximum kinetic energy of a pre-equilibrium neutron is 11.9 MeV. Since the maximum kinetic neutron kinetic energy cut−off was set at 10 MeV this 11.9 MeV cut−off was not observable in this experiment. The fitted magnitude of 0.492 assumes a full Maxwellian spectrum out to infinity. For a Maxwellian with T=2.77, 93% of the spectrum is below 11.9 MeV. Correcting for this, the total pre-equilibrium multiplicity is 0.458 $\pm$ 0.023.

B Figures and Data

B.1 Fission fragment Coincidences

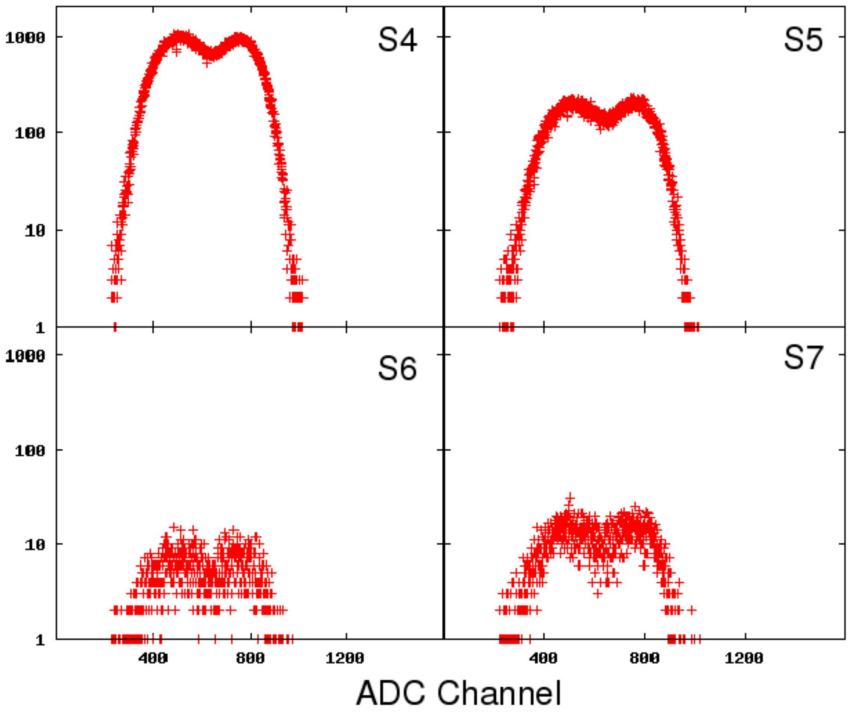

FIGURE 0.1: Good fission events in each strip detector coincident with a good fission event in S0.

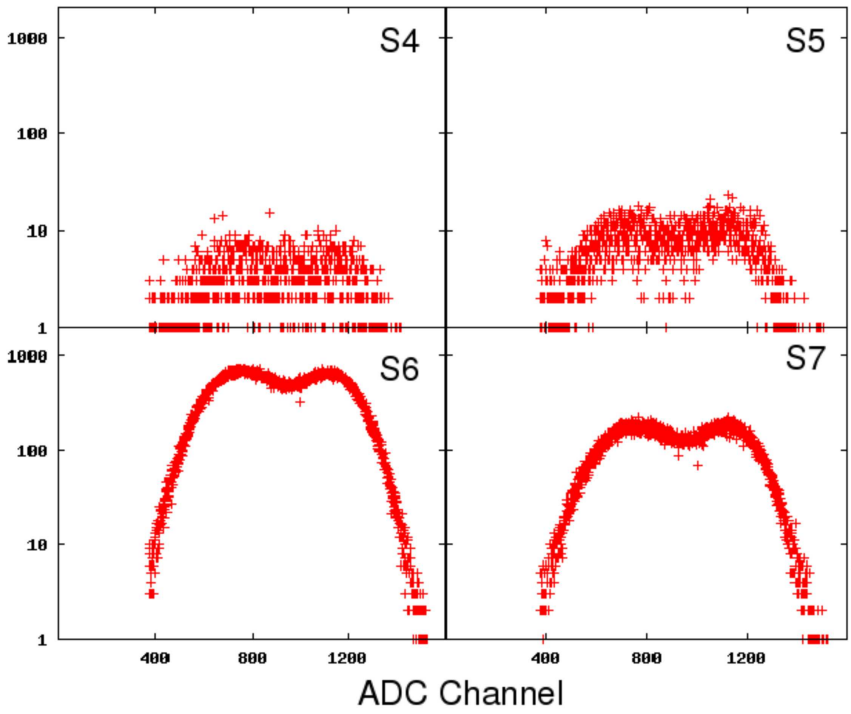

FIGURE 0.2: Good fission events in each strip detector coincident with a good fission event in S1.

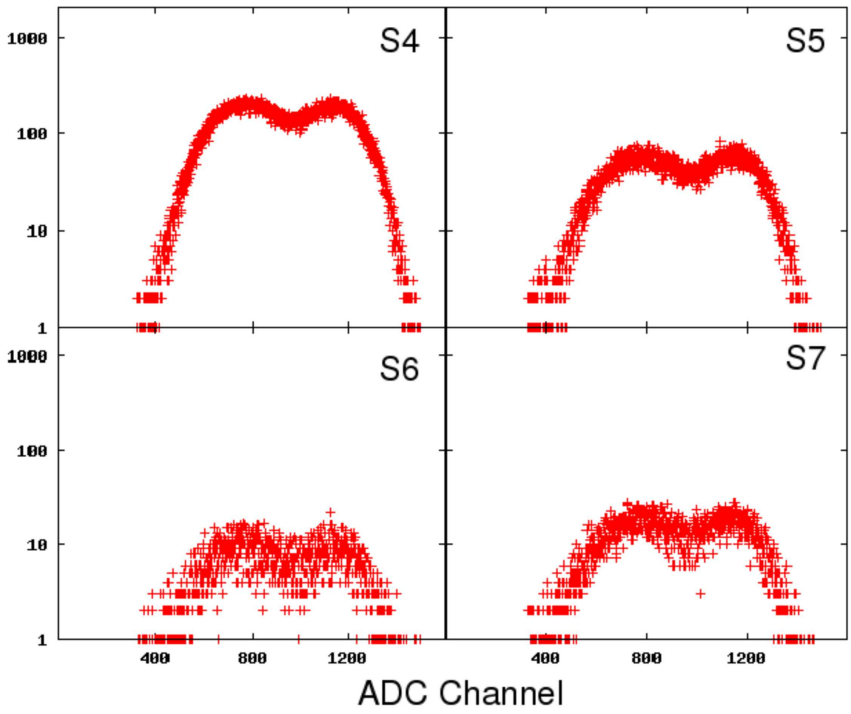

FIGURE 0.3: Good fission events in each strip detector coincident with a good fission event in S2.

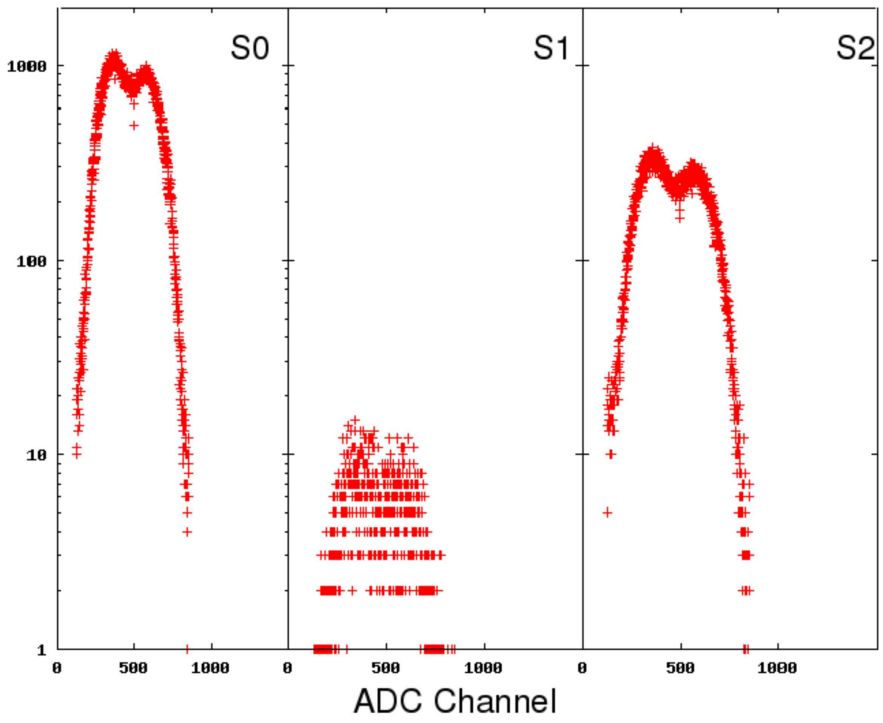

FIGURE 0.4: Good fission events in each forward array detector coincident with a good fission event in S4.

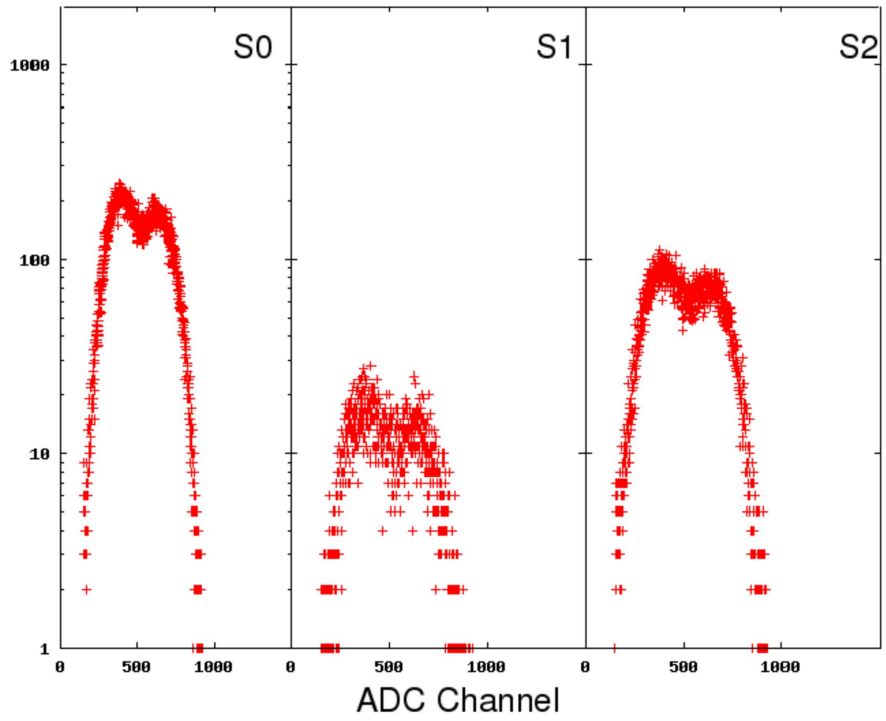

FIGURE 0.5: Good fission events in each strip detector coincident with a good fission event in S5.

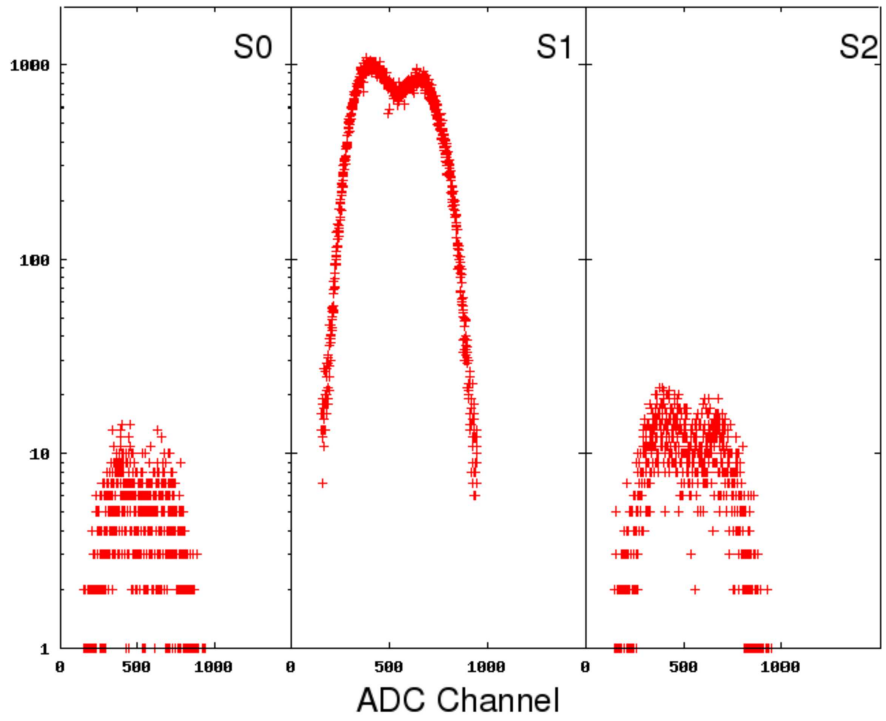

FIGURE 0.6: Good fission events in each strip detector coincident with a good fission event in S6.

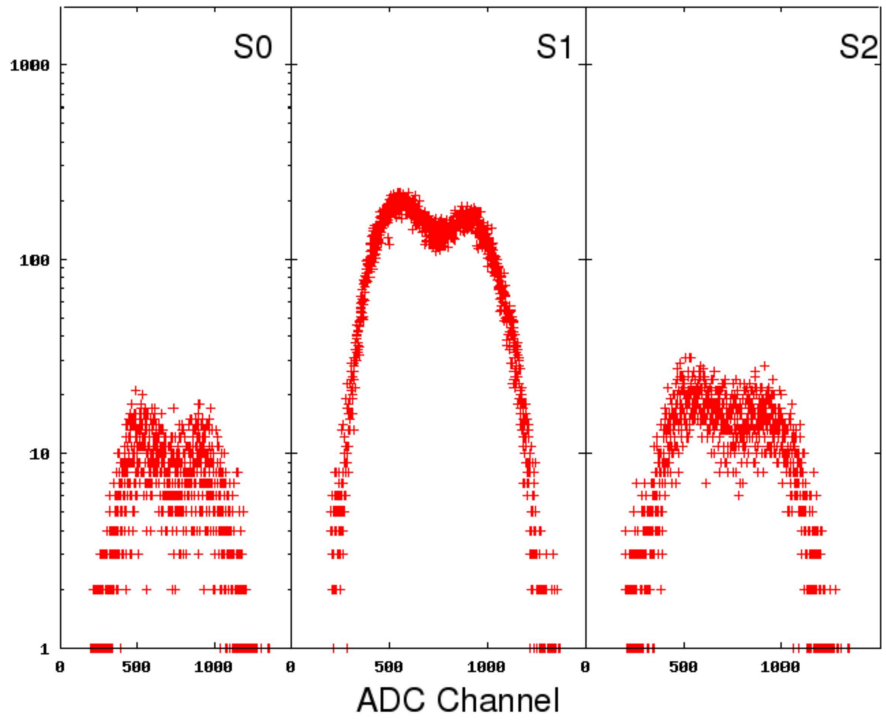

FIGURE 0.7: Good fission events in each strip detector coincident with a good fission event in S7.

B.2 Raw TDC Spectra

Below are the raw TDC spectra for each fission detector - neutron detector pair.

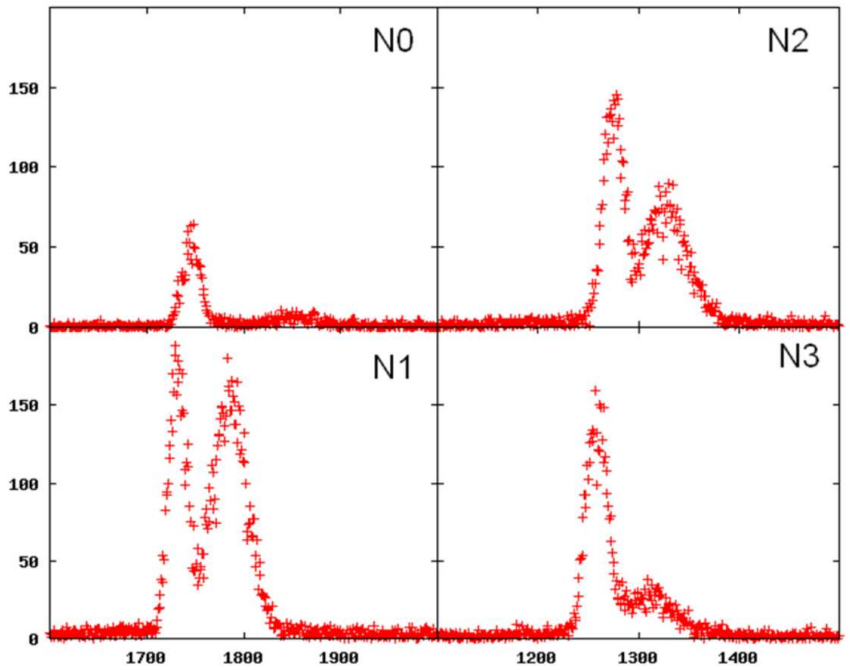

FIGURE 0.8: Raw TDC spectra for neutrons in coincidence with a fission in S0.

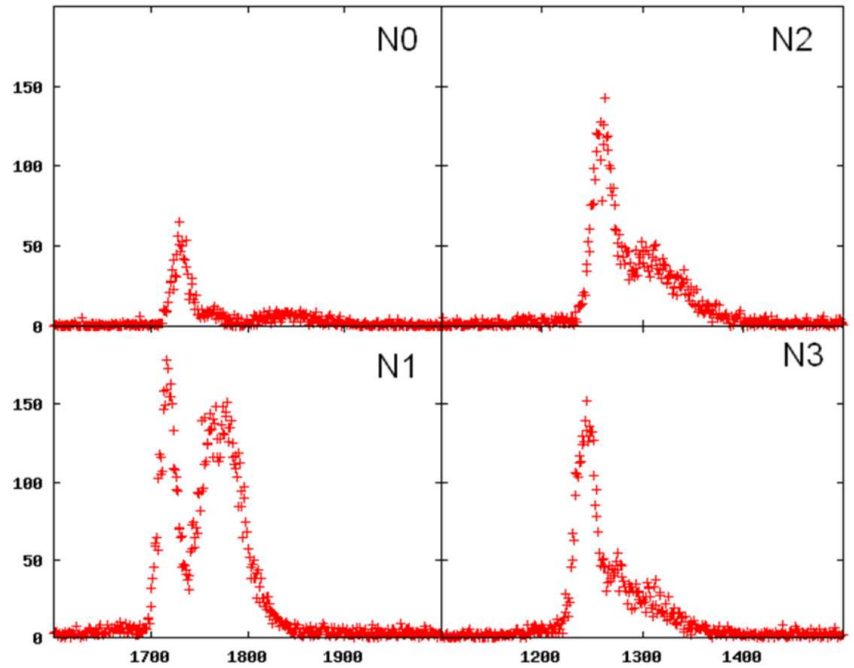

FIGURE 0.9: Raw TDC spectra for neutrons in coincidence with a fission in S1.

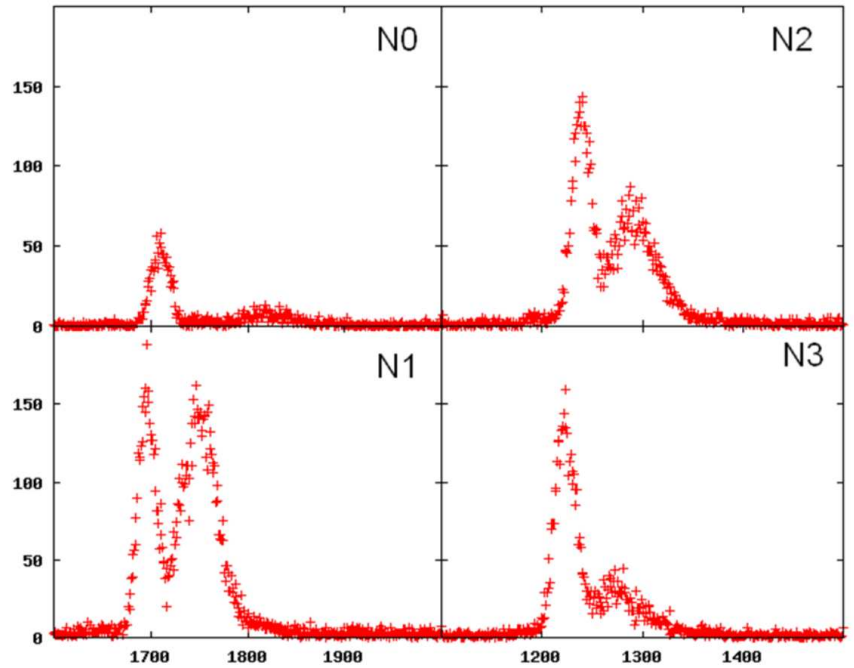

FIGURE 0.10: Raw TDC spectra for neutrons in coincidence with a fission in S2.

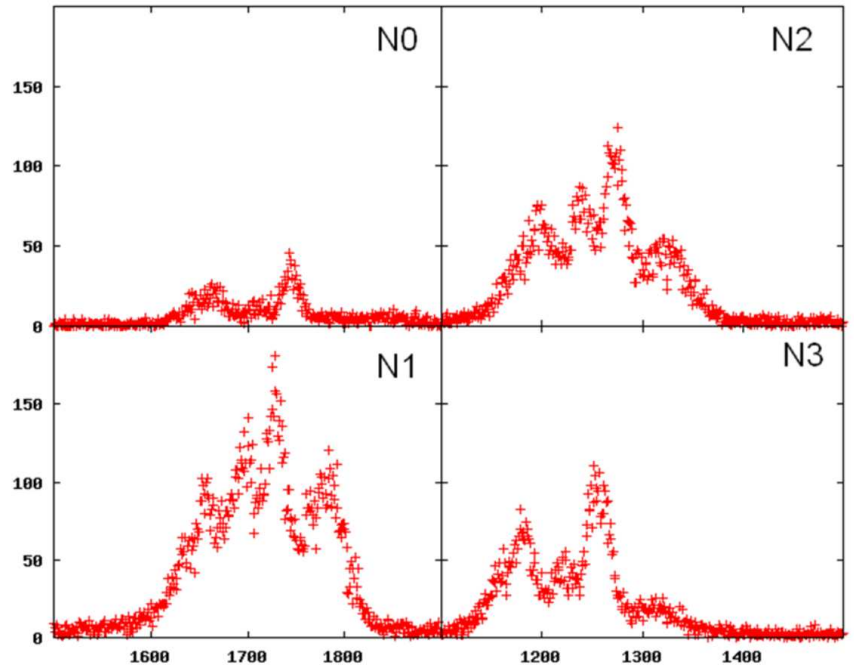

FIGURE 0.11: Raw TDC spectra for neutrons in coincidence with a fission in S4.

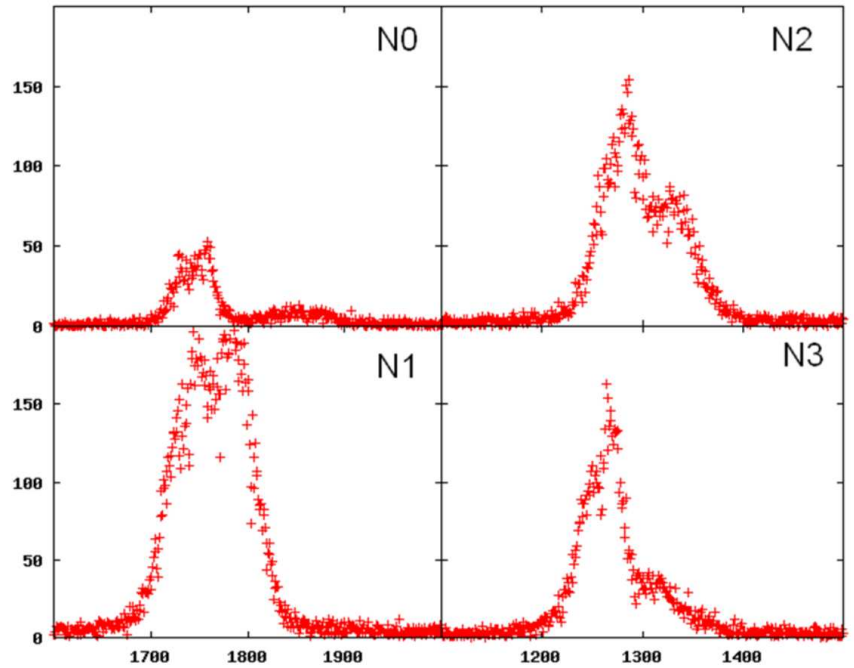

FIGURE 0.12: Raw TDC spectra for neutrons in coincidence with a fission in S5.

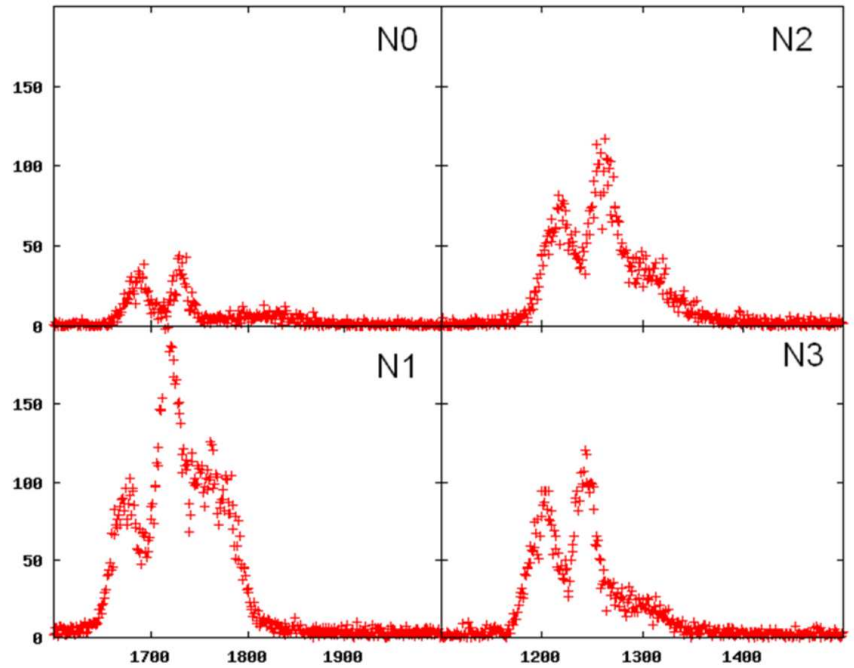

FIGURE 0.13: Raw TDC spectra for neutrons in coincidence with a fission in S6.

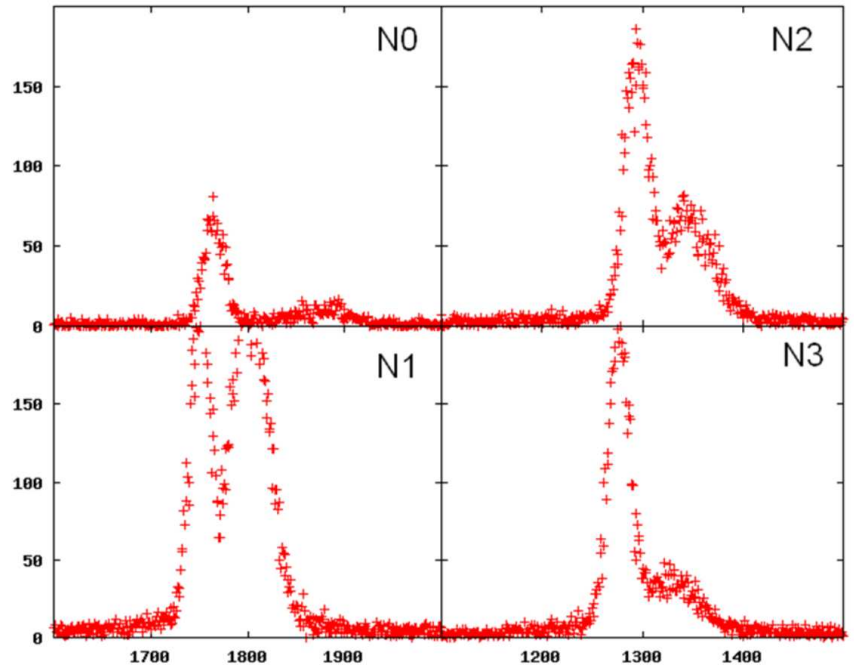

FIGURE 0.14: Raw TDC spectra for neutrons in coincidence with a fission in S7.

B.3 Neutron Data

Energy	S1N0	S2N0	S3N0	S7N0
1.25	0.09342±0.02412	0.18287±0.03543	0.16852±0.03404	0.13099±0.02569
1.75	0.06865±0.01206	0.08521±0.01397	0.08947±0.01468	0.10222±0.01495
2.25	0.04505±0.00811	0.05736±0.00958	0.05826±0.00984	0.05547±0.00865
2.75	0.03396±0.00649	0.03910±0.00709	0.05266±0.00894	0.03423±0.00587
3.25	0.02746±0.00553	0.02241±0.00482	0.02523±0.00530	0.02870±0.00507
3.75	0.01598±0.00394	0.01942±0.00436	0.02060±0.00462	0.01644±0.00347
4.25	0.01320±0.00350	0.01248±0.00335	0.01308±0.00352	0.01426±0.00314
4.75	0.01229±0.00334	0.00917±0.00284	0.01014±0.00306	0.00772±0.00222
5.25	0.00553±0.00224	0.00453±0.00204	0.00512±0.00220	0.00585±0.00193
5.75	0.00447±0.00203	0.00228±0.00156	0.00469±0.00210	0.00917±0.00245
6.25	0.00402±0.00194	0.00248±0.00158	0.00489±0.00214	0.00410±0.00163
6.75	0.00284±0.00166	-0.00054±-0.00064	-0.00040±-0.00068	0.00334±0.00148
7.25	0.00228±0.00150	0.00147±0.00128	0.00375±0.00188	0.00256±0.00131
7.75	0.00236±0.00151	0.00717±0.00259	0.00248±0.00156	0.00176±0.00111
8.25	0.00176±0.00132	0.00161±0.00126	0.00120±0.00116	0.00180±0.00111
8.75	0.00180±0.00132	0.00347±0.00178	0.00190±0.00136	0.00142±0.00100
9.25	0.00118±0.00109	0.00107±0.00104	0.00125±0.00112	0.00264±0.00132
9.75	0.00118±0.00105	-0.00004±-0.00055	0.00243±0.00148	0.00256±0.00130

TABLE 0.2: Neutron data from N0. Units are neutrons/(MeV·fission·steradian).

Energy	S1N1	S2N1	S3N1	S7N1
1.25	0.22262±0.02946	0.38275±0.04825	0.27881±0.03617	0.23633±0.03012
1.75	0.21256±0.02327	0.26609±0.02869	0.21159±0.02322	0.20629±0.02215
2.25	0.19985±0.02223	0.22025±0.02433	0.22309±0.02471	0.19894±0.02174
2.75	0.19668±0.02244	0.18416±0.02104	0.19131±0.02189	0.18970±0.02132
3.25	0.16234±0.01890	0.13899±0.01630	0.14885±0.01745	0.15091±0.01730
3.75	0.12993±0.01530	0.09571±0.01151	0.12946±0.01529	0.11236±0.01304
4.25	0.10249±0.01216	0.09197±0.01098	0.10328±0.01228	0.10720±0.01233
4.75	0.08703±0.01031	0.07494±0.00898	0.07477±0.00904	0.08828±0.01009
5.25	0.07545±0.00890	0.06818±0.00811	0.05664±0.00698	0.07649±0.00866
5.75	0.05922±0.00708	0.06053±0.00718	0.04969±0.00615	0.06772±0.00760
6.25	0.04765±0.00581	0.04334±0.00534	0.04311±0.00539	0.05986±0.00669
6.75	0.02829±0.00380	0.03592±0.00454	0.03359±0.00437	0.04215±0.00487
7.25	0.02829±0.00376	0.03564±0.00447	0.03108±0.00407	0.03543±0.00419
7.75	0.02349±0.00324	0.02358±0.00322	0.02348±0.00326	0.03227±0.00388
8.25	0.01955±0.00280	0.02630±0.00350	0.01911±0.00277	0.02067±0.00270
8.75	0.01281±0.00202	0.01264±0.00198	0.01310±0.00207	0.01837±0.00246
9.25	0.01073±0.00175	0.01020±0.00167	0.01225±0.00195	0.01373±0.00195
9.75	0.00995±0.00163	0.00855±0.00144	0.00784±0.00138	0.01029±0.00155

TABLE 0.3: Neutron data from N1. Units are neutrons/(MeV·fission·steradian).

Energy	S1N2	S2N2	S3N2	S7N2
1.25	0.16981±0.02134	0.14805±0.01890	0.17269±0.02241	0.12641±0.01577
1.75	0.15886±0.01889	0.11853±0.01452	0.16333±0.02003	0.12558±0.01473
2.25	0.14824±0.01784	0.07456±0.00972	0.12965±0.01636	0.09421±0.01142
2.75	0.13097±0.01598	0.05943±0.00797	0.11971±0.01524	0.06964±0.00871
3.25	0.10237±0.01275	0.04655±0.00645	0.08966±0.01172	0.05987±0.00758
3.75	0.08270±0.01048	0.04262±0.00594	0.06646±0.00896	0.04863±0.00628
4.25	0.04885±0.00662	0.03561±0.00508	0.05651±0.00774	0.03859±0.00510
4.75	0.05073±0.00677	0.02223±0.00350	0.05093±0.00703	0.03636±0.00481
5.25	0.04115±0.00564	0.02275±0.00352	0.03687±0.00534	0.02329±0.00331
5.75	0.03257±0.00463	0.02158±0.00334	0.02774±0.00422	0.02234±0.00317
6.25	0.02923±0.00421	0.01476±0.00250	0.02609±0.00399	0.01721±0.00256
6.75	0.01938±0.00304	0.01474±0.00246	0.02315±0.00360	0.01301±0.00205
7.25	0.01776±0.00281	0.01110±0.00198	0.01403±0.00244	0.00999±0.00166
7.75	0.01362±0.00228	0.00818±0.00157	0.00776±0.00159	0.00943±0.00157
8.25	0.01080±0.00189	0.00725±0.00141	0.01027±0.00188	0.00670±0.00120
8.75	0.00830±0.00153	0.00548±0.00114	0.00738±0.00146	0.00653±0.00116
9.25	0.00535±0.00110	0.00514±0.00106	0.00683±0.00134	0.00353±0.00073
9.75	0.00556±0.00109	0.00351±0.00079	0.00413±0.00092	0.00321±0.00066

TABLE 0.4: Neutron data from N2. Units are neutrons/(MeV·fission·steradian).

C Codes

C.1 Code used to determine the angle between two detectors.

Since the java programming language does not have an upper limit on line length, the codes below contain lines which are longer than allowed by the format of this thesis. The codes below were edited to take this into account. A line begining with a series of asterisks is a line that is continued.

```
import java.io.*;       //Location of PrintWriter
import java.util.*;     //Location of Random
import java.lang.*;     //Location of Math

public class solid_da2
{public static void main(String[] argv)
     throws IOException, FileNotFoundException
{

    int numevents=1000000,events=0,trials=0;
    //all lengths in cm

    //positions:
    double ds=10,rs=0.977;//distance to silicon and radius of silicon
    double dn=28.3,rn=3.75;//distance and radius of neutron detector
    double sw=0.625,sh=2.5;//width and height of strip
    double coss=ds/Math.sqrt(ds*ds+(sw*sw+sh*sh));//min z component
****required for striphit
    double cosn=dn/Math.sqrt(dn*dn+rn*rn);//min z component required
****for neuthit
    double theta;//angle between the two particles
    double ii=0;//variable in the for loop
```

```
    //counters and arrays
    //int silhits=0, neuthits=0;
    int angle[] = new int[181];

    //velocities:
    double xf,yf,zf,phif;//positions of the fission
    double xn,yn,zn,phin;//positions of the neut
    double xnr,znr;//positions of the neut after rotation

    String filename="nfg";
    boolean neuthit,silhit;
    long seed=16797;
    Random randnum = new Random();
    // To access next random double: randnum.nextDouble()
    // Double is between 0 and 1

for(int i=0;i<=10;i++)
{
    if(i==0){ii=169.8;filename="16980.csv";}
    if(i==1){ii=176.6;filename="17660.csv";}
    if(i==2){ii=124.9;filename="12490.csv";}
    if(i==3){ii=131.6;filename="13160.csv";}
    if(i==4){ii=138.4;filename="13840.csv";}
    if(i==5){ii=145.1;filename="14510.csv";}
    if(i==6){ii=79.6;filename="7960.csv";}
    if(i==7){ii=86.3;filename="8630.csv";}
    if(i==8){ii=93.1;filename="9310.csv";}
    if(i==9){ii=99.9;filename="9990.csv";}
    if(i==10){ii=90.0;filename="9000.csv";dn=48.3;}
```

```
/*/    if(i==2){ii=10.44;filename="1044.csv";}
    if(i==3){ii=10.59;filename="1059.csv";}
    if(i==4){ii=14.01;filename="1401.csv";}
    if(i==5){ii=20.62;filename="2062.csv";}
    if(i==6){ii=24.62;filename="2462.csv";}
    if(i==7){ii=31.23;filename="3123.csv";}
    if(i==8){ii=34.34;filename="3434.csv";}
    if(i==9){ii=34.8;filename="3480.csv";}
    if(i==10){ii=38.47;filename="3847.csv";}
    if(i==11){ii=41.29;filename="4129.csv";}
    if(i==12){ii=41.81;filename="4181.csv";}
    if(i==13){ii=45.55;filename="4555.csv";}
    if(i==14){ii=48.37;filename="4837.csv";}
    if(i==15){ii=48.89;filename="4889.csv";}
    if(i==16){ii=55.37;filename="5537.csv";}
    if(i==17){ii=55.83;filename="5583.csv";}
    if(i==18){ii=69.55;filename="6955.csv";}
    if(i==19){ii=76.16;filename="7616.csv";}
    if(i==20){ii=83.4;filename="8340.csv";}
    if(i==21){ii=90.48;filename="9048.csv";}
    if(i==22){ii=0.31;filename="031.csv";}
    if(i==23){ii=3.44;filename="344.csv";}*/

    double neutdetangle=ii*3.14159/180.;
    PrintWriter q = new PrintWriter(new FileOutputStream(filename),
*****true);
    events=0;trials=0;
//loop through for each trial
do
{
```

```
    trials++;
    //reset the positions
    xf=0;yf=0;xn=0;yn=0;neuthit=false;silhit=false;

    /****find the vectors **************/
    //find the x,y,z, vectors of the neutron
    zn=1-(1-cosn)*randnum.nextDouble();
    phin=2*3.14159*randnum.nextDouble();
    xn=Math.sqrt(1-zn*zn)*Math.cos(phin);
    yn=Math.sqrt(1-zn*zn)*Math.sin(phin);
    if(Math.sqrt(xn*xn+yn*yn)/zn<(rn/dn)){neuthit=true;}

    //finding the x,y,z vectors of the fission
    //make sure the particle will hit the silicon
    zf=1-(1-coss)*randnum.nextDouble();
    phif=2*3.14159*randnum.nextDouble();
    xf=Math.sqrt(1-zf*zf)*Math.cos(phif);
    yf=Math.sqrt(1-zf*zf)*Math.sin(phif);
    //need to check x & y positions of strip
    if(Math.abs(xf*(ds/zf))<sw)
    {
if(Math.abs(yf*(ds/zf))<sh)
    {
silhit=true;
    }
    }

    if(silhit==true && neuthit==true)
        {
    events++;
```

```
    //System.out.println(events);
    if(events==250000){System.out.println(events);}
    if(events==500000){System.out.println(events);}
    if(events==750000){System.out.println(events);}
    //first we need to rotate the neutron detector into place
    //rotation about the y axis
    xnr=xn*Math.cos(neutdetangle)+zn*Math.sin(neutdetangle);
    znr=-Math.sin(neutdetangle)*xn+Math.cos(neutdetangle)*zn;
            //find the angle between the angles using the dot product
    theta=180/3.14159*Math.acos(xnr*xf+yn*yf+znr*zf);
    angle[(int) theta]++;
}


}while(events<numevents);// end of do loop through trials
System.out.println(filename);
System.out.println("# trials: " + trials);
System.out.println("# events: " + events);
for(int j=0;j<=180;j++){q.println(angle[j]);angle[j]=0;}

}//end of for loop
}}//end of program
```

C.2 Fission fragment filtering code.

```
import java.io.*;
import java.util.*;
import java.text.NumberFormat;
public class cp283_new
{
public static void main(String[] argv)
throws java.io.IOException, java.text.ParseException
{

//******************** definitions ****************************///
//input variables
//the structure of the raw data file is
//c0 c1 c2 c4 c5 c6 c7 c12 c13 c14 c15 t0 t1 t2 t3
//The telescope data (c0 c1 & c2) is now irrelevant
//as are the silicon strip detectors (c12-c15) and c7
double fission[] = new double[8];// raw data for the fission events
double rawneut[] = new double[4];// raw data for the neutrons
int fi1=15,fi2=15; // fission detector index
int c4count=0,c5count=0,c6count=0,c7count=0,c12count=0,c13count=0,
*****c14count=0,c15count=0;
int goodc4count=0,goodc5count=0,goodc6count=0,goodc7count=0;
int goodc12count=0,goodc13count=0,goodc14count=0,goodc15count=0;

//conditions
boolean single=false;
boolean doublearray=false,doublestrip=false,nothinghit=false;
boolean random;

//intermediate variables
```

```
int index=0,channel;
int arraycount=0,stripcount=0;
int arraysingle=0,stripsingle=0,coincidenceevent=0,nothing=0;
int nans=0,nass=0,nads=0,nats=0,naqs=0;
int sans=0,sass=0,sads=0,sats=0,saqs=0;
int dans=0,dass=0,dads=0,dats=0,daqs=0;
int tans=0,tass=0,tads=0,tats=0,taqs=0;
int qans=0,qass=0,qads=0,qats=0,qaqs=0;
int da=0,ds=0,ta=0,ts=0,qa=0,qs=0;
String line="";

//input and output files
File infile = new File("run283.txt"); //file with the raw data
BufferedReader r = new BufferedReader(new FileReader(infile));
PrintWriter s = new PrintWriter(new FileOutputStream
*****("283singles_new.csv"),true);
s.println("index fi1 fi2 n0 n1 n2 n3");

//formatting objects
NumberFormat number = NumberFormat.getInstance();
//*************************************************************//

//*************************************************************//
//******* START READING EVENT BY EVENT **********************//
while(true)
{
index++;//System.out.println(index);
//if(index>2500000){break;}

single=false;arraycount=0;stripcount=0;fi1=15;fi2=15;
```

```
doublearray=false;doublestrip=false;nothinghit=false;
random=false;

line=r.readLine();
//check for "EOF" (End Of File)
if(line.charAt(0)=='E'&&line.charAt(1)=='O'&&line.charAt(2)=='F')
*****{break;}
if(line.charAt(0)=='"'&&line.charAt(1)=='E'&&line.charAt(2)=='O')
*****{break;}

//****** get the telescope, fission, and neut #'s ***********//
StringTokenizer tok = new StringTokenizer(line);
//Read the scope data
tok.nextToken();tok.nextToken();tok.nextToken();

//Read the fission fragment data
for(int i=0;i<=7;i++){fission[i]=number.parse(tok.nextToken()).
*****doubleValue();}

//Read the neutron data
for(int i=0;i<=3;i++){rawneut[i]=number.parse(tok.nextToken()).
*****doubleValue();}

//Check to see if the event is good
if(fission[0]>225 && fission[0]<1025){fi1=0;arraycount++;c4count++;}
if(fission[1]>375 && fission[1]<1525){fi1=1;arraycount++;c5count++;}
if(fission[2]>325 && fission[2]<1500){fi1=2;arraycount++;c6count++;}
if(fission[3]>325 && fission[3]<1325){fi1=3;arraycount++;c7count++;}
if(fission[4]>125 && fission[4]<850){fi2=4;stripcount++;c12count++;}
if(fission[5]>150 && fission[5]<925){fi2=5;stripcount++;c13count++;}
```

```
if(fission[6]>150 && fission[6]<950){fi2=6;stripcount++;c14count++;}
if(fission[7]>200 && fission[7]<1375){fi2=7;stripcount++;c15count++;}

// If there is only one hit in the array we're good
if(arraycount==2){doublearray=true;da++;}
if(stripcount==2){doublestrip=true;ds++;}
if(arraycount==3){doublearray=true;ta++;}
if(stripcount==3){doublearray=true;ts++;}
if(arraycount==4){doublearray=true;qa++;}
if(stripcount==4){doublearray=true;qs++;}
if((fi1==0 || fi1==2) && (fi2==6 || fi2==7)){random=true;}
if((fi1==1) && (fi2==4 || fi2==5)){random=true;}
if(arraycount==0 && stripcount==0){nothinghit=true;nothing++;}
if(arraycount==1 && stripcount==0){arraysingle++;}
if(arraycount==2 && stripcount==0){dans++;}
if(arraycount==3 && stripcount==0){tans++;}
if(arraycount==4 && stripcount==0){qans++;}
if(arraycount==0 && stripcount==1){stripsingle++;}
if(arraycount==1 && stripcount==1){coincidenceevent++;}
if(arraycount==2 && stripcount==1){dass++;}
if(arraycount==3 && stripcount==1){tass++;}
if(arraycount==4 && stripcount==1){qass++;}
if(arraycount==0 && stripcount==2){nads++;}
if(arraycount==1 && stripcount==2){sads++;}
if(arraycount==2 && stripcount==2){dads++;}
if(arraycount==3 && stripcount==2){tads++;}
if(arraycount==4 && stripcount==2){qads++;}
if(arraycount==0 && stripcount==3){nats++;}
if(arraycount==1 && stripcount==3){sats++;}
if(arraycount==2 && stripcount==3){dats++;}
```

```
if(arraycount==3 && stripcount==3){tats++;}
if(arraycount==4 && stripcount==3){qats++;}
if(arraycount==0 && stripcount==4){naqs++;}
if(arraycount==1 && stripcount==4){saqs++;}
if(arraycount==2 && stripcount==4){daqs++;}
if(arraycount==3 && stripcount==4){taqs++;}
if(arraycount==4 && stripcount==4){qaqs++;}



//********************** PRINTOUT ********************//
if(doublearray==false && doublestrip==false && nothinghit==false
***** && random==false && fi1 != 3)
{
if(fi1!=15)
{
s.println(index+" "+fi1+" "+rawneut[0]+" "+rawneut[1]
***** +" "+rawneut[2]+" "+rawneut[3]);
}
if(fi2!=15)
{
s.println(index+" "+fi2+" "+rawneut[0]+" "+rawneut[1]
***** +" "+rawneut[2]+" "+rawneut[3]);
}
if(fi1==0){goodc4count++;}
if(fi1==1){goodc5count++;}
if(fi1==2){goodc6count++;}
if(fi1==3){goodc7count++;}
if(fi2==4){goodc12count++;}
if(fi2==5){goodc13count++;}
if(fi2==6){goodc14count++;}
```

```
if(fi2==7){goodc15count++;}
}
//*********************************************************//
}//end of while loop
s.println("EOF");
s.close();
System.out.println("index="+index+" arraysingle="+arraysingle
***** +" stripsingle="+stripsingle);
System.out.println("coincidenceevent="+coincidenceevent
***** +" da="+da+" ds="+ds);
System.out.println("ta="+ta+" ts="+ts+" qa="+qa+" qs="+qs
***** +" nothing="+nothing);
System.out.println("nans="+nans+" nass="+nass+" nads="+nads
***** +" nats="+nats+" naqs="+naqs);
System.out.println("sans="+sans+" sass="+sass+" sads="+sads
***** +" sats="+sats+" saqs="+saqs);
System.out.println("dans="+dans+" dass="+dass+" dads="+dads
***** +" dats="+dats+" daqs="+daqs);
System.out.println("tans="+tans+" tass="+tass+" tads="+tads
***** +" tats="+tats+" taqs="+taqs);
System.out.println("qans="+qans+" qass="+qass+" qads="+qads
***** +" qats="+qats+" qaqs="+qaqs);
System.out.println("c4="+c4count+" goodc4="+goodc4count);
System.out.println("c5="+c5count+" goodc5="+goodc5count);
System.out.println("c6="+c6count+" goodc6="+goodc6count);
System.out.println("c7="+c7count+" goodc7="+goodc7count);
System.out.println("c12="+c12count+" goodc12="+goodc12count);
System.out.println("c13="+c13count+" goodc13="+goodc13count);
System.out.println("c14="+c14count+" goodc14="+goodc14count);
System.out.println("c15="+c15count+" goodc15="+goodc15count);
```

```
}}//EOP
```

C.3 Neutron filtering code.

```
import java.io.*;
import java.util.*;
import java.text.NumberFormat;
public class neuts283singles_new
{
public static void main(String[] argv)
throws java.io.IOException, java.text.ParseException
{

//****************** definitions ************************///
//input variables
//the structure of the raw data file is
//index fi1 t0 t1 t2 t3
int index=0,fi,event=0;
double neut[] = new double[4];

//neut
double eneutlab=0,tof=0,vneutlab=0,gammatime;
double n[][][] = new double[4096][8][4];
int ni=15;
double npc[] = new double [4];//npc = ns per channel
       npc[0]=0.1909;
       npc[1]=0.1962;
       npc[2]=0.1959;
       npc[3]=0.1939;

double centroids[][] = new double[4][4];//[fission][neut]
```

```
// variables used in convolution
double con,prob;
double tofdelta[][] = new double[4][4];//[fission][neut]
Boolean convoluted=false;

//conditions
Boolean goodneut=false,goodfission=true;
//intermediate variables and counters
int count=0;
String line="";
Random randnum = new Random();


//input and output files
File infile = new File("283singles_new.csv");
BufferedReader r = new BufferedReader(new FileReader(infile));
r.readLine();
PrintWriter p = new PrintWriter(new FileOutputStream
***** ("283neutsingles_new.csv"),true);
/*PrintWriter c4t0 = new PrintWriter(new FileOutputStream
***** ("283t0c4.csv"),true);
PrintWriter c4t1 = new PrintWriter(new FileOutputStream
***** ("283t1c4.csv"),true);
PrintWriter c4t2 = new PrintWriter(new FileOutputStream
***** ("283t2c4.csv"),true);
PrintWriter c4t3 = new PrintWriter(new FileOutputStream
***** ("283t3c4.csv"),true);
PrintWriter c5t0 = new PrintWriter(new FileOutputStream
***** ("283t0c5.csv"),true);
PrintWriter c5t1 = new PrintWriter(new FileOutputStream
```

```
***** ("283t1c5.csv"),true);
PrintWriter c5t2 = new PrintWriter(new FileOutputStream
***** ("283t2c5.csv"),true);
PrintWriter c5t3 = new PrintWriter(new FileOutputStream
***** ("283t3c5.csv"),true);
PrintWriter c6t0 = new PrintWriter(new FileOutputStream
***** ("283t0c6.csv"),true);
PrintWriter c6t1 = new PrintWriter(new FileOutputStream
***** ("283t1c6.csv"),true);
PrintWriter c6t2 = new PrintWriter(new FileOutputStream
***** ("283t2c6.csv"),true);
PrintWriter c6t3 = new PrintWriter(new FileOutputStream
***** ("283t3c6.csv"),true);
PrintWriter c12t0 = new PrintWriter(new FileOutputStream
***** ("283t0c12.csv"),true);
PrintWriter c12t1 = new PrintWriter(new FileOutputStream
***** ("283t1c12.csv"),true);
PrintWriter c12t2 = new PrintWriter(new FileOutputStream
***** ("283t2c12.csv"),true);
PrintWriter c12t3 = new PrintWriter(new FileOutputStream
***** ("283t3c12.csv"),true);
PrintWriter c13t0 = new PrintWriter(new FileOutputStream
***** ("283t0c13.csv"),true);
PrintWriter c13t1 = new PrintWriter(new FileOutputStream
***** ("283t1c13.csv"),true);
PrintWriter c13t2 = new PrintWriter(new FileOutputStream
***** ("283t2c13.csv"),true);
PrintWriter c13t3 = new PrintWriter(new FileOutputStream
***** ("283t3c13.csv"),true);
PrintWriter c14t0 = new PrintWriter(new FileOutputStream
```

```
***** ("283t0c14.csv"),true);
PrintWriter c14t1 = new PrintWriter(new FileOutputStream
***** ("283t1c14.csv"),true);
PrintWriter c14t2 = new PrintWriter(new FileOutputStream
***** ("283t2c14.csv"),true);
PrintWriter c14t3 = new PrintWriter(new FileOutputStream
***** ("283t3c14.csv"),true);*/
PrintWriter c15t0 = new PrintWriter(new FileOutputStream
***** ("283t0c15.csv"),true);
PrintWriter c15t1 = new PrintWriter(new FileOutputStream
***** ("283t1c15.csv"),true);
PrintWriter c15t2 = new PrintWriter(new FileOutputStream
***** ("283t2c15.csv"),true);
PrintWriter c15t3 = new PrintWriter(new FileOutputStream
***** ("283t3c15.csv"),true);
PrintWriter conout = new PrintWriter(new FileOutputStream
***** ("con.csv"),true);

p.println("index fi ni energy");

//formatting objects
NumberFormat number = NumberFormat.getInstance();
//*********************************************************//

//*** read in the neut peak centroids ***********************//
centroids[0][0]=1746.08;
centroids[0][1]=1731.53;
centroids[0][2]=1274.52;
centroids[0][3]=1258.18;
centroids[1][0]=1730.1;
```

```
centroids[1][1]=1717.04;
centroids[1][2]=1260;
centroids[1][3]=1243.66;
centroids[2][0]=1710.15;
centroids[2][1]=1695;
centroids[2][2]=1238.76;
centroids[2][3]=1223.3;
centroids[3][0]=1764;
centroids[3][1]=1750.4;
centroids[3][2]=1293.2;
centroids[3][3]=1276.3;
//****** read in the gamma peak widths *************************//
tofdelta[0][0]=1.83;
tofdelta[0][1]=1.90;
tofdelta[0][2]=1.96;
tofdelta[0][3]=2.14;
tofdelta[1][0]=1.53;
tofdelta[1][1]=1.59;
tofdelta[1][2]=1.85;
tofdelta[1][3]=1.70;
tofdelta[2][0]=1.86;
tofdelta[2][1]=1.78;
tofdelta[2][2]=1.80;
tofdelta[2][3]=1.95;
tofdelta[3][0]=2.12;
tofdelta[3][1]=2.04;
tofdelta[3][2]=2.33;
tofdelta[3][3]=1.92;

for(int i=0;i<4096;i++)
```

```
{
for(int j=0;j<8;j++)
{
for(int k=0;k<4;k++){n[i][j][k]=0;}
}
}

//******* START READING EVENT BY EVENT ************************//
while(true)
{
event++;//System.out.println(index);
goodneut=true;goodfission=true;
ni=15;count=0;gammatime=29.0/30.0;
eneutlab=0;vneutlab=0;tof=0;
line=r.readLine();
//Check for EOF (End Of File)
if(line.charAt(0)=='E'&&line.charAt(1)=='O'&&line.charAt(2)=='F')
***** {break;}
if(line.charAt(0)=='"'&&line.charAt(1)=='E'&&line.charAt(2)=='O')
***** {break;}

//********** get the fission, and neut #'s ***************//
StringTokenizer tok = new StringTokenizer(line);
index=number.parse(tok.nextToken()).intValue();
fi=number.parse(tok.nextToken()).intValue();
for(int i=0;i<=3;i++){neut[i]=number.parse(tok.nextToken()).
***** doubleValue();}

//Make sure the fission is good
if(fi>2 && fi<7){goodfission=false;}
```

```
if(fi==7){fi=3;}

if(goodfission==true)
{
//*************************************************************//
//******************* THE NEUTRON ***************************//
for(int i=0;i<=3;i++)//loop through the four detectors
{
goodneut=true;convoluted=false;
ni=i;
if(neut[ni]>0 && fi==3){n[(int) neut[ni]][fi][ni]++;}
//if(neut[ni]>0 && fi2<15){n[(int) neut[ni]][fi2][ni]++;}

if(neut[ni]<centroids[fi][ni]){goodneut=false;}

if(goodneut==true)
{
if(index==316){System.out.println(ni);}
count++;
gammatime=29/30;
if(ni==0){gammatime=49/30;}
tof=npc[ni]*((neut[ni]+randnum.nextDouble())
***** -centroids[fi][ni])+gammatime;

// Need to convolute the tof
do
{
// pick a delta tof at random that is within 3 sigma of zero
// then determine the relative probability of this delta tof
con=3*tofdelta[fi][ni]*(2*randnum.nextDouble()-1.0);
```

```
prob=Math.exp(-0.5*(con*con)/(tofdelta[fi][ni]*tofdelta[fi][ni]));
if(randnum.nextDouble()<prob)
{
tof=tof+con;
convoluted=true;
}
}while(convoluted == false);
if(fi==0 && ni==1){conout.println(con);}

vneutlab=28.3/tof;
if(ni==0){vneutlab=48.3/tof;}
eneutlab=0.5*939.6/900*vneutlab*vneutlab;
// if the energy is too low or too high, exclude it
if(eneutlab<0.75 || eneutlab>10.75){goodneut=false;}
//  PRINTOUT
if(goodneut==true)
{
p.println(index+" "+fi+" "+ni+" "+eneutlab);
}
}//end of goodneut if*/
}//end of for loop through detectors
}//end of good fission
}//end of while loop1


for(int i=0;i<4095;i++)
{
/*c4t0.println(i+" "+n[i][0][0]);
c5t0.println(i+" "+n[i][1][0]);
c6t0.println(i+" "+n[i][2][0]);
```

```
c12t0.println(i+" "+n[i][4][0]);
c13t0.println(i+" "+n[i][5][0]);
c14t0.println(i+" "+n[i][6][0]);*/
//c15t0.println(i+" "+n[i][3][0]);
//c4t1.println(i+" "+n[i][0][1]);
//c5t1.println(i+" "+n[i][1][1]);
//c6t1.println(i+" "+n[i][2][1]);
//c12t1.println(i+" "+n[i][4][1]);
//c13t1.println(i+" "+n[i][5][1]);
//c14t1.println(i+" "+n[i][6][1]);
//c15t1.println(i+" "+n[i][3][1]);
//c4t2.println(i+" "+n[i][0][2]);
//c5t2.println(i+" "+n[i][1][2]);
//c6t2.println(i+" "+n[i][2][2]);
//c12t2.println(i+" "+n[i][4][2]);
//c13t2.println(i+" "+n[i][5][2]);
//c14t2.println(i+" "+n[i][6][2]);
//c15t2.println(i+" "+n[i][3][2]);
//c4t3.println(i+" "+n[i][0][3]);
//c5t3.println(i+" "+n[i][1][3]);
//c6t3.println(i+" "+n[i][2][3]);
//c12t3.println(i+" "+n[i][4][3]);
//c13t3.println(i+" "+n[i][5][3]);
//c14t3.println(i+" "+n[i][6][3]);
//c15t3.println(i+" "+n[i][3][3]);
}

p.println("EOF");
p.close();
}}//EOP
```

C.4 Neutron Detector Geometrical Correction code

This code generates the function W(θ) which is the probability (or the weight) of a neutron interacting with a detector at an angle θ. The code works by randomly generating a trajectory and then calculating the detector depth at that trajectory. The deepest trajectory occurs at angle θ_C which has magnitude of

$$d = \frac{8}{cos(\theta_C)} = 8.051cm \tag{C.1}$$

The calculated trajectory is then divided by 8.051 which yields a number between 0 and 1. A random number is then generated between 0 and 1 and if the random number is smaller than the distance fraction a neutron hit is registered. The angle between the fission fragment and the neutron is then calculated and binned. 100,000 events were recorded for each neutron detector placement in order to ensure a smooth angular distribution curve. This spectrum was then normalized to an area of one. Note that the correction is energy independent because the ratio of time spent in the detector between two angles is constant regardless of the velocity.

```
import java.io.*;       //Location of PrintWriter
import java.util.*;     //Location of Random
import java.lang.*;     //Location of Math

public class solid_neutcal
{public static void main(String[] argv)
     throws IOException, FileNotFoundException
{

    int numevents=100000,events=0,trials=0;
    //all lengths in cm

    //positions:
    double ds=10.5,rd=0.977;//distance to silicon and radius of
***** silicon
    double dn=25,rn=3.75,thetan,noffset=16.25*3.14159/180.;//thetan
```

```
***** is the angle of incidence into the det
    double theta;//angle between the two detectors

    //counters and arrays
    int silhits=0, neuthits=0;
    int spectra[] = new int [91];
    for(int i=0;i<=90;i++){spectra[i]=0;}

    //velocities:
    double xf,yf,zf,phif;//positions of the fission
    double xn,yn,zn,phin;//positions of the neut
    double xnr,znr;//positions of the neut after rotation

    long seed=16797;
    Random randnum = new Random();
    boolean fission=false,neutron=false;
    boolean silhit=false,neuthit=false;
    // To access next random double: randnum.nextDouble()
    // Double is between 0 and 1

    PrintWriter q = new PrintWriter(new FileOutputStream
***** ("MC16.25.csv"),true);



//loop through for each trial
do
{
    trials++;
    //reset the positions and booleans
    xf=0;yf=0;xn=0;yn=0;fission=true;neutron=false;theta=0;
```

```
    silhit=false;neuthit=false;

    /****find the vectors ***************/
    //finding the x,y,z vectors of the fission
    //restricted to positive z, and it should hit a fission detector
    zf=randnum.nextDouble()/1000.0+0.995;
    phif=2*3.14159*randnum.nextDouble();
    xf=Math.sqrt(1-zf*zf)*Math.cos(phif);
    yf=Math.sqrt(1-zf*zf)*Math.sin(phif);

    //find the x,y,z, vectors of the neutron
    zn=randnum.nextDouble();
    phin=2*3.14159*randnum.nextDouble();
    xn=Math.sqrt(1-zn*zn)*Math.cos(phin);
    yn=Math.sqrt(1-zn*zn)*Math.sin(phin);


    // now see if the fission hits the detectors
    // we want tan(theta_particle)<tan(theta_detector)
    if(Math.sqrt(xf*xf+yf*yf)/zf<(rd/ds))
{
    silhits++;
    silhit=true;
}
    //neuts are harder because they need to be weighted do to the
***** trajectory
    //into the detector

    thetan=Math.atan(Math.sqrt(xn*xn+yn*yn)/zn);
```

```
    if(thetan<Math.atan(rn/dn))// if it impinges on the detector
***** surface
        {    //It is normalized to the trajectory of a neutron
***** leaving the corner
    //this distance is 8/Math.cos(6.48)=8.05144
    if(thetan<Math.atan(rn/(dn+8)))// if it is heading out
***** the back
{
    if((8*Math.cos(thetan)/8.05144)>randnum
***** .nextDouble())
{
    neuthits++;
    neuthit=true;
}
}
    else // if the neutron goes out the side
        {
    if(((3.75/Math.tan(thetan)-25)/8.05144*
***** Math.cos(thetan))>randnum.nextDouble())
        {
    neuthits++;
    neuthit=true;
}
}
}



    if(silhit==true && neuthit==true)
        {
    events++;
```

```
    if(events==1000){System.out.println(events);}
            if(events==25000){System.out.println(events);}
    if(events==50000){System.out.println(events);}
    if(events==75000){System.out.println(events);}
    //first we need to rotate the neutron detector into place
    xnr=xn*Math.cos(noffset)+zn*Math.sin(noffset);
    znr=-Math.sin(noffset)*xn+Math.cos(noffset)*zn;
    //find the angle between the angles using the dot product
    thetan=180/3.14159*Math.atan(Math.sqrt(xnr*xnr+yn*yn)/znr);
    theta=180/3.14159*Math.acos(xnr*xf+yn*yf+znr*zf);
    spectra[(int) theta]++;
}


}while(events<numevents);// end of do loop through trials

System.out.println("# trials: " + trials);
System.out.println("# events: " + events);
System.out.println("# silhits: " + silhits);
System.out.println("# neuthits: " + neuthits);
for(int i=0;i<=90;i++){if(spectra[i]>0)
***** {q.println(i+" "+spectra[i]);}}
}}//end of program
```

C.5 MCNPX input file

```
 c    Cell Cards
1    0        -1           imp:n=1      $ before the block
2    1 -2.7   1 -2         imp:n=1      $ in the block
3    0        2 -3         imp:n=1      $ after the block
4    1 -2.7   3 -4         imp:n=1      $ in the dome
5    0        4            imp:n=0      $ after the dome

c    Surface Cards
1    SO 10.5      $inside edge of block
2    SO 11.77     $outside edge of block
3    SO 20.3      $inside edge of dome
4    SO 20.64     $outside edge of dome

c    Material Cards & source cards
m1   013027 1     $aluminum
mode n
phys:n 15
sdef erg=5 vec=0 0 1 dir=1 par=n
F16:n 2  $energy deposited in block
E16  0.001 6
F26:n 4  $energy deposited in dome
E26  0.001 6
nps  100000
```

C.6 χ^2 Minimization Code

```
// code calculates the chi square of the
// Bowman data using Isaev's equations

import java.io.*;
import java.util.*;
import java.text.*;

public class minimize
{
public static void main(String[] argv)
throws java.io.IOException, java.text.ParseException
{
//multiplicities and temperatures
double Tf,Tcn,Tcn1,Tcn2,Tcn3,Tpre;
double mh,ml,mf,mcn,mcn1,mcn2,mcn3,mpre;
double Tfmin=10,Tcnmin=10,Tpremin=10;
double mhmin=10,mlmin=10,mfmin=10,mcnmin=10,mcn1min=10,
***** mcn2min=10,mcn3min=10,mpremin=10;
double ehmin=10,elmin=10;

//chisquared variable
double wssr=0,minwssr=1000000000;
double diff,function;
int goodpoint,goodpointmin=300;

// kinematics, solid angles, and contributions of the fragments
double lff,lfb,lf;//the light fragment components
double hff,hfb,hf;//the heavy fragment components
double cm,cm1,cm2,cm3,pe,pre;//the cm & pre-equilibrium components
```

```
double elab,elf,elb,ehf,ehb,epe;//lab & cm energy of the neutron
double eh=0.51,el=1.01,epre=1.86;//kinetic energies of the light
***** and heavy fragments/nucleon
             //TKE = 173 from Viola systematics and Ah=140, Al=100
double Ah,Al;//masses of the two fragments
double costheta,cospre;

//other control variables
boolean badpoint=false;
int minenergy=3,maxenergy=16;
int minneutdet=0,maxneutdet=3;
int minfissdet=0,maxfissdet=3;
int angle=15;
String line="",line2="";
NumberFormat number = NumberFormat.getInstance();
DecimalFormat dec = new DecimalFormat("0.0000");
DecimalFormat dec2 = new DecimalFormat("0000.00");
//PrintWriter o = new PrintWriter(new FileOutputStream
***** ("outputlog.csv"),true);

// ARRAY DEFINITIONS
//************************
// data[neutdet][fissdet][energy][quantity]
// where the actual data is stored
// neutdet: t0->0, t1->1, ...
// fissdet: c4->0, c5->1, c6->2, c15->3
// quantity: counts -> 0, uncertainty -> 1
double data[][][][] = new double[4][4][20][2];
BufferedReader datareader = new BufferedReader(new FileReader
***** (new File("alldata.csv")));
```

```
BufferedReader errorreader = new BufferedReader(new FileReader
***** (new File("alldata_errors.csv")));
datareader.readLine();//read the titles line
errorreader.readLine();//read the titles line

for(int j=0;j<16;j++)
{
line=datareader.readLine();
line2=errorreader.readLine();
StringTokenizer tok = new StringTokenizer(line);
StringTokenizer tok2 = new StringTokenizer(line2);
for(int i=0;i<4;i++)
{
for(int k=0;k<4;k++)
{
data[i][k][j][0]=number.parse(tok.nextToken())
***** .doubleValue();
data[i][k][j][1]=number.parse(tok2.nextToken())
***** .doubleValue();
//System.out.print(dec.format(data[i][k][j][0])+" ");
}
}
}//System.out.print("\n");}

//**********************************
//fractions data
//fractions[energy][angle][lff,lfb,hff,hfb]
double fraction[][][] = new double[20][8][4];
BufferedReader fractionreader = new BufferedReader
***** (new FileReader(new File("omegas130.csv")));
```

```
fractionreader.readLine();//read the titles line
for(int j=0;j<8;j++)//angles
{
for(int i=0;i<20;i++)//energies
{
line=fractionreader.readLine();
StringTokenizer tok = new StringTokenizer(line);
for(int k=0;k<4;k++)
{
fraction[i][j][k]=number.parse
***** (tok.nextToken()).doubleValue();
//System.out.print(fraction[i][j][k]+" ");
}
//System.out.print("\n");
}
}

//END OF DATA ARRAY INITIALIZATION
//************************************************************

minenergy=0;maxenergy=15;
minneutdet=0;maxneutdet=2;
minfissdet=0;maxfissdet=3;

////////////////////////////////////////////////////////////
//o.println("mcn mf");
for(int q1=0;q1<=0;q1++){
for(int q2=0;q2<=0;q2++){
for(int q3=0;q3<=0;q3++){
for(int q4=0;q4<=0;q4++){
```

```
for(int q5=0;q5<=0;q5++){
for(int q6=0;q6<=0;q6++){
for(int q7=0;q7<=0;q7++){
if(q3==0 && q4==0 && q5==0 && q6==0 && q7==0)
{System.out.println("q's="+q1+" "+q2);}

//mcn1=q1/100.0+0.0;
//mcn2=q2/100.0+0.0;
//mcn3=q3/100.0+0.0;
//if(mcn2<=mcn1 && mcn3<=mcn2)
//el=q2/100.0+0.52;
//eh=q3/100.0+0.52;
//if(eh<=el)
{
mcn=q1/100.0+0.0;
//mcn2=q2/100.0+0.0;
ml=q5/100.0+2.26;
mh=q4/100.0+2.26;
Tcn=q5/100.0+0.50;
Tf=q6/100.0+1.27;
//Tpre=q7/100.0+0.23;
//Tcn1=0.873;//Bn = 5.06
//Tcn2=0.733;//Bn = 6.2
//Tcn3=0.53;//Bn = 5.49

//ml=mf/2.0;
//mh=mf/2.0;

wssr=0;
goodpoint=0;
```

```
////////////////////////////////////////////////////////////////
//Loop through angles and energies to find each each data point
for(int neutdet=minneutdet;neutdet<=maxneutdet;neutdet++)
// loop through neutron detectors
{
for(int fissdet=minfissdet;fissdet<=maxfissdet;fissdet++)
// loop through fission detectors
{
costheta=0.139;angle=3;//most common angle
if((neutdet==1&&fissdet==0)||(neutdet==1&&fissdet==1)||
***** (neutdet==1&&fissdet==2)){costheta=0.978;angle=0;}
if((neutdet==2&&fissdet==0)||(neutdet==2&&fissdet==2))
***** {costheta=0.799;angle=1;}
if(neutdet==2&&fissdet==1){costheta=0.588;angle=2;}
if(neutdet==0&&fissdet==3){costheta=0.0;angle=4;}
if((neutdet==0&&fissdet==2)||(neutdet==3&&fissdet==1)||
***** (neutdet==3&&fissdet==3)){costheta=-0.139;angle=5;}
if(neutdet==2&&fissdet==3){costheta=-0.558;angle=6;}
if(neutdet==1&&fissdet==3){costheta=-0.978;angle=7;}
if(neutdet==3&&fissdet==3){costheta=0.187;}

cospre=-2;
if(neutdet==0){cospre=0;}
if(neutdet==1){cospre=0.866;}
if(neutdet==2){cospre=0.259;}
if(neutdet==3){cospre=-0.5;}
if(cospre==-2){System.out.println("bad pre");}

for(int j=minenergy;j<=maxenergy;j++)// loop through energies
```

```
{
badpoint=false;
/// eliminate single bad data points
if(neutdet==0 && (fissdet == 1 && (j==13 || j==15))){badpoint=true;}
if(neutdet==0 && (fissdet == 2 && j==11)){badpoint=true;}
if(neutdet==0 && (fissdet == 3 && j==9)){badpoint=true;}
//if(neutdet==1 && fissdet==3){badpoint=true;}

if(badpoint==false)
{
elab=j/2.0+1.25;
//System.out.println(elab+" "+data[neutdet][fissdet][j][0]+" "
***** +data[neutdet][fissdet][j][1]);
elf=elab+el-2*costheta*Math.sqrt(elab*el);
elb=elab+el+2*costheta*Math.sqrt(elab*el);
ehf=elab+eh-2*costheta*Math.sqrt(elab*eh);
ehb=elab+eh+2*costheta*Math.sqrt(elab*eh);
epe=elab+epre-2*cospre*Math.sqrt(elab*epre);

//the light component is forward
lff=Math.exp(-elf/Tf);//*fraction[j][angle][0];
hfb=Math.exp(-ehb/Tf);//*fraction[j][angle][3];
// half of the time the light fragment
// is forward hence the factor of 0.5
lf=0.5*0.09*ml/(Math.pow(Tf,1.5))*Math.sqrt(elab)*(lff+hfb);
//if(i==minangle && j==0){System.out.println(vl+" "+exp1+" "
***** +exp2+" "+exp3+" "+rhol);}

//the heavy component is forward
hff=Math.exp(-ehf/Tf);//*fraction[j][angle][2];
```

```
lfb=Math.exp(-elb/Tf);//*fraction[j][angle][1];
hf=0.5*0.09*mh/(Math.pow(Tf,1.5))*Math.sqrt(elab)*(hff+hfb);
//if(i==minangle && j==0){System.out.println(vh+" "+exp1
***** +" "+exp2+" "+exp3+" "+rhoh);}

//the cm component
cm=0.09*mcn/Math.pow(Tcn,1.5)*Math.sqrt(elab)*Math.exp(-elab/Tcn);
//cm1=0.08*mcn1/(Tcn1*Tcn1)*elab*Math.exp(-elab/Tcn1);
//cm2=0.08*mcn2/(Tcn2*Tcn2)*elab*Math.exp(-elab/Tcn2);
//cm3=0.08*mcn3/(Tcn3*Tcn3)*elab*Math.exp(-elab/Tcn3);
//cm1=0.09*mcn1/Math.pow(Tcn1,1.5)*Math.sqrt(elab)*Math.exp(-elab/Tcn1);

//the pre-equilibrium component
//pe=Math.exp(-epe/Tpre);
//pre=0.08*mpre/(Tpre*Tpre)*elab*pe;

//least squares value
function=cm+hf+lf;
diff=(function-data[neutdet][fissdet][j][0]);
if((data[neutdet][fissdet][j][0]-data[neutdet][fissdet][j][1])
***** <function && (data[neutdet][fissdet][j][0]
***** +data[neutdet][fissdet][j][1])>function)
{
goodpoint++;
}

// Determine the WSSR
wssr=wssr+diff*diff/(data[neutdet][fissdet][j][1]*
***** data[neutdet][fissdet][j][1]);
//if(i==minangle && j==1){System.out.println(wssr);}
```

```
if(data[neutdet][fissdet][j][1]*data[neutdet][fissdet][j][1]
***** < 0.0000001){System.out.println(elab+" "+neutdet+" "
***** +fissdet+" "+q1+" "+q4+" "+q5+" "+q6);}

}//End loop through good points
}}}//End of loop through detectors and energies

////////////////////////////////////////////////////////////////
//out[q1][q2]=wssr;
if(wssr<minwssr)
{
minwssr=wssr;
goodpointmin=goodpoint;
ehmin=eh;
elmin=el;
//Tcnmin=Tcn;
Tfmin=Tf;
        mhmin=mh;
mlmin=ml;
mcnmin=mcn;
//mfmin=mf;
//mcn1min=mcn1;
//mcn2min=mcn2;
//mcn3min=mcn3;
//mpremin=mpre;
//Tpremin=Tpre;
System.out.print(dec2.format(wssr)+" ");
//System.out.print(dec.format(mcn1)+" "+dec.format(mcn2)
***** +" "+dec.format(mcn3)+" ");
System.out.print(dec.format(mcn)+" ");
```

```
System.out.print(dec.format(ml)+" "+dec.format(mh)+" ");
//System.out.print(dec.format(mpre)+" ");
//System.out.print(dec.format(mf)+" ");
System.out.print(dec.format(Tcn)+" ");
System.out.print(dec.format(Tf)+" ");
//System.out.print(dec.format(Tpre)+" ");
//System.out.print(dec.format(eh)+" "+dec.format(el));
System.out.print("\n");
//o.println(dec2.format(wssr)+" "+dec.format(mcn)+" "
***** +dec.format(mf)+" "+dec.format(Tcn)+" "+dec.format(Tf));
}

}//End restriction on mcn's
}}}}}}}//End of loop through quantities

//////////////////////////
System.out.println("chisquare="+minwssr);
System.out.println("goodpoints="+goodpointmin);
System.out.println("mcn="+mcnmin);
//System.out.println("mcn1="+mcn1min);
//System.out.println("mcn2="+mcn2min);
//System.out.println("mcn3="+mcn3min);
System.out.println("ml="+mlmin);
System.out.println("mh="+mhmin);
//System.out.println("mf="+mfmin);
//System.out.println("mpre="+mpremin);
System.out.println("Tcn="+Tcnmin);
System.out.println("Tf="+Tfmin);
//System.out.println("Tpre="+Tpremin);
System.out.println("eh=" + ehmin);
```

```
System.out.println("el="+elmin);

//for(int i=0;i<q1limit;i++){for(int j=0;j<q2limit;j++)
***** {o.println((i/q1divisor)+" "+(j/q2divisor)+" "+out[i][j]);}}
//o.close();

}}//EOP
```

C.7 Modeling Code

```
 //predicts the decay of the $^{239}$Np branch using the classic formula
import java.io.*;
import java.util.*;
import java.text.*;

public class decayNp239c
{
public static void main(String[] argv)
throws java.io.IOException, java.text.ParseException
{
double Estart=17.914,Tstart=4.13;
double a,ac=8.0,anaf=1.00;
double t,t239=0,t238=0,t237=0;
double estar239=0,estar238=0,estar237=0;
double estar239tot=0,estar238tot=0;
double prob,max,decaye=0;
double Bn240=5.06,Bn239=6.2,Bn238=5.49,Bn237=5.488;
double ef240=6.0,ef239=5.85,ef238=6.0,ef237=5.7;
double gngf;// Gn/Gf
double fissneuts1=0,fissneuts2=0,fissneuts3=0,fissneuts=0,preneuts=0;
double d,delta,chi,epsilon,Sn,Sf,Nn,Nf;
//variable for the Swiatecki formula
int f239=0,f238=0,f237=0;
int n239=0,n238=0,n237=0;
int gamma=0;
int numevents=500000,A,Astart=239;
Boolean goode=false,stop=false,goodevent=false;
Boolean fission1=false,fission2=false,fission3=false;
Boolean neut1=false,neut2=false,neut3=false;
```

```
Random randnum = new Random();
File outfile = new File("decayout.csv");
PrintWriter q = new PrintWriter(new BufferedWriter
***** (new FileWriter(outfile)));
q.println("index T1 preneuts fissneuts 1Type 2Type 3Type");
DecimalFormat dec = new DecimalFormat("0.00");

//loop through events
for(int i=0;i<numevents;i++)
{
System.out.println(i);
goode=false;stop=false;goodevent=false;
fission1=false;fission2=false;fission3=false;
neut1=false;neut2=false;neut3=false;
t=Tstart;A=Astart;
estar239=0;estar238=0;estar237=0;
fissneuts1=0;fissneuts2=0;fissneuts3=0;preneuts=0;

//Start by finding the excitation energy of the $^{239}$Np
while(goode==false)
{
// choose a candidate energy at random and put it
// through a maxwellian criteria
decaye=20*randnum.nextDouble();
max=decaye*Math.exp(-decaye/t)/(t*t);
if((Estart-decaye)>0 && randnum.nextDouble()<max){goode=true;}
}
a=A/ac;
estar239=Estart-decaye;
goode=false;
```

```
t=Math.sqrt(estar239/a);
//System.out.println(estar+" "+ti);
//if(i==55){System.out.println("estar1:"+estar);}

// Determine whether the Np239 does neutron or fission
//Bn239=6.2, ef239=5.85
//if(estar<0){stop=true;q.println(i+" 0 0 pre all");}
if(estar239<ef239 && stop==false){stop=true;gamma++;}
if(stop==false && estar239<Bn239)
{
n239++;
neut1=true;
stop=true;
//q.println(i+" 0 pre NE");
}
if(stop==false)
{
////////////// CLASSIC ////////////////////////
//gngf=0.41*Math.pow(A,0.667)*(estar239-Bn239)
***** /(anaf*(2*Math.sqrt(a*(estar239-ef239))-1));
//gngf=gngf*Math.exp(2*Math.sqrt(anaf*a*(estar239-Bn239))
***** -2*Math.sqrt(a*(estar239-ef239)));

if(randnum.nextDouble()<(1/(gngf+1)))
{
f239++;
fission1=true;
fissneuts1=fissneuts1+0.144*estar239+1.78;
fissneuts=fissneuts+fissneuts1;
stop=true;
```

```
q.println(i+" 0 "+dec.format(fissneuts1)+" f1");
}
else{neut1=true;n239++;}

//if we have a neutron continue on
if(neut1==true && stop==false){
//find neut E
while(goode==false)
{
// choose a candidate energy at random and put it through
// a maxwellian criteria
decaye=10*randnum.nextDouble();
max=decaye*Math.exp(-decaye/t)/(t*t);
if((estar239-Bn239-decaye)>0 && randnum.nextDouble()<max)
***** {goode=true;}
}// end good E while
A=A-1;
a=A/ac;
goode=false;
estar238=estar239-Bn239-decaye;
t=Math.sqrt(estar238/a);
//if(i==55){System.out.println("estar2:"+estar);}

// Determine whether the Np238 does neutron or fission
//Bn238=5.49, ef238=6.0
//if(estar<0){stop=true;q.println(i+" 1 0 n1 all");}
if(estar238<Bn238 && stop==false){stop=true;gamma++;}
if(stop==false && estar238<ef238)
{
f238++;
```

```
estar239tot=estar239tot+estar239;
fission2=true;
fissneuts2=fissneuts2+0.144*estar238+1.63;
fissneuts=fissneuts+fissneuts2;
stop=true;
q.println(i+" 1 "+dec.format(fissneuts2)+" n1 f2");
}
if(stop==false)
{
////////////// CLASSIC ////////////////////////
//gngf=0.41*Math.pow(A,0.667)*(estar238-Bn238)
***** /(anaf*(2*Math.sqrt(a*(estar238-ef238))-1));
//gngf=gngf*Math.exp(2*Math.sqrt(anaf*a*(estar238-Bn238))
***** -2*Math.sqrt(a*(estar238-ef238)));

if(randnum.nextDouble()<(1/(gngf+1)))
{
f238++;
estar239tot=estar239tot+estar239;
fission2=true;
fissneuts2=fissneuts2+0.144*estar238+1.63;
fissneuts=fissneuts+fissneuts2;
stop=true;
q.println(i+" 1 "+dec.format(fissneuts2)+" n1 f2");
}
else{neut2=true;n238++;}

if(neut2==true && stop==false){
//find neut E
while(goode==false)
```

```
{
// choose a candidate energy at random and put it
// through a maxwellian criteria
decaye=10*randnum.nextDouble();
max=decaye*Math.exp(-decaye/t)/(t*t);
if((estar238-Bn238-decaye)>0 && randnum.nextDouble()<max)
***** {goode=true;}
}// end good E while
A=A-1;
a=A/ac;
estar237=estar238-Bn238-decaye;
goode=false;
t=Math.sqrt(estar237/a);
//if(i==55){System.out.println("estar3:"+estar);}

// Determine whether the Np237 does neutron or fission
//Bn3=5.488, ef3=5.7
//if(estar<0){stop=true;q.println(i+" 2 0 n1 n2 all");}
if(estar237<Bn237 && stop==false)
***** {stop=true;gamma++;/*q.println(i+" 2 0 n1 n2 NE");*/}
if(stop==false && estar237<ef237 && estar237>Bn237)
{
neut3=true;
n237++;
stop=true;
//q.println(i+" 2 0 n1 n2 n3");
}
if(stop==false && estar237>ef237)
***** {System.out.println("Not done yet!");}
```

```
}//end good neut2
}//end of second stop
}//end good neut1
}//end of first stop
//if(neut3==false && neut2==false && neut1==false)
***** {q.print("NA NA NA NA NA NA NA NA ");}
//if(neut3==false && neut2==true){preneuts=2;q.print("NA NA 2 ");}
//if(neut3==false && neut2==false && neut1==true)
***** {preneuts=1;q.print("NA NA NA NA 1");}
//,nfissneuts=fissneuts1+fissneuts2+fissneuts3;
//q.print(fissneuts+"\n");
}//end loop through events
q.close();
System.out.println("f239,f238,f237:"+f239+" "+f238+" "+f237);
System.out.println("n239,n238,n237:"+n239+" "+n238+" "+n237);
System.out.println("gamma:"+gamma);
System.out.println("estar239tot:="+dec.format(estar239tot/f238));
System.out.println("fissneuts:="+fissneuts/(f239+f238+f237));
}}
```